The Dissertation Committee for Jacob Lachenmyer Yates
certifies that this is the approved version of the following dissertation:

Signal transformation and noise correlation in the primate dorsal stream during sensory decision-making

Committee:

Alexander Huk, Supervisor

Jonathan Pillow, Co-Supervisor

Eyal Seidemann

Nicholas Priebe

Daniel Johnston

Wilson Geisler

Signal transformation and noise correlation in the primate dorsal stream during sensory decision-making

by

Jacob Lachenmyer Yates, B.A.

DISSERTATION

Presented to the Faculty of the Graduate School of

The University of Texas at Austin

in Partial Fulfillment

of the Requirements

for the Degree of

DOCTOR OF PHILOSOPHY

THE UNIVERSITY OF TEXAS AT AUSTIN

May 2016

Dedicated to F.E.Y.

Acknowledgments

This dissertation would not have been possible without the support of many people. First and foremost, I could not have been more privileged to have the pair of advisors I had. The joint mentorship of Alex and Jonathan played an enormous role in guiding my work, and they have had a tremendous influence on the way I think scientifically. They have been more than mentors to me; serving as role models both in science and in life.

I would also like to thank my committee: Bill Geisler, Eyal Seidemann, Nicholas Priebe, and Dan Johnston for enduring my scattered interests. Collectively their guidance has helped me understand each and every aspect of my work at an intuitive level. Additionally, I have had the fortune of having the support of unofficial advisors who were around CPS: in particular, Larry Cormack, whose door was always open. And whether it was at work or over a round disc golf, he always found a way to drop some incredibly sage advice.

Thanks to my Smith-Kettlewell Family: Tony, Suzanne, Alex, Justin and Melanie, for helping me get where I am.

To UT Austin, which has a brilliant cast of people around to bounce ideas off or grab beers with: Akram, Steve, Johannes, Kate, Jonas, Yoon – you were all a huge part of keeping science fun. Additionally, I owe a very special thanks to Ben for being an incredible friend and roommate, always excited

to talk shop; Memming, for entertaining my wild ideas and helping me check derivations; Kenneth, for being a great friend, for brewing delicious beer and for the collaboration; Kenny for helping out during many long basement days; and last but not least Leor, for being there every step of the way.

I would like to thank my family, in particular my mother, for decades of support. Finally, Milly, thank you for everything.

Signal transformation and noise correlation in the primate dorsal stream during sensory decision-making

Publication No. _____

Jacob Lachenmyer Yates, Ph.D.
The University of Texas at Austin, 2016

Supervisor: Alexander Huk
Co-Supervisor: Jonathan Pillow

Neuroscientists have long sought a link between the activity of single neurons and our thoughts, perceptions and ultimately our mental experiences. As our senses provide the input into the brain, understanding the computations that transform signals along the sensory pathways has remained central to this endeavor. Remarkable progress has been made by studying neural correlates of perceptual decisions in motion-processing and oculomotor areas of the primate brain. In particular, when monkeys indicate their decisions about the direction of motion with eye movements, neurons in the middle temporal area (MT) represent the instantaneous motion evidence and neurons in the lateral intraparietal area (LIP) resemble the integration of motion evidence, effectively transforming the sensory signal into a decision variable.

In the main body of this thesis, I describe the results of an effort to measure the sensorimotor transformation between MT and LIP on single trials. First, I describe a motion-discrimination task that is amenable to reverse correlation analysis, allowing the experimenter to measure the temporal dependencies of neural responses and choices on the instantaneous motion energy. I then use a unified statistical framework to analyze simultaneous recordings from both areas during decision-making. Primarily, I found that MT neurons exhibited time-varying sensitivity to motion direction, with important consequences for the behavior and neurophysiology in downstream areas. Individual LIP neurons also carried a signature of an integrated motion signal in their spike rates, however, it was unlikely that this signal results from direct MT input. Finally, I show that a biologically plausible simple decoder can perform as well as the monkey at coarse direction-discrimination task.

In the appendix, I describe the results of pharmacological inactivations of MT and LIP and statistical models of single trial dynamics in LIP that were performed in collaboration with fellow graduate students, Leor Katz and Kenneth Latimer, respectively.

Table of Contents

List of Figures

Chapter 1

Introduction

"Whoever, in the pursuit of science, seeks after immediate practical utility may rest assured that he seeks in vain" - Hermann von Helmholtz

1.1 Overview

The external world is encoded by our visual system through a hierarchy of areas in our cerebral cortex (Lennie 1998). To accomplish even the simplest tasks, the brain requires circuits that can decode task-relevant information from sensory neural populations. I emphasize *populations*, because it is now widely accepted that these sensory representations exist at the level of populations of neurons, at least for primate cortex (Graf, Kohn, Jazayeri & Movshon 2011). In recent years neuroscientists have gained the ability to record from many neurons simultaneously (Stevenson & Kording 2011), yet much of what is known about the perceptual readout of sensory areas to guide perceptual decisions is extrapolated from recordings of single neurons in the parietal lobe of macaque monkeys making judgements about the direction of motion.

When a monkey makes a decision about the direction of motion and

indicates her choice with an eye-movement, neurons in the middle temporal area (MT) are thought to represent the instantaneous motion evidence and neurons in the lateral intraparietal area (LIP) resemble the accumulation of evidence, effectively transforming the MT activity into a decision variable. These observations have been articulated mathematically in the form of two-stage computational models, where MT is integrated by LIP, forming a feedforward process where both signal and noise in MT are propagated downstream to LIP (Mazurek, Roitman, Ditterich & Shadlen 2003, Gold & Shadlen 2007, Beck, Ma, Kiani, Hanks, Churchland, Roitman, Shadlen, Latham & Pouget 2008).

In this thesis, I probe the MT-LIP circuit using statistical models of neural activity and simultaneous recordings from both areas during decision-making to track the propagation of signal and noise on the scale of single decisions. This chapter is structured to cover the relevant experimental and theoretical results that pertain to the MT-LIP circuit as well as the methodology that is employed in this thesis. It begins with an overview of the field of sensory decision-making. I then review the theoretical frameworks that lay crucial groundwork for the study of perceptual decisions. I cover MT and LIP physiology as well as the computational modeling approaches to understanding their link to perceptual decisions. Finally, I review statistical methods for studying neural and behavioral data.

1.1.1 Signal and noise in sensory neurons during perceptual decisions

25 years ago, Bill Newsome and colleagues performed a set of seminal experiments by recording from single neurons in MT while monkeys made perceptual decisions about the direction of motion. In these experiments they made two key observations that have shaped the field of sensory decision-making. First, they found that single MT neurons were often as sensitive as the monkey to motion direction (Britten, Shadlen, Newsome & Movshon 1992). They concluded the monkey would only have to use a few neurons to solve this task. Second, they found that for stimuli near perceptual threshold, when the monkey's choices were variable, the MT neurons exhibited trial-to-trial variability that was correlated with animal's perceptual report. They called this correlation *choice probability* (CP) and interpreted it as evidence that MT neurons sent spikes forward to decision areas. In other words, the signal to noise ratio (SNR) of MT neurons paralleled the SNR of the monkey and the noise of MT neurons was correlated with the noise of the monkey, suggesting that the monkey was "reading out" MT activity.

To understand how the MT neurons could exhibit such widespread correlation with the perceptual report, the authors used computational experiments to implement a possible scheme to readout MT. The intuition that motivated the study is that averaging samples from a noisy distribution (spikes from multiple neurons in this case) improves the SNR if the samples are independent. However, that improvement in SNR is diminished if the samples

are positively correlated. The Shadlen, Britten, Newsome & Movshon (1996) model built a "decision neuron" that could discriminate up and down motion by receiving excitatory input from a pool of upward selective MT neurons and inhibitory input from a pool of downward selective MT neurons. By including a covariation (noise correlation) between individual MT neurons in their model, the Shadlen et al. (1996) model explained both the observed choice probabilities and the perceptual thresholds.

In the subsequent years, the "decision neuron" in the second stage of Shadlen et al. (1996) was mapped explicitly onto a model of area LIP neurons (Shadlen & Newsome 2001, Mazurek et al. 2003). LIP was targeted because it has anatomical projections to oculomotor areas involved in generating the saccadic eye-movements that the monkey uses to indicate his choice (Barbas & Mesulam 1981, Lynch, Graybiel & Lobeck 1985), and because it receives input from MT (Maunsell & Van Essen 1983*b*, Ungerleider & Desimone 1986), placing it at an intermediate stage between the purely sensory and purely motor (Gnadt & Andersen 1988). Indeed, during motion-discrimination, LIP neurons have average firing rates that resemble an idealized decision process: they ramp up or down preceding the two choices, where the slope of the ramp is a function of the motion strength (Shadlen & Newsome 2001). There have been many iterations of this model and it has had a broad impact on neuroscience at large (Shadlen & Newsome 2001, Mazurek et al. 2003, Huk & Shadlen 2005, Gold & Shadlen 2007, Beck et al. 2008, Shadlen & Kiani 2013).

The expert reader will note that there are at least three notable caveats

to this story: First, recent experiments involving shorter duration stimuli have constrained the measurements on neural sensitivity (Cohen & Newsome 2009). In a response-time version of the dots task, where the monkey is allowed to indicate his choice whenever he has sufficient evidence without waiting for the whole stimulus to finish, single MT neurons are never more sensitive than the monkey. Second, theoretical studies have greatly changed our understanding of the effect of neural correlations on population codes (Ecker, Berens, Tolias & Bethge 2011, Moreno-Bote, Beck, Kanitscheider, Pitkow, Latham & Pouget 2014). Noise correlations can help or hurt coding depending on their structure in relation to the signal and simultaneous recordings from oppositely tuned pairs of neurons have revealed positive noise correlations (Cohen & Newsome 2009) providing empirical evidence of potentially beneficial noise correlations. Third, the decision-like ramping activity observed in LIP has been seen in many other brain areas (both cortical and subcortical)(Shadlen & Kim 1999, Horwitz, Batista & Newsome 2004, Ding & Gold 2013). Despite these caveats, the basic idea that choice probability indicates a feedforward readout strategy has largely been maintained until recently.

1.1.2 Choice probability more than a neuron's causal role

In standard models of sensory decision-making, sensory areas project to decision areas which in turn project to motor systems (Gold & Shadlen 2007). In this framework, choice probability results from the feed-forward propagation of noise in sensory areas and as such, has largely been interpreted as

purely feed-forward. However, the completely feed-forward interpretation of choice probability was recently brought into question by a study that compared the time-course of choice probability to the perceptual strategy of the monkey (Nienborg & Cumming 2009). Nienborg & Cumming (2009) recorded from disparity selective V2 neurons while monkeys performed coarse depth-discrimination. Importantly, on a subset of trials, the stimulus disparity was drawn at random such that the instantaneous disparity was independent over time and there was no net expected near versus far disparity (ie. no signal). On these trials, the monkey was still trying to do the task (but was rewarded randomly). By correlating the instantaneous fluctuations in disparity with the animal's choice, the experimenters could measure the subject's strategy in the task. The logic here is that if there is a particular time in trial when the the animal is using the stimulus, then the stimulus should be correlated with choice at that time but not any other time. This technique, referred to as either classification image analysis or psychophysical reverse correlation (discussed below), approximates the strategy of the observer with a linear template (Murray 2011).

The monkeys had psychophysical kernels that peaked early in the stimulus presentation. This was interpreted as evidence that the monkeys were using the stimulus at the beginning more than the end to inform their choices. The prediction here is that if choice probability is reflecting feedforward correlation with choice– that is, the stochastic variability in spiking response is correlated with animals choice because it is "read out" – then choice probabil-

ity should also peak early in the stimulus presentation. However, although the psychophysical kernel decayed throughout the stimulus presentation, choice probability increased over time. This result suggested that at least some component of choice probability, the portion that showed up late, could not be explained with the feedforward interpretation, because the neural noise was still correlated with the animal's choice after the animal had stopped using the stimulus.

By comparing the time-course of psychophysical weighting to the time-course of choice probability, Nienborg & Cumming (2009) took the relationship between sensory neural activity and choice explicitly into the time domain, which has been a central component of the MT-LIP story, but which has not been directly characterized (Gold & Shadlen 2007). The basic premise of my work was to test this idea feed-forward readout in the motion-discrimination paradigm at two levels of the hierarchy: the sensory representation, and the putative decision process. Psychophysical reverse correlation provided a means to directly compare the monkey's temporal strategy to the encoding of neural responses in MT and LIP (Neri & Levi 2006).

1.1.3 General approach

So far in this chapter I have described a line of research that integrates threshold psychophysics and single neuron recordings to probe the mechanisms of perceptual readout. In this thesis, I bring this approach to the level of small populations in multiple stages of the cortical hierarchy. I focus on the tem-

poral strategy of the psychophysical observer and how that is related to the responses of small populations of neurons in MT and LIP. To make measurements of the strategy, the neural encoding mechanisms and the residual noise correlation (both with choice and across simultaneously recorded neurons), I used a systems identification approach which forms a unified framework for measuring neural and behavioral responses to visual stimuli. In particular, I developed a motion-discrimination stimulus based on sequential motion pulses such that we could reverse correlate the stimulus with choice, or with spikes in MT and LIP. I recorded from multiple neurons simultaneously in both areas to address whether activity in MT and LIP was correlated across trials, and I employed a statistical framework both to measure the psychophysical kernel, and the temporal receptive fields of the neurons.

Many of the analyses in this these utilize a generalized linear model (GLM), which is a highly flexible, empirically tractable regression model that has been widely successful in describing early sensory areas and has been used to understand both MT and LIP responses independently in the past (Cui, Liu, Khawaja, Pack & Butts 2013, Park, Meister, Huk & Pillow 2014). Importantly, using a likelihood based approach, we were able to explain away variance due to the stimulus and ask an important question: does single trial MT activity influence single trial LIP activity or vice-versa? Additionally, likelihood-based methods answer that question in units that are immediately relevant: How much more likely is this result if X is the case than if Y is?

In Chapter 2, I describe a motion-discrimination stimulus and task I

developed that is amenable to white-noise systems identification techniques. Monkeys were trained to integrate independent samples ("motion pulses") of motion evidence over a second-long window and indicate their choices with an eye movement. This stimulus allowed us to measure the contribution of each motion pulse to behavior and to neural activity in MT and LIP.

In chapter 3, I use a generalized linear model (GLM) to describe the responses of simultaneously recorded MT and LIP neurons to the motion-pulse stimulus during decision-making. I found that, contrary to the MT-LIP model, both MT and LIP exhibited time-varying responses to motion. LIP's stimulus referenced responses to motion (the signal) could be explained with temporal integration of MT's average time-varying signal without appeal to additional mechanisms. However, the trial-by-trial variability in LIP activity (the noise) was not coupled to fluctuations in MT activity. Surprisingly, task-modulated coupling was observable in the feedback direction.

In chapter 4, I analyze the information available in small populations of simultaneously recorded MT neurons. I show that a simple, neurally plausible, decoder is as accurate as the monkey and is more accurate than the best single neuron on each session. I show that for this task, the decoder can be quite simple over neurons and over time. Additionally, the information about motion direction was greatest early in motion viewing.

1.2 The theoretical basis for simple perceptual decisions

1.2.1 Signal Detection Theory

Psychophysicists have long thought of perception and perceptual decisions as statistical inference about environmental stimuli (von Helmholtz & Southall 1924, Fechner 1860). The basic idea is that a perceptual decision is an inference about the state of the world given the signals on the sensor array. The goal of the psychophysicist is to understand the rules of this process mathematically. A major step towards this goal was formalized in Signal Detection Theory (SDT)(Green & Swets 1966). SDT begins with the sensory evidence, s, as it is available to the observer. s is a noisy internal variable that results from the noisy response of the sensory transducers to the true state of the world. The world can two states: the signal is present, or the signal is absent. The observer's goal is to decide which state of the world generated the sensory evidence observed ("signal present" or "signal absent", denoted a and b respectively from here on). SDT formalizes this general idea probabilistically. The observer should should choose "a" if the probability of a given s is greater than the probability of b given s (choose a if $p(a|s) > p(b|s)$). Using Bayes' theorem, the previous statement can be rewritten in terms of the probability of s given a or b. These two distributions are the *likelihood* of the observed sensory signal given the two possible states of the world. To make an optimal choice, the observer then simply has to compare the likelihood ratio to a criterion – which, in a world where a and b are equally likely and have equal value,

is 1. SDT provides the theoretical groundwork to allow psychophysicists to understand internal sensory mechanisms while measuring only the behavior. This approach was extended to understand the sensitivity of single neurons and compare them to psychophysical sensitivity (Mountcastle, Talbot, Sakata & Hyvärinen 1969, Parker & Newsome 1998).

1.2.2 Sequential Analysis

Sequential Analysis (SA) extends SDT into the time domain (Wald 1947, Link 1992) If time effectively gives the observer multiple samples from $p(s|a)$ and $p(s|b)$, then the observer can increase the SNR by combining these samples. If the samples are independent, than they can be combined by taking the logarithm and summing them. Thus, the observer gains SNR by summing log-likelihood ratios over time. A criterion can then be set depending on the value and prior probability of the two outcomes as well as the desired accuracy of the observer. The sequential sampling framework has been a powerful tool for understanding psychological processes that take time, including memory retrieval and the accumulation of evidence for perceptual decisions (Ratcliff 1978, Gold & Shadlen 2001). SDT and SA play a major role in the interpretation of behavioral and neural data in this chapter, and ultimately in the formulation of the MT-LIP model. Many experimental observations loosely conform to the assumptions laid out in SDT and SA such that during motion-discrimination, area MT can be thought of as the sensory evidence and LIP reflects the accumulation of evidence (Gold & Shadlen 2007). In the

next sections I review basic physiological properties of area MT and its role in perceptual decision-making.

1.3 Physiology

1.3.1 Area MT

Originally discovered and named over four decades ago in the owl monkey (Allman & Kaas 1971), the middle temporal area (MT) has had a major influence on studies of perception, decision-making and neural coding (Born & Bradley 2005). Composing less than 1% of the macaque cerebral cortex (Felleman & Van Essen 1991), MT is remarkably homogenous (Lennie 1998), with 90% of neurons exhibiting directionally selective responses (Albright 1984). MT receives feedforward input from V1 (Burkhalter & Van Essen 1986, Maunsell & Van Essen 1983*b*), V2 (Maunsell & Van Essen 1983*b*), V3 (Maunsell & Van Essen 1983*b*), superior colliculus (Berman & Wurtz 2010) and LGN (Sincich, Park, Wohlgemuth & Horton 2004). Of the many inputs to MT, the input from V2 seems to be strongest (Maunsell & Van Essen 1983*b*, Markov, Vezoli, Chameau, Falchier, Quilodran, Huissoud, Lamy, Misery, Giroud, Ullman, Barone, Dehay, Knoblauch & Kennedy 2014), and the cortical input from V1 is the most well understood (Movshon & Newsome 1996). MT neurons are also sensitive to disparity (Maunsell & Van Essen 1983*a*), speed (Maunsell & Van Essen 1983*b*), and motion-through-depth (Czuba, Huk, Cormack & Kohn 2014, Sanada & DeAngelis 2014). Additionally, there is evidence that MT neurons solve the *aperture problem* and respond to ve-

locity at a range of spatial and temporal frequencies (Movshon, Adelson, Gizzi & Newsome 1985, Priebe, Cassanello & Lisberger 2003). Additionally, many of these selectivities are organized across cortical columns (DeAngelis & Newsome 1999). For the purposes of this dissertation, I focus on the role of MT in the perception of frontoparallel motion with little concern for how MT neurons acquire that selectivity.

1.3.1.1 Role in visual perception

Many studies have established area MT's causal role in the perception of motion. Early lesion studies showed that inactivation of MT impairs the ability to pursue moving objects (Newsome, Wurtz, Dürsteler & Mikami 1985) or perform coarse direction-discrimination (Newsome & Pare 1988). Microstimulation of MT biases coarse direction-discrimination (Salzman, Britten & Newsome 1990, Salzman, Murasugi & Britten 2003). In tasks with more than two directions, microstimulation biases direction estimates towards the direction of the column that the stimulating electrode is in (Salzman & Newsome 1994), regardless of whether the direction is indicated with an eye movement or manually (Nichols & Newsome 2002). Area MT indeed seems to be a bottleneck in many perceptual tasks involving the perception of motion or depth (Parker & Newsome 1998, Kim, Angelaki & DeAngelis 2015).

Another piece of supporting evidence for MT's role in the perception of motion is that neural sensitivity to direction is sufficient to explain psychophysical performance (Newsome, Britten & Movshon 1989, Britten et al.

1992) and the trial-by-trial variability in spiking in MT is correlated with the perceptual report (Britten, Newsome, Shadlen, Celebrini & Movshon 1996). This correlation with choice for stimuli near perceptual threshold has been observed for coarse discrimination (Britten et al. 1996), fine-discrimination (Purushothaman & Bradley 2005), and at much higher levels during bi-stable perceptions (Logothetis & Schall 1989, Dodd, Krug, Cumming & Parker 2001). Taken together, the causal manipulations and choice probabilities have established MT as a central locus for motion processing. One notable exception to the above studies is Hedges, Gartshteyn, Kohn, Rust, Shadlen, Newsome & Movshon (2011). In this study, the authors found that when presented with an apparent motion stimulus where, as the individual elements appear they drift locally, human observers perceive the global motion and MT tracks the local motion. However, this study was performed by comparing macaque MT neurons to human psychophysics and it there is no psychophysical data from macaques to suggest that they perceive the global motion.

1.3.1.2 Sensitivity to motion

Many studies have focused on how MT gains its velocity selectivity (See Bradley & Goyal (2008) for a comprehensive review). Neurons in MT have been studied extensively using bars (Albright 1984, Okamoto, Kawakami, Saito, Hida, Odajima, Tamanoi & Ohno 1999), gratings (Movshon et al. 1985, Priebe et al. 2003) and random dots (Britten, Shadlen, Newsome & Movshon 1993, Priebe & Lisberger 2002). MT neurons are tuned for the direction of

moving stimuli in a way that is well described by a circular gaussian or von Mises tuning curve (Albright 1984, Rust, Mante, Simoncelli & Movshon 2006). MT neurons are often broadly tuned for the speed of motion with a log Normal function describing the sensitivity (Priebe et al. 2003, Nover, Anderson & DeAngelis 2005). To be truly speed tuned, the neurons must be selective to all combinations of spatial and temporal frequencies that produce a certain speed and many MT neurons have this feature (Priebe et al. 2003).

1.3.1.3 Readout Mechanisms

Area MT has been a fruitful testing bed for electrophysiologists and theorists. Its comparatively homogenous population of directionally selective neurons (Lennie 1998) have allowed experimenters to consistently find the responses they are interested in studying, and have allowed theorists to model responses with relatively simple analytic forms (Shadlen et al. 1996, Jazayeri & Movshon 2006). Population readout mechanisms have been studied for many decades in sensory and motor areas (Georgopoulos, Schwartz & Kettner 1986). Most of the early studies have relied on simple *ad hoc* population readout mechanisms such as vector averaging or winner-take-all. In more recent years, probabilistic inference has dominated as a framework for studying population readout (Seung & Sompolinsky 1993, Jazayeri & Movshon 2006).

Many studies have demonstrated causally using microstimulation that image velocity is read out from MT, yet they often disagree on the particular algorithm. In the earliest studies, stimulating a column of MT neurons was

shown to bias a monkey's perceptual report for coarse discrimination of direction alternatives in a way that was consistent with a winner-take-all read out scheme, regardless of whether there were two or eight alternatives (Salzman et al. 1990, Salzman & Newsome 1994). However, microstimulation affected smooth pursuit eye-movements in a manner consistent with a vector averaging readout scheme (Groh, Born & Newsome 1997).

In a continuous motion estimation task, the readout scheme switched systematically between the two (Nichols & Newsome 2002). This suggests that the animal has a fairly sophisticated mechanism for reading out MT. Probably the most compelling evidence that the animal's readout is sophisticated comes from microstimulation at different time intervals (Seidemann, Zohary & Newsome 1998) and for neurons that were selective for task irrelevant features (DeAngelis & Newsome 2004). By delivering current stimulation at different times relative to the motion stimulus, the first study showed that the animal can selectively gate its read out of MT over time. The second showed that an MT column's contribution to choice about direction depends strongly on how well tuned the neurons were for a task-irrelevant feature (disparity) of the discriminated stimulus.

There are two interrelated questions when it comes to the read out algorithms employed by the brain. The first, which is closely linked to the studies described in the previous two paragraphs, is directed at how the animal *does* read out the brain area. The second takes a normative approach: Given the neural responses, how *should* the animal read out the stimulus? This

second approach has played a large role in the interpretations of signals that are present downstream from MT, and which will be discussed at length in the following sections as I introduce the downstream areas that are thought to be involved in this process.

1.3.2 Area LIP

The lateral intraparietal area (LIP) has played a major role in studies of perceptual decision-making as well as a host of other cognitive and sensorimotor functions(Rao, DeAngelis & Snyder 2012)(Louie & Glimcher 2012). Here I focus on the subset of the literature that speaks directly to its role in decisions. LIP is located on the lateral bank of the intrapariaetal sulcus and has neurons that encode the spatial location of upcoming saccades (Andersen, Essick & Siegel 1985). It projects to brain centers involved in eye movements: super colliculus (SC) (Lynch et al. 1985, Wurtz, Sommer, Paré & Ferraina 2001, Andersen, Asanuma, Essick & Siegel 1990), the frontal eye fields (FEF) (Andersen et al. 1990, Ferraina, Paré & Wurtz 2002) and receives input from visual areas (including MT) (Lewis & Van Essen 2000, Ungerleider & Desimone 1986, Blatt, Andersen & Stoner 1990)and has an established role in oculomotor planning(Lynch 1992, Andersen & Buneo 2002).

The motivation for studying LIP in the context of perceptual decision-making is two-fold. First, in the original (and current) motion-discrimination task, the monkeys indicated their choices with saccadic eye movements, thus, any area involved in the decision process logically had to have access to modify

saccade motor plans (Shadlen & Newsome 1996). Second, several brain areas involved in eye-movement planning had previously been identified and shown to have neurons with persistent activity (Gnadt & Andersen 1988, Barash, Bracewell, Fogassi, Gnadt & Andersen 1991*a*, Barash, Bracewell, Fogassi, Gnadt & Andersen 1991*b*). That is, activity that continued (persisted) after a stimulus disappeared as long as that stimulus was used in preparation of an eye movement to the region of space coded for by the neuron (the response field; RF) (Gnadt & Andersen 1988). This activity is strongly predictive of whether the monkey's eye movement would be in or out of the RF(Graf & Andersen 2015).

1.3.2.1 Role in decision-making

The first recordings from LIP during motion-discrimination of motion revealed that the persistent activity resembles ramps that ramp up for choices into the RF and down for choices out of the RF. This ramping activity builds up at different rates as a function of the motion strength such that the predictive relationship with choice was dependent on the motion strength (Shadlen & Newsome 1996). The existing literature on integrators in the oculomotor system (Fuchs, Kaneko & Scudder 1985), as well as the previously hypothesized decision neurons that sum pools of MT neurons (Shadlen et al. 1996) invited the authors to interpret these motion-dependent ramps in LIP as resembling the integration of MT. The reasoning here was very directly linked to the normative approach for LIP was additionally shown to exhibit coher-

ence dependent ramps in a reaction time version of the task (Roitman & Shadlen 2002) and to reflect the integration of motion evidence directly (Huk & Shadlen 2005).

Around the same time, coming from a different decision-theoretic perspective Platt & Glimcher (1999) showed that LIP neurons code for the the prior probability and expected value of a target. Additionally LIP has been shown to track other decision-theoretic quantities including the subjective value of a choice (Sugrue, Corrado & Newsome 2004), confidence (Kiani & Shadlen 2009) and elapsed time (Leon & Shadlen 2003, Janssen & Shadlen 2005, Jazayeri & Shadlen 2015). Despite that fact that integration alone cannot explain the representation of priors, value or reward; despite the existence of similar responses in the frontal lobes (Shadlen & Kim 1999), superior colliculus (Horwitz et al. 2004) and caudate(Gold & Ding 2013); and despite the disappointing conclusion that integration itself is not identifiable in the behavior (Ditterich 2006), many computational models of decision-making reference the MT-LIP link in motion discrimination directly (Mazurek et al. 2003, Law & Gold 2008, Beck et al. 2008, Wimmer, Compte, Roxin, Peixoto, Renart & de la Rocha 2015) and LIP has remained central to the study of perceptual decision-making, at least in part because of its physical proximity to MT (Shadlen & Newsome 1996) and this putative link (Gold & Shadlen 2007).

1.3.3 MT-LIP model

Although even the earliest papers suggested that LIP reflects the integration of MT (Shadlen & Newsome 1996), the first explicit formulation of the MT-LIP model comes from (Mazurek et al. 2003). The model begins with pools of MT neurons (similar to (Shadlen et al. 1996)) that code for the two directions of motion (Figure 1.1a). Assuming that motion is discriminated along the horizontal axis, such that the two directions are left and right, Mazurek et al. (2003) represented MT with two pools of neurons (righward and leftward preferring neurons) with rates that were flat over time and generated spikes with a process that created slightly sub-poisson noise (Mazurek & Shadlen 2002). However, the instantaneous averaged ensemble activity was taken as output at each stage, such that MT was essentially represented by two rate functions. The output of the two pools were then compared (differenced) and then integrated by LIP neurons (Figure 1.1a). At this point, it is important to reflect on the realism of this simulation. Although the parameters of the MT stage were set based on empirical measurements, many features of MT responses are ignored (such as short-term adaptation (Priebe, Churchland & Lisberger 2002, Bair & Movshon 2004) and temporal autocorrelation (Uka & DeAngelis 2003, Osborne, Bialek & Lisberger 2004)). These features may contribute to certain failures of the model (discussed in the following paragraphs).

A key feature of the Mazurek et al. (2003) model was the addition of a decision bound. The bound is an important feature because it allows

for the description of both speed and accuracy during RT tasks. The bound also served to limit the monkey's performance on the fixed duration version of the discrimination task (Mazurek et al. 2003). The only parameter fit to the behavior was the height of the bound. The model provided a surprisingly accurate account of the neural data and behavior. Importantly, and I believe quite unusually for neuroscience, this bounded integrator model made several predictions for future experiments. First, it predicted that MT neurons should be half as sensitive during an RT task, since less spikes are available. Second, CP should be much larger during the RT task, since all of the spikes are being used by the monkey. Third, RT should be weakly anti-correlated with spike rate in MT. The first prediction was false. MT neurons were slightly less sensitive during RT task, but not by half. The second prediction turned out to be false as well. CP was not larger during RT version of the dots task (Cohen & Newsome 2009). However, the third prediction held (Price & Born 2010), but again, at a different magnitude. The failure of the accumulator model predictions strongly suggests that this model is incorrect, or at least incomplete.

The single most compelling piece of evidence for the MT-LIP accumulation model comes from an experiment with time-varying motion texture pulses superimposed behind the usual motion stimulus(Huk & Shadlen 2005). LIP neurons had spike rates that showed lasting effects of the direction of a motion pulse. The change in spike rate that resulted from a motion pulse began roughly 200ms after the onset of motion and lasted for 800ms, revealing a

response to motion that was substantially smoothed over time compared to average MT responses. Additionally, the experimenters found that LIP neurons were shift-variant in a way that could be reconciled by bounded accumulation. In particular, they found that early pulses exerted larger effects on spike rate than later pulses. Together, these two pieces of evidence provided the best empirical support for the idea that LIP reflects the accumulation of MT spikes to bound.

Over the past decade, the basic form of the model has remained the same. Pools of MT neurons represent motion direction and LIP integrates the pools until a bound is reached. Some variations of the model involve attractor networks with neural circuit implementations (Wong, Huk, Shadlen & Wang 2008), probabilistic population codes (Beck et al. 2008), and spiking neural networks (Wimmer et al. 2015). In many cases the explicit MT stage is dropped and LIP spike rates were just qualitatively mapped on to diffusion models that were fit to behavior (Ditterich 2006, Kiani, Hanks & Shadlen 2008, Kiani & Shadlen 2009). A version was used to gain insight into perceptual learning (Law & Gold 2008). More recently, MT-LIP models have been used to understand the source of choice probabilities in MT (Wimmer et al. 2015). In every single one of these models, there is either a comparator stage between MT and LIP (that takes the difference between the two pools of MT neurons) or there is no stage between MT and LIP and the connection is direct. In most cases, the comparator stage is implemented by LIP itself in that on pool delivers excitatory input and the other inhibitory input to each LIP neuron.

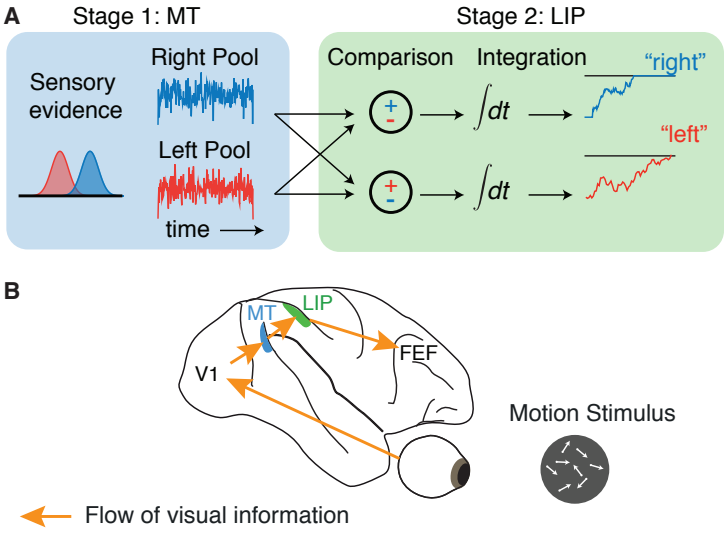

Figure 1.1: Schematic of the MT-LIP model. **A** Cartoon of the two stage MT-LIP accumulation to bound model (Inspired by Mazurek et al. (2003)). Blue box: Area MT represents the instantaneous sensory evidence. Two distributions represent the probability of spike rate for rightward (blue) and leftward (red) selective MT pools given the stimulus. The MT response over time represents samples from these distributions such that the instantaneous LLR can be measured by subtracting the two traces. Green box: LIP neurons receive excitatory input from rightward selective MT neurons (blue) and inhibitory input from leftward selective MT neurons (red) and vice verse. The difference is accumulated over time until a bound is reached. The choice is determined by a race to threshold. In this example, where the likelihood that left motion generated the stimulus was lower than for right, LIP neurons that preferred right hit the threshold before the leftward selective group. **B** The flow of visual information in cortex. MT receives input from V1. LIP receives input from MT and feeds forward to oculomotor area FEF and SC (not shown). This cartoon is widely present in the neuroscience literature.

1.3.3.1 Anatomical and functional evidence

There are monosynaptic connections between MT and LIP (Ungerleider & Desimone 1986, Maunsell & Van Essen 1983*b*), although it's unclear whether

the timescale of computations in LIP could be governed by those (Shadlen & Newsome 1996). LIP does have feedforward connections to FEF and SC (Lynch et al. 1985, Andersen et al. 1990), but LIP also receives excitatory feedback from FEF, direct projections from SC and is in many ways better thought of as part of a computational unit in tandem with SC and FEF(Ferraina et al. 2002). Additionally LIP feeds back to MT (Andersen et al. 1990, Markov et al. 2014). FEF also feeds back to MT (Stanton, Bruce & Goldberg 1995, Anderson, Kennedy & Martin 2011). Thus, the anatomical evidence does a poor job of constraining the relationship between MT and LIP because both MT and LIP are interconnected with every other area that is hypothesized to be involved in the process (Wurtz et al. 2001).

Functionally, there is a 100ms latency between the visual responses in MT (or LIP for that matter) and the onset of ramping activity in LIP (Kiani et al. 2008). It's important to note that the motion stimulus is not in the RF of LIP neurons in this model. Somehow, the brain has to map the visual information from one area of the visual field to a motor plan to another place entirely (Shadlen & Kiani 2013). The logic of the task suggests that this comes from MT and does seem to be reflected in LIP (Huk & Shadlen 2005), but the latencies and flexible mapping alone are reason to expect that the relationship is not governed by direct anatomical connections.

Additionally, there is a dearth of simultaneous data from MT and LIP and no study to date has recorded from both areas during a motion-discrimination task. Only three studies to date have recorded simultane-

ously and only two of them have analyzed the simultaneous nature of the data. All found evidence that suggests feedback from LIP to MT (Herrington & Assad 2010, Saalmann, Pigarev & Vidyasagar 2007, Siegel, Buschman & Miller 2015).

1.4 Methodology

One of the key methodological goals of this work was to compare the monkey's temporal strategy to the neural responses in MT and LIP. Measurement of the psychophysical strategy and neural encoding rules both fall under the domain of *systems identification*. The principles are the same for both the neural encoding and behavioral strategy. In this section I review existing statistical approaches to reverse correlation of both psychophysics and neural responses and show that both can be understood within the framework of a generalized linear model (GLM) (Figure 1.2).

1.4.1 Psychophysical Reverse Correlation

Psychophysical reverse correlation is a technique for measuring the features in a stimulus that are driving behavior. In a typical psychophysical reverse correlation experiment, a psychophysical observer is tasked with detecting a signal that is embedded in gaussian white noise. On half of the trials, the signal is present. On the other half, only noise is present. In the absence of the noise, this task would be unambiguous, but the noise is titrated such that the observer is only correct 75% of the time. The resulting error trials provide

an intuition for how the method works: Sometimes the signal is present and the subject missed it because of the noise and sometimes the signal was absent and the noise caused the subject to say it was present. Because the noise is known explicitly, it is possible to learn what features contributed to the errors. By separating the trials into the two choices and averaging the noise that led to each choice, the psychophysicist can build an image of the average noise that led to each choice. The difference between these two images is known as the classification image or psychophysical kernel (PK), because it can be used to classify the choice that the observer will make given a noise stimulus and is directly related to the first-order kernel of Wiener or Volterra expansion (Murray 2011).

The PK forms a linear predictor for the subjects response: The dot-product between the noise-sequence on a given trial and the PK is an estimate of the subject's internal decision variable. Placing a criterion on this value produces estimates of the subject's choices. This model of the psychophysical observer can also be formed probabilistically, by including a soft threshold and a noise model. With only two possible stimulus states, choices are described by a Bernoulli random variable. The probability of a response can be written:

$$p(y(t)|\vec{s}(t), \vec{w}) = \rho(t)^{y(t)}(1 - \rho(t))^{(1-y(t))} \tag{1.1}$$

where $y(t) \in \{0, 1\}$ is the choice on trial t and $\rho(t)$ is the probability the subject chooses $y(t) = 1$, which can be represented by the equation $f(\vec{s(t)} \cdot \vec{w})$ where f is a sigmoidal nonlinearity, $\vec{s(t)}$ is the spatiotemporal stimulus on trial

t and $\vec{w}$ is the subject's template (the PK). In this formulation, the PK, $\vec{w}$, can be estimated using maximum likelihood of the distribution $p(\mathbf{y}|\mathbf{s}, \vec{w})$ or by maximum aposteriori estimation of $p(\vec{w}|\mathbf{y}, \mathbf{s})$ where $\mathbf{y}$ is a vector of choices on each trial and $\mathbf{s}$ is a matrix that depicts the spatiotemporal stimulus on each trial (Knoblauch & Maloney 2008, Mineault, Barthelme & Pack 2009).

Since its introduction in auditory perception (Ahumada 1971, Ahumada 1975), psychophysical reverse correlation has been most widely used to probe the neural mechanisms that underly a perceptual categorization without recording from neurons (Neri & Levi 2006). They have been successful in describing internal mechanisms of (but not limited to) processing contrast (Neri & Heeger 2002, Shimozaki, Eckstein & Abbey 2005), stereopsis(Neri, Parker & Blakemore 1999, Neri 2004), orientation(Mareschal, Morgan & Solomon 2008, Mareschal, Dakin & Bex 2006), contour formation(Gold, Murray, Bennett & Sekuler 2000).

Typically, when vision scientists use classification images, the subject is looking for a particular feature in the stimulus and the experimenter is trying to learn the features of sensory neurons that are representing the signal the observer is searching for (Murray 2011). An example of this type of interpretation is apparent in classification images for simple detection. In these images, if the subject is trained to detect a a white bar embedded in noise, the classification image reveals that the subject is indeed looking for a white bar, but that bar is surrounded by negative lobes. These negative flanks are interpreted as evidence for the shape of sensory receptive fields, that have cen-

ter surround properties (Neri & Levi 2006). An alternative interpretation is that the subject reads out neurons that do not have surrounds with negative weights. This can only be unpacked by recording from neurons at different stages in the brain. In fact, if neuroscientists hadn't already observed center-surround mechanisms in the retina and LGN, they would not have known if the center-surround mechanism existed at the encoding or the readout stage in the PK (Neri & Levi 2006).

Psychophysical reverse correlation studies often seek to understand how the sensory neurons shape the observer's template. For example, Neri & Heeger (2002) looked at contrast detection and found that nonlinear mechanisms preceded linear mechanisms of detection. They interpreted this as evidence that complex cells in V1, which respond strongly to contrast energy regardless of luminance sign, were priming the readout of simple cells in a way that is akin to bottom up attention. Since the classification image is approximating the entire visual system in one linear stage, it is comprised of multiple linear and nonlinear steps.

More recently, scientists have begun looking at the dynamics of PKs over time, and interpreting these dynamics as evidence for decision strategies. The first example of this comes from Kiani et al. (2008), where they measured the PK over time for motion-discrimination. They found that the motion energy in the stimulus was most correlated with the animal's choices early in the trial and they interpreted this as evidence for bounded accumulation of motion energy. Of course, this could also result if the sensory neurons had temporal

dynamics (Priebe et al. 2002). Interpreting PKs as read out has become increasingly popular in recent years (Nienborg & Cumming 2009, Tsetsos, Gao, McClelland & Usher 2012, Wyart, de Gardelle, Scholl & Summerfield 2012, Wimmer et al. 2015, Raposo, Kaufman & Churchland 2014, Erlich, Brunton, Duan, Hanks, Brody & Carandini 2015)

1.4.2 Statistical models of neural activity

To study the representation of motion information in MT and LIP, I employed statistical models of single neuron and multi-neuron activity. The models used here follow the same principles as psychophysical reverse correlation. In this section I briefly review the generalized linear models (GLMs) that are employed in this thesis.

1.4.2.1 Single neuron models

Sensory neurons do not fire the same pattern of action potentials when repeatedly shown the same sensory stimulus (Tolhurst, Movshon & Dean 1983). This variability, or noise, is the primary motivation for treating neural responses probabilistically. The "neural coding problem", as it is often called ultimately requires a statistical approach to understand the transformations that generate neural responses to stimuli: Given a certain spatiotemporal stimulus, $s(t)$, at time t, what is the probability of a particular neural response $r(t)$. At first glance, it seems we could empirically build up $p(\vec{r}|\vec{s})$, however, s occupies a high-dimensional space and thus suffers from the so-called "curse of

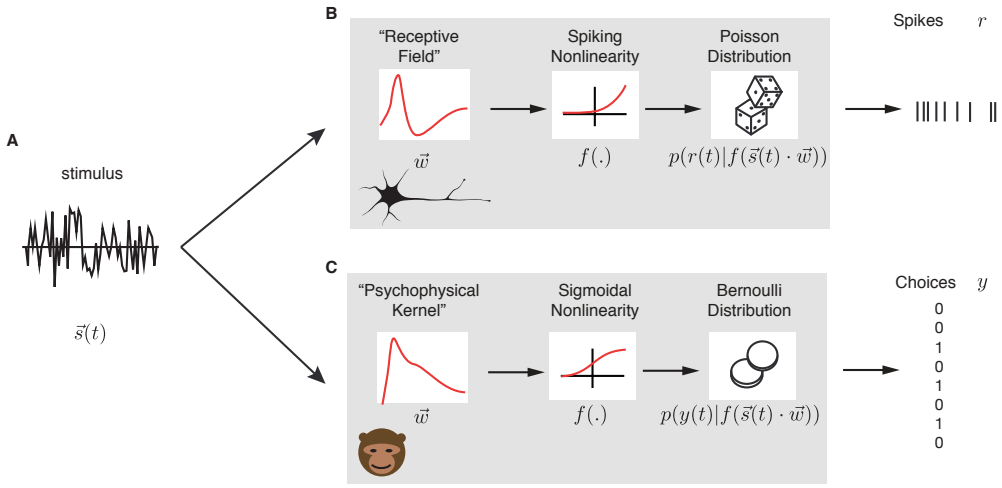

Figure 1.2: Systems Identification for neuron and behavior. **A** A noisy stimulus is shown to a monkey (C) in the receptive field of a neuron (B) and spikes are recorded while the monkey makes perceptual judgements about the stimulus. **B** Statistical model of neural activity: The receptive field takes a weighted sum of the stimulus over time. The output of the linear stage is passed through a point nonlinearity. This enforces that spike rates do not go negative. The probability of spiking is described by a Poisson distribution with rate that is the output of the nonlinear stage. Here t indexes into time bins. **C** Psychophysical observer model. The observer has a linear template that performs a weighted sum of the stimulus. This corresponds to the psychophysical kernel in the psychophysical reverse correlation literature. The output of the linear stage corresponds to the internal decision variable and is passed through a static, sigmoidal nonlinearity that maps the decision variable into a probability of a particular choice. The probability of a choice is given by the Binomial distribution, or since there are only two possible outcomes on each trial, the Bernoulli distribution. Here t corresponds to each trial.

dimensionality". As the dimensionality grows, samples in a high-dimensional space effectively become sparse. Take for example a stimulus that covers only a 10 x 10 grid of pixels of the computer monitor. It would take 2^{100} samples just to have 1 sample in each orthant of the stimulus space. It is immedi-

ately evident that this approach is intractable and instead statistical tools are required to reduce the dimensionality of the problem. There are additional reasons why the naiive approach to measuring $p(\vec{r}|\vec{s})$ is hindered.

Although it is theoretically possible to characterize complex nonlinear responses using a polynomial expansion to white noise input, the amount of data required scales with the stimulus size and the polynomial order to a dimensionality well beyond what we can typically collect in a physiology experiment and the higher order terms are difficult to interpret. The first-order (linear) kernel can be measured fairly straightforwardly. In fact, it is a similar procedure to the psychophysical reverse correlation described above. If the stimulus is white noise, the linear filter can be measured by simply averaging all stimuli that preceded a spike (Chichilnisky 2001). This measurement, known as the spike-triggered average (STA) has been widely used to estimate linear receptive fields in many early visual areas.

$$\hat{w} = \frac{1}{N}\sum_{t=1}^{N} r(t)s(t) \tag{1.2}$$

where N is the number of spikes. The STA is an unbiased estimate of the linear receptive field if the stimulus is white noise – that is, if the stimulus is zero mean and circularly symmetric. This assumption can be relaxed slightly by correcting for the stimulus covariance. This method is called whitened-STA and is the STA multiplied by the inverse of the stimulus covariance matrix. Thus the STA can be extended to more complicated stimuli than simple white noise.

However, neurons exhibit clear nonlinearities. The simplest observable nonlinearity is that neurons cannot emit negative spike rates, and as such have response that cannot be described with a single linear filter. It is possible to estimate the spiking nonlinearity sequentially by projecting the estimated linear weights on the stimulus vector $s(t) \cdot \hat{w}$ to produce an estimated rate and then quantitizing the spiking response as a function of that generator signal (Chichilnisky 2001). Of course, the assumption that the neuron depends only on the recent stimulus history is false, as can be immediately seen from the presence of refractory periods: Neurons cannot fire an action potential within a roughly 1ms window after their last action potential. This and other measurable dependencies led to extensions that fit the neural response within a probabilistic framework while simultaneously accounting for the multiple input dependencies and the spiking nonlinearity (Truccolo, Eden, Fellows, Donoghue & Brown 2005).

1.4.2.2 Generalized linear models

Generalized Linear Models (GLMs) have been a popular tool for understanding neural encoding because they are flexible, tractable, and interpretable (Stevenson & Kording 2011). The GLM can be flexibly extended to include parameters to capture stimulus dependencies, spike history effects, and coupling between neurons because it is log-concave and thus easy to fit to neural datasets (Paninski 2004). The parameters themselves often directly map to features neuroscientists are comfortable with, such as the "receptive field". In

its simplest form, the GLM is a linear nonlinear poisson (LNP) model with a set of linear weights to represent the "receptive field", and a nonlinearity to map to spike rate and a poisson process for generating spikes. In this model, the spike trains are produced as an inhomogeneous poisson process with rate

$$\lambda(t) = f(\vec{s}(t) \cdot \vec{w}) \tag{1.3}$$

The linear stage $\vec{s}(t) \cdot \vec{w}$ is the linear projection of the stimulus on the receptive field. When using white noise, the STA described above is an unbiased estimator of $\vec{w}$ (Paninski 2004). A substantial effort in systems neuroscience has been focused on estimating $\vec{w}$ for different levels of the visual system. The nonlinearity, $f(.)$, maps the linear stage into a spike rate, enforcing that $\lambda(t)$ does not go negative. If the spike generation process is poisson, then the likelihood is given by

$$p(\mathbf{r}|\mathbf{s}, \theta) = \prod_{t=1}^{T} p(r(t)|\lambda(t)) = \prod_{t=1}^{T} \frac{\lambda(t)^{r(t)}}{r(t)!} e^{-\lambda(t)} \tag{1.4}$$

where $\theta \in \{b, \vec{w}\}$ gives the baseline firing rate b and the receptive field $\vec{w}$, such that $\lambda(t) = f(\vec{s}(t) \cdot \vec{w})$. The goal here is to estimate θ. This is possible via maximum likelihood. The logarithm is a monotonic transform of $p(r|\lambda)$ so we can maximize the quantity:

$$\arg\max_{\theta} \log(p(\mathbf{r}|\lambda, \theta)) \propto \sum_{t=1}^{T} r(t) \log(\lambda(t)) + \sum_{t=1}^{T} \lambda(t) \tag{1.5}$$

This basic form makes up the MT and LIP model in chapter 3. The form holds, even for extensions of λ, which can include the neuron's own spike history as

input and can be extended to include spike trains from simultaneously recorded neurons. The inclusion of parameters for capturing neural interactions plays a significant role in relating MT and LIP in chapter 3 and will be explored in the following section.

1.4.3 Statistical methods for measuring functional connectivity

Since the invention of multi-electrode recordings, it has been clear that neuronal activity is correlated across neurons. Recording technology has progressively advanced over the decades (Stevenson & Kording 2011). In this dissertation I record from ensembles (up to 23) of neurons simultaneously using linear electrode arrays. These arrays have up to 24 electrode leads along a single shaft. These linear electrode arrays allowed me to record from MT and LIP, which are both buried deep within sulci (Lewis & Van Essen 2000) as had never been done before. The advancement in technology available for recording populations of neurons developed concurrently with methodology for analyzing simultaneous activity (Stevenson & Kording 2011).

The most straightforward classic analysis of connectivity is the cross-correlogram. This plots the excess spike rate of one neuron, conditioned on a spike from another neuron. It has been used primarily to infer connectivity (Alonso, Usrey, Reid & others 1996), but also to measure coding principles (Bair, Zohary & Newsome 2001). An extension of the cross-correlogram is the joint-peri-stimulus-time histogram which plots the joint activity of two neurons aligned to an experimenter controlled stimulus or task variable (Brody

1999). This extension can capture lags and dynamic correlations. Both of these methods are pairwise, are subject to misleading sources of variability, and require ad hoc shuffling methods to correct for slow-timescale fluctuations and assess statistical significance. They require fixed task-timing and stimulus to measure accurately (Stevenson, Rebesco, Miller & Kording 2008, Stevenson & Kording 2011).

It is also possible to extend the GLM framework to include multiple neurons within the same probabilistic framework. Here, the response of n simultaneously recorded neurons can be expressed

$$p(\mathbf{r}_1, \mathbf{r}_2, ..., \mathbf{r}_n | \vec{s}, \theta, ...) = \prod_{i=1}^{n} \prod_{t=1}^{T} p(r_i(t) | \lambda_i(t)) \tag{1.6}$$

Where the rate for the ith neuron λ_i is

$$\lambda_i(t) = f\Big(\vec{s}(t) \cdot \vec{w} + \sum_{i=1}^{n} \vec{k}_i \cdot r_i(t-1)\Big) \tag{1.7}$$

Importantly, the Poisson noise model is independent so equation 1.6 can be expressed as a product over neuron and time. However, the rate for each neuron is dependent on the spiking activity of other simultaneously recorded neurons (eq. 1.7). This formulation has been used to measure correlations in simultaneously recorded populations of retinal ganglion cells (Pillow, Shlens, Paninski, Sher, Litke, Chichilnisky & Simoncelli 2008), in human and monkey motor cortex (Truccolo, Hochberg & Donoghue 2010) and many sensory and motor areas (Stevenson, London, Oby, Sachs, Reimer, Englitz, David, Shamma, Blanche, Mizuseki, Zandvakili, Hatsopoulos, Miller & Kording 2012). Additionally, it has been shown to be a decent proxy for anatomical connectivity

in a system where all neurons are observable (Gerhard, Kispersky, Gutierrez, Marder, Kramer & Eden 2013) and can be used to test for directional dependencies (Kim, Putrino, Ghosh & Brown 2011, Stevenson & Kording 2010). This measure forms the basis of how I interrogate whether LIP spike trains depend on MT in chapter 3.

1.4.4 Decoding

There are two sides of the neural coding problem. So far I have discussed the *encoding* problem. That is, I have described statistical tools for describing the probability of a neural response given a stimulus. The other side is called *decoding* and describes the opposite relationship: the probability of a stimulus given a neural response. Decoding was discussed briefly above in the section on MT readout mechanisms.

In chapter 4, I use a simple, neurally plausible, decoder to read out of the direction of the motion stimulus from small populations of MT neurons. Population decoding methods have proven useful in understanding the information available in populations of neurons in motor cortex (Georgopoulos et al. 1986) and primary visual cortex of anesthetized (Graf et al. 2011) and alert fixating macaques (Berens, Ecker, Cotton, Ma, Bethge & Tolias 2012), and behaving macaques (Chen, Geisler & Seidemann 2006), as well as the dynamics of decision-making in frontal cortex (Kiani, Cueva, Reppas & Newsome 2014) and oculomotor planning in LIP (Graf & Andersen 2015). Decoding approaches offer perspective on how the brain might accomplish the task at hand

given only the neural signals.

1.5 Summary

This thesis approaches the problem of perceptual decision-making by integrating the advances in psychophysical reverse correlation, statistical models for neural data, and large-scale recording techniques. The analysis relies heavily on the use of generalized linear models (GLMs) which are a class of statistical models that can be easily fit to many types of data. The following chapters describe a unique application of these techniques at the intersection between sensation and cognition.

Chapter 2

Psychophysical reverse correlation motion-discrimination task

Our goal was to develop a motion-discrimination task that was amenable to reverse-correlation analysis to probe the subject's psychophysical strategy as well as the responses of neurons in MT and LIP. We had four specific requirements for the stimulus: First, the motion evidence should be controlled in a temporally precise manner. Second, the "noise" should be explicitly known by the experimenter. Third, it should produce a percept of motion that is supported by a conventional sigmoidal psychometric function. Fourth, it should target known selectivities of MT neurons. In this chapter, I introduce the Gabor-pulse stimulus and compare its spatiotemporal properties to the spatiotemporal properties of the classic random dot motion stimulus (referred to as either RDM or "the dots" from here on). I show that the Gabor-pulse stimulus has distinct advantages over classic dot stimuli for reverse correlation and that it supports conventional psychophysical behavior and drives area MT lawfully.

This work has been presented in part at the Workshop on Natural Environments Tasks and Intelligence (NETI) 2014 meeting, but can be treated

primarily as the extended general methods for the experiments described in this dissertation.

2.1 Introduction

The dots have been used extensively to probe properties of motion perception (Morgan & Ward 1980, Newsome & Pare 1988) and the responses of motion sensitive neurons in MT (Britten et al. 1993, Britten et al. 1992, Osborne et al. 2004, Bosking & Maunsell 2011, Price & Prescott 2012). However, we chose not to use the random dots in this study because the mapping between experimenter controlled motion strength and the stimulus shown is stochastic and the explicit noise is difficult to estimate without pre-filtering with an MT-like mechanism.

2.1.1 Motion-discrimination tasks

Discrimination tasks are a central component of the study of decision-making and evidence accumulation (Gold & Shadlen 2007). Motion discrimination in particular has played a major role in studies of MT and LIP during decision-making, even when investigating cognitive mechanisms such as reward expectation, confidence or prior expectation (Kiani & Shadlen 2009, Rao et al. 2012). This is largely because a large body of research has established area MT's causal role in representing the sensory evidence for decisions about motion (Newsome & Pare 1988, Salzman et al. 1990, Nichols & Newsome 2002, Ditterich, Mazurek & Shadlen 2003). Many iterations of

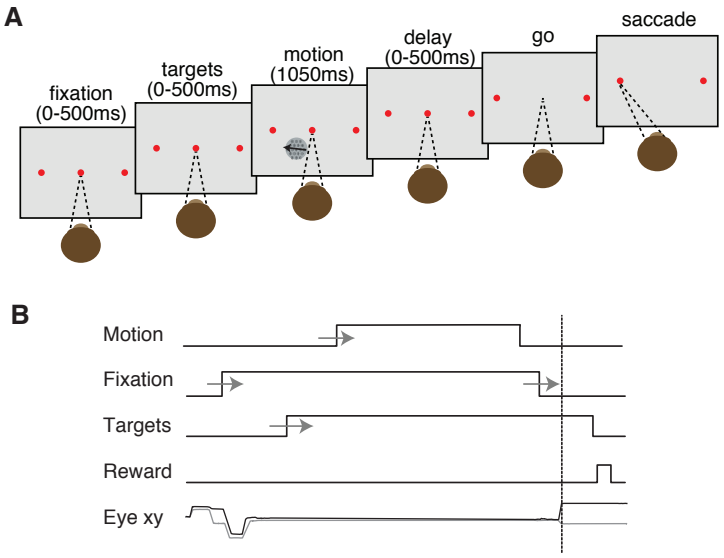

Figure 2.1: Motion discrimination task (**A**) Monkeys maintain fixation through a 1050ms stimulus and then wait for the fixation point to dim before indicating their choice about motion with an eye-movement to one of two targets. (**B**) Timing of task components. Gray arrows indicate that the onset of each of the experimenter controlled task components are jittered by a 500ms uniform distribution.

motion-discrimination tasks have a standard generic form with subtle manipulations to probe different aspects of the decision process. We kept to the basic discrimination paradigm, by implementing a task where monkeys integrate the direction of motion in a perifoveal motion stimulus and indicate their choices with an eye-movement to one of two peripheral targets (Figure 2.1).

We used a fixed-duration (FD) paradigm, where the experimenter controls the duration of the motion stimulus and it is the same duration on every trial. We chose a FD paradigm because it gives us the same number of samples

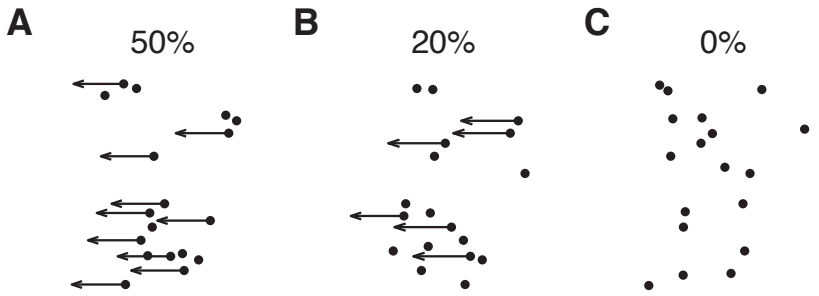

Figure 2.2: Experimenter control of motion strength using dot stimuli (**A**) A sample frame of dots at 50% coherence. 50% of the dots are selected at random to be signal dots. On this frame, 10 of 18 dots were randomly selected to translate to the left (indicated with arrow vectors). The remaining dots are replotted at random within the stimulus aperture. (**B,C**) Same as in A, but for 20% and 0% coherence, respectively. The 0% coherence level means no dots are coherently replotted.

of the stimulus on each trial to use in the reverse correlation analysis. Alternatives to FD are to vary the duration from trial to trial in what is known as a variable duration (VD) paradigm or to let the animal dictate the duration of the stimulus by training them to make an eye-movement whenever they are ready, which is known as a response time (RT) task. The disadvantages to VD or RT paradigms for reverse correlation are that many of the trials cannot be used to estimate the temporal strategy because their duration is too short, and that they essentially enforce an optimal strategy of early weighting because the animal either ends the stimulus when it has seen enough (RT) or knows the stimulus might end early (VD). The optimal strategy in a fixed duration task is to integrate the entire stimulus – assuming a perfect representation of the stimulus in sensory areas and no cost for fixation. In general, FD stimuli are widely used in reverse correlation paradigms as they let the subject use

what information is most useful to it, and let the experimenter measure that relationship with psychophysical reverse correlation (Murray 2011).

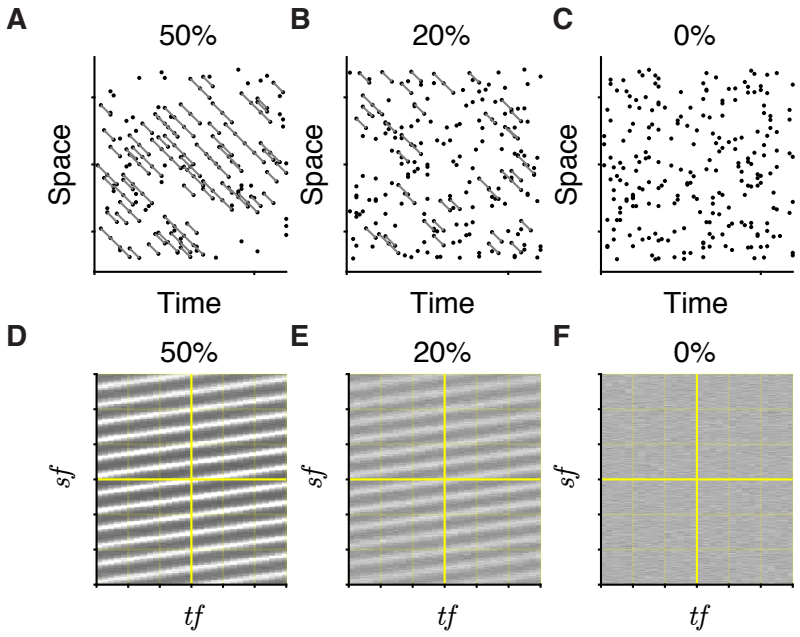

Figure 2.3: A look at dot motion in space-time and the spatiotemporal frequency domain **A** Space-time slice of a single trial of 50% coherent dots presented with a 60Hz refresh rate. Gray lines connect signal dots across frames. Notice that motion appears as orientation in the space-time domain. Using the classic algorithm, dots are replotted every three frames. This demonstrates that the dots are stroboscopic or apparent motion which enforces a minimum temporal integration of 3 x frame rate or 50ms in this case. **B,C** Same as in a, but for 20% and 0% coherence, respectively. **D** Single-trial of dot motion as energy in the frequency domain. The oriented line through the origin represents the velocity of the signal dots. The parallel lines are due to the stroboscopic presentation. **E,F** Same as in a, except for 20% and 0% coherent dots. The color scale is fixed across all three subplots. 20% coherent dots have the same oriented structure, but a lower power.

2.1.2 Motion in random dot stimuli

The focus on random dot stimuli in the decision-making literature is is in part historical (Born & Bradley 2005), but there are several nice features of RDM stimuli that allow for a close examination of signal and noise in the perception of motion. Unlike low contrast stimuli, RDM stimuli have external noise and the SNR in the stimulus can be manipulated by the experimenter. The dots themselves can be "signal" dots or "noise" dots, and the experimenter controls the strength of the stimulus by changing this proportion. The signal dots represent a coherent translational motion and are replotted in one of two possible directions over frames. The noise dots are replotted at random on each frame Figure 2.2. This ratio, termed "coherence", ranges from 100% (all dots are replotted in the direction of first target) through 0% coherence (all dots are randomly replotted) to -100% (where all dots are replotted in the direction of the second target). In the standard dot algorithm, the signal dots are replotted every 40ms such that the motion signal is *apparent* motion (Newsome & Pare 1988, Britten et al. 1992, Roitman & Shadlen 2002).

As with any sequence of images that generates visual motion, the motion of RDM stimuli can be visualized either in space-time or in the Fourier domain (Watson & Ahumada 1983). In space-time, the signal dots are replotted at fixed spatial and temporal intervals consistent with a fixed velocity. This appears as oriented structure in the xt plane. Figure 2.3a shows an example of this, with 50% coherent dots plotted in the xt plane. The signal dots are connected across frames with gray lines, which were added to illustrate

the velocity signal but are not there in the stimulus. This orientation in xt is consistent with the speed of the motion ($x = vt$ where v is the velocity). Because the signal dots are replotted stroboscopically, each signal dot is offset by $\Delta x = v\Delta t$. As the coherence is reduced, the oriented structure in space time is diminished (Figure 2.3b,c).

Motion also appears as orientation in the frequency domain (Watson & Ahumada 1983). To visualize the stimulus in the frequency domain, $f(\omega x, \omega t)$, we take the 3D Fourier transform:

$$f(\omega x, \omega t) = \iiint_{-\infty}^{\infty} c(x, y, t) \exp(-2\pi i(\omega x + \omega y + \omega t))\partial x \partial y \partial t \qquad (2.1)$$

Where $c(x, y, t)$ is the luminance of the stimulus on our monitor at each pixel, on each frame, ωx and ωt are spatial and temporal frequency at each point in the frequency plot. The full 3-dimensional space is difficult to visualize so we consider a stimulus in which coherent motion is along only the x dimension and then marginalize across the y dimension.

Figure 2.3d shows the same dots from panel a now plotted in the Fourier domain. The oriented structure is apparent immediately. The oriented line passing through the origin is the stimulus velocity. This reflects the orientation that was present in space-time, except now the slope is $-\frac{1}{v}$. The many parallel lines result from aliasing due to the stroboscopic presentation of the signal dots. As the coherence is reduced, the Fourier amplitude along the oriented lines is reduced until all that is left is broadband noise (Figure 2.3e,f). This reveals two nice properties of RDM. The first is that there is power along all

combinations of spatial and temporal frequencies that are consistent with the signal velocity (The signal dots are broadband). The second feature is that the noise is also broadband and has power at all directions and speeds. In the 0% coherence stimulus, only white noise is left, spanning all frequencies equally.

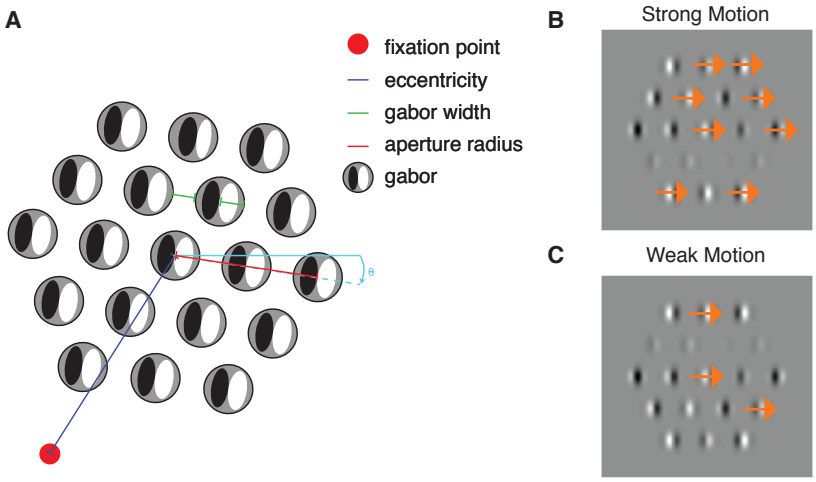

Figure 2.4: Parameters of the Gabor-pulse based motion stimulus (**A**) The stimulus consists of a hexagonal grid of Gabor patches. Each Gabor was scaled to have a half-width equal to .1 x eccentricity so as to be roughly the size of V1 neuron receptive fields. The Gabors were also spaced by this value. The entire grid spanned 1 x eccentricity to roughly equal the size of the average MT neuron receptive field. The entire grid and each Gabor within it was oriented by θ such that all motion energy was along the direction of discrimination. (**B,C**) Motion strength is controlled by changing the fraction of elements that drift in a fixed direction.

2.1.3 Precise control of direction information

In the previous sections, I highlighted appealing spatiotemporal and spectral properties of RDMs. However, there are several limitations to dot

motion. The main limitations that caused us to search for an alternative is that the specific spatiotemporal motion energy is hard to control and harder to measure. The dots are not continuous moving objects in the world. They are plotted with a refresh rate on a computer monitor. As such, on any two frames, each dot on the current frame can in theory be any of the dots on the subsequent frame (Watamaniuk, Grzywacz & Yuille 1993). Thus, the dots suffer from a "correspondence problem" and the experimenter has little control over how this noise plays out (Barlow & Tripathy 1997).

One option for measuring the motion that is present in RDM stimuli is to calculate the n^2 possible motion vectors for each frame transition, where n is the number of dots. This type of analysis has been used to estimate the ideal observer for dot stimuli and to estimate MT receptive fields (Watamaniuk et al. 1993, Cook 2004). However, it would fail to measure any motion at the signal velocity in the classic RDM we have discussed so far. The dots from (Britten et al. 1992) are replotted with a spatial and temporal offset that spans several frames. This highlights a larger problem with this analysis, which is that the number of motion vectors for each frame transition scales with the number of frames lags as the experimenter considers motions that could span multiple frames. A second approach to measure motion in the stimulus is to use a filtering mechanism that mimics early motion detectors in the visual system (Adelson & Bergen 1985). This approach introduces substantial temporal integration that can contaminate any estimates of neural or behavioral integration times and is inappropriate for MT characterization,

because it is a model of visual processes. Given these limitations, we developed a stimulus based on Gabor patches, where we could precisely control the local motion energy.

2.2 Methods

2.2.1 Stimulus Apparatus

All stimuli were presented using the Pychophysics Toolbox with Matlab (The Mathworks) using a Datapixx I/O box (Vpixx) for precise temporal registration (Eastman & Huk 2012). Monkeys sat in a primate chair (Crist Instruments) and faced a 55 inch LCD (LG) display (resolution = 1920 x 1080p, refresh rate = 60Hz, background luminance = 26.49 cd/m2) that was corrected to have a linear gamma function. Monkeys viewed the stimulus from a distance of 118cm such that the screen subtended 100 degrees of visual angle. Eye position was tracked using an Eyelink eye tracker (SR Research), sampled at 1kHz. Reward was delivered through a computer controlled solenoid.

2.2.2 Subjects

Data were recorded from two adult rhesus macaque monkeys (one male and one female, referred to as P and N hereafter), aged 14 and 10, weighing 10 and 7.7kg, respectively. All procedures were performed in accordance with US National Institutes of Health guidelines and Institutional Animal Care and Use Committee at the University of Texas at Austin.

2.2.3 Gabor stimulus

The Gabor-pulse stimulus consisted of a hexagonal grid (5-7 degrees across, scaled by eccentricity) of 19 Gabor patches (.9 cyc/deg, σ = .1 x eccentricity). Figure 2.4a shows a schematic of the stimulus arrangement and parameters that govern its appearence. The spatial frequency (.9 cyc/deg) was selected to roughly match the peak selectivity of MT neurons (Bair & Movshon 2004). The inter-element spacing and spatial standard deviation of each Gabor element were scaled by 10% of the eccentricity of the center of the aperture to match the average RF size of a V1 neuron at that eccentricity (Van Essen, Newsome & Maunsell 1984). This ensured that all of the Gabors were non-overlapping. All motion was presented by varying the phase of the sinewave carrier of each Gabor and all positions and Gaussian-envelopes were fixed across trials in each experiment. The temporal frequency of the Gabors was 7Hz (Monkey P) or 5Hz (Monkey N), yielding velocities of 7.78 and 5.55 degrees/second respectively. Subjects were trained to report the net direction of motion in a field of drifting and flickering Gabor elements with an eye movement to one of two saccade targets.

Motion strength was manipulated by changing the proportion of "signal" vs. "noise" elements (Figure 2.4b). To precisely control this, all elements in the grid were implemented as the sum of two overlapping Gabor functions with identical orientation and spatial frequency. This can be rewritten (and appears) as a single Gabor with a contrast modulation, but it allowed us to precisely control the state of each Gabor as either pulsing (signal) or flickering

(noise). Mathematically, the entire stimulus can be written

$$S = \sum_{i=1}^{n} G_i \tag{2.2}$$

where each G_i is the sum of two Gabor filters that only differ in phase (ϕ, ω)

$$G_i = g(x_i, y_i, \sigma, \theta, f, \phi_i) + g(x_i, y_i, \sigma, \theta, f, \omega_i) \tag{2.3}$$

$$g(x, y, \sigma, \theta, f, \phi, t) = \exp\left(-\frac{x'^2 + y'^2}{2\sigma^2}\right) \cos\left(2\pi f x' + \phi(t)\right) \tag{2.4}$$

where

$$x' = x\cos\theta + y\sin\theta$$

and

$$y' = -x\sin\theta + y\cos\theta$$

This is equivalent to the superposition of two cosine waves windowed by an unnormalized gaussian, $\mathcal{N}$, which can be rearranged to show each G_i is a single gabor with an amplitude that is modulated sinusoidally

$$\begin{aligned} G_i(x, y, t) &= \mathcal{N}(\mu, \sigma^2)\left(\cos(2\pi f x + \phi(t)) + \cos(2\pi x + \omega(t))\right) \\ &= \underbrace{\mathcal{N}(\mu_i, \sigma_i^2)\cos(2\pi f x + \frac{\phi(t) + \omega(t)}{2})}_{\text{gabor}} \underbrace{2\cos(\frac{\phi(t) - \omega(t)}{2})}_{\text{amplitude}} \end{aligned}$$

The Gabors can be in one of two states: *flicker*(noise) or *pulse*(signal) In flicker mode, the carrier phase does not change over frames, but the amplitude changes sinusoidally (Figure 2.5a). In pulse mode, the carrier phase drifts and the amplitude changes sinusoidally (Figure 2.5b).

Each trial consisted of seven consecutive motion pulses, each lasting 9 or 10 video frames (150 or 166ms). The strength of each pulse, X_i, was drawn from a Gaussian and rounded to the nearest integer value: $X_i \sim \mathcal{N}(\mu, \nu)$, where μ and ν enforce the expected motion strength and were fixed on each trial (Figure 2.9a). On a subset of sessions, X_i was drawn from a uniform distribution over fixed pulse strengths (Figure 2.9d). On pulse i, $|X_i|$ Gabors are randomly assigned to pulse and all change their phase in the same direction ($\text{sign}(X_i)$) at the specified temporal frequency. The remaining Gabors undergo a counter-phase flicker at the specified temporal frequency. The initial phase of each Gabor was assigned randomly to minimize grouping of flicker. The difficulty on each trial was modulated by manipulating both μ, and σ, which effectively biases the probability of a rightward pulse at each time.

The monkey was rewarded based on the net motion that was actually shown on each trial, not based on the stimulus distribution that a pulse sequence was drawn from. That is, for motion discriminated on a horizontal axis, the monkey was rewarded for making a choice to the target on the right if the sum of the seven pulses shown was greater than zero, and for making a saccade to the target on the left if the sum was less than zero. On trials that summed to zero, the monkey was rewarded at random with 50% probability.

2.2.4 Measuring Motion with Motion-Energy Filters

To compute the instantaneous motion energy on each trial, we use two pairs of spatiotemporal filters (Adelson & Bergen 1985, Kiani et al. 2008).

Each pair was either selective for the the coherent direction of motion or the opposite. Motion energy filters are formed as the sum of two space-time separable filters and are described in detail in Adelson & Bergen (1985). To match to previous literature on RDM, we used identical filters to Kiani et al. (2008). The spatial filters we used were even and odd symmetric fourth-order Cauchy functions:

$$s_1(x,y) = \cos^4(\alpha)\cos(4\alpha)\exp\left(-\frac{\gamma^2}{2\sigma_s^2}\right) \tag{2.5}$$

$$s_2(x,y) = \cos^4(\alpha)\sin(4\alpha)\exp\left(-\frac{\gamma^2}{2\sigma_s^2}\right) \tag{2.6}$$

where $\alpha = \tan^- 1(x/\sigma_c)$. In the y dimension, we windowed the filters with a gaussian envelope with standard deviation σ_s. For the temporal filters, we used

$$t_1(t) = (60t)^3\exp(-60t)\left[\frac{1}{3!} - \frac{(60t)^2}{(3+2)!}\right] \tag{2.7}$$

$$t_2(t) = (60t)^5\exp(-60t)\left[\frac{1}{5!} - \frac{(60t)^2}{(5+2)!}\right] \tag{2.8}$$

Again, for any direct comparisons to previous literature using RDM, we matched the filters to those described in Kiani et al. (2008). For comparisons of measured motion energy to the average change of phase in the stimulus, we tried to avoid having filters that integrate over 150ms as the ones described above do. Therefore, in all direct comparisons of the change in phase of the Gabors over time to motion energy estimates from filtering the stimulus image sequence, we

used oriented Gabors in quadrature that were matched to the spatiotemporal frequency of the stimulus. This was not meant to be a model of MT responses (or V1), but instead a relatively direct comparison of the experimenter controlled stimulus parameters (phase) and the measurable local velocity using filters tailored for the signal.

Psychophysical Kernel

To measure the contribution of each pulse to the monkey's choice on each trial, we used logistic regression, where the probability of the monkey's choices across the dataset is given by:

$$p(\mathbf{Y}|\mathbf{X}, \mathrm{w}) = \frac{\exp(Y^T \mathbf{X}\mathrm{w})}{1 + \exp(\mathbf{X}\mathrm{w})} \tag{2.9}$$

Where $\mathbf{Y} \in \{0, 1\}$ is a vector of the choice on each trial, $\mathbf{X}$ is a matrix of the seven pulses on each trial, augmented by a column of ones to capture the bias, and w is the seven pulse weights plus a bias term. This model was fit using maximum likelihood (Knoblauch & Maloney 2008).

$$\arg\max_{\mathrm{w}} Y^T \mathbf{X}\mathrm{w} - \log(1 + \exp(\mathbf{X}\mathrm{w})) \tag{2.10}$$

Error bars were derived from the matrix of partial second derivatives.

2.3 Results

Here I examine the properties of the Gabor-pulse stimulus in relation to the four criterion for a reverse-correlation motion-discrimination task laid out

in the introduction. I use the dots as a reference point for each. Gabors are gaussian-windowed sinusoids and have a property of being local in space-time and local in the Fourier domain. This is an important contrast to the dots in that the Gabor has a precise mapping from space-time to a representation in the frequency domain. Sinewaves in space time are points in the Fourier domain and Gaussians have the special property of being Gaussians in both space-time and the frequency domain. Figure 2.6 depicts the components of the Gabor stimulus in the Fourier domain. A purely drifting Gabor shows up as two gaussian blobs in the frequency domain. Again, the orientation represents a velocity, except now the stimulus is narrowband and only a one spatial and temporal frequency are combined. Figure 2.7 shows a space-time slice of of the Gabor-pulse stimulus at multiple stimulus strengths and the corresponding view in the Fourier domain. The oriented structure trades off as a function of stimulus strength. The advantages to the Gabor pulse stimulus are clear when trying to control or measure motion energy, which are the first two requirements of our reverse correlation stimulus.

2.3.1 Precise experimenter control of motion strength

We directly compared the time-varying motion energy in the Gabor stimulus and RDM using motion energy filters that have been previously used to measure motion in the dots (Kiani et al. 2008). The output of these filters for different motion strengths (Figure 2.4b,c) shows that the Gabor-pulse stimulus has substantially less variance in motion energy as a function of the

experimenter controlled motion strength. We quantified this as the ratio of mean to standard deviation (or SNR) and found that the experimenter has five times more SNR in controlling the motion energy than would be possible with the dots. Thus, we establish that the Gabor-pulse stimulus meets the requirements for criterion two: the motion energy can be delivered with precise experimenter control over the strength.

2.3.2 Temporal precision of motion evidence

We addressed the second criterion, i.e.. that the "noise" is known explicitly, by comparing the change in phase averaged across Gabors to the motion energy measured with filters. In principle, Gabors have a parametric correspondence between their representation in space-time and in the Fourier domain. We should be able to know the motion energy by simply tracking the change in phase of each Gabor over frames. Here we compared this theoretical value of motion energy to what could be measured from the sequence of images on the monitor. Figure 2.4 e and f shows the spatially averaged change in phase and the spatially averaged motion energy for three randomly sampled trials. There is a close correspondence between the phase of the Gabors and the measured motion energy. Of course, motion energy filters assume a bandwidth and add some temporal integration which are free parameters to be set by the experimenter. The phase is a parameter of the stimulus that is known by the experimenter for each Gabor. This close correspondence between the average change in phase and the output of the motion energy filters shows that

the motion energy noise is known from its generating signal (proportionally) without having to measure it with filters. Thus, the Gabor-pulse stimulus overcomes the two main shortcomings of the dots. First, the experimenter can precisely control the motion strength and second, the experimenter knows the change in phase of each Gabor which is proportional to the motion energy.

2.3.3 Psychophysical performance during motion discrimination

The third requirement of a motion-discrimination reverse correlation task is that the subject's percept of motion depends systematically on the signal strength. Here I briefly analyze psychophysical performance and show that the Gabor-pulse stimulus supports standard sigmoidal psychometric function of the net motion strength. There are two ways to calculate psychophysical performance in this task. The first is in line with classic signal detection theory, in which the signal strength is based on the experimenter manipulated expectation of net signal. This is how psychophysical performance is measured in the dots. The subject is rewarded for selecting a target consistent with the generating distribution. For example, say the trial was 3% coherent motion to the right. It is possible with such a low signal strength that a random draw from the distribution will result in leftward motion by chance (due to the noise dots). We can either reward for correctly inferring that the generating distribution was biased to the right, or we can reward based on the motion sequence that was actually shown.

We attempted to keep the animals vigilant across the reverse-correlation

trials that had zero expected motion (equivalent to zero coherence trials) by rewarding based on the motion that was empirically realized (shown) on each trial. Both types of reward support learning the same criterion and both types of reward support conventional psychometric functions (Figure 2.9).

2.3.4 Reverse correlation reveals the subject's strategy

The main goal of the stimulus is to measure the subject's temporal strategy during motion discrimination. We sought to do this with a low-dimensional parameterization of the stimulus. In many psychophysical reverse correlation studies, the number of parameters estimated is linked to either the number of pixels or number of frames in the stimulus. Here, by parameterizing the motion across seven distinct pulses, we were able to use the number of drifting Gabors during each pulse as a proxy for the motion energy in that epoch and reverse correlate temporal weights across seven pulses. This allows us to reduce the number of parameters that govern our estimate of the subjects strategy to the number of pulses (seven), which results in a huge computational advantage over the dots. We estimated the monkey's temporal weights with maximum likelihood of a logistic model and found that both monkeys preferentially weighed the early pulse more than the later ones on average. Figure 2.10 shows the psychophysical kernels for the two monkeys estimated using all trials and zero-coherence trials only. We consistently found that the monkeys tended towards early weighting strategies.

Of course, it is possible that the monkeys are only using one pulse to

inform their choice, and simply switch which pulse they use on each trial. This likely not the case and there is evidence, based on the monkeys' accuracy that they are using more than one pulse. Across all stimulus strengths, the average expected performance if the monkey was using only one pulse is 75% (±2%) correct. Monkeys typically exceeded that, averaging 80% (±1.2%) correct. The average % correct on the zero-expected motion trials if the monkey was using only one pulse was 51% (±2.2%) correct . Monkeys averaged 64% (±2.4%) correct on these trials. This suggests that the monkeys are integrating across more than one pulse to inform their choices.

2.3.5 The Gabor Pulse stimulus drives area MT

Chapters 3 and 4 focus on the response of MT neurons to this stimulus in detail. Here I briefly focus on the selected parameters of the stimulus and their justification with regard to previous studies of MT. I then highlight the responses of an example MT neuron to reverse-correlation trials only.

The lack of broadband motion energy is a disadvantage of the Gabors for driving MT neurons when compared to the dots. However, area MT has also been studied extensively with sinewave gratings and many MT neurons are selective for a range of spatial frequencies with a peak sensitivity near .9 cycles/degree (Bair & Movshon 2004). The Gabors all have a spatial frequency of .9 cycles/degree, selected for this very reason. Figure 2.11 shows the average spike rate of an MT neuron sorted by pulse strength for each of the seven pulses. This neuron was recorded while the animal viewed the reverse

correlation condition, where each pulse was drawn independently on each trial. It is clear from the PSTHs that the pulse has an effect on spike rate that is independent in time and dependent on the number and direction of pulsing Gabors. We also established that area MT is required for performance on this task using reversible inactivations (Appendix A).

2.4 Discussion

This chapter described the properties of the reverse correlation motion-discrimination paradigm that is used throughout this thesis. I detailed four requirements of a reverse correlation motion discrimination stimulus and then showed how the Gabor pulse stimulus meets those requirements. The first two refer to the experimenter control of signal and noise and the measurement of motion energy. Using motion energy filters to estimate the instantaneous motion energy, I showed that the experimenter has substantially more control of motion energy using Gabor-based stimuli than with dots, and that the parameters of the stimulus itself (namely, the change in phase of each Gabor) are roughly proportional to the motion energy.

I then showed that the stimulus supports standard psychophysics and that it can be used to measure a subject's temporal strategy. Our monkeys weighed the early pulses more than late ones. Finally, I showed that area MT responds to the direction and strength of the motion pulses.

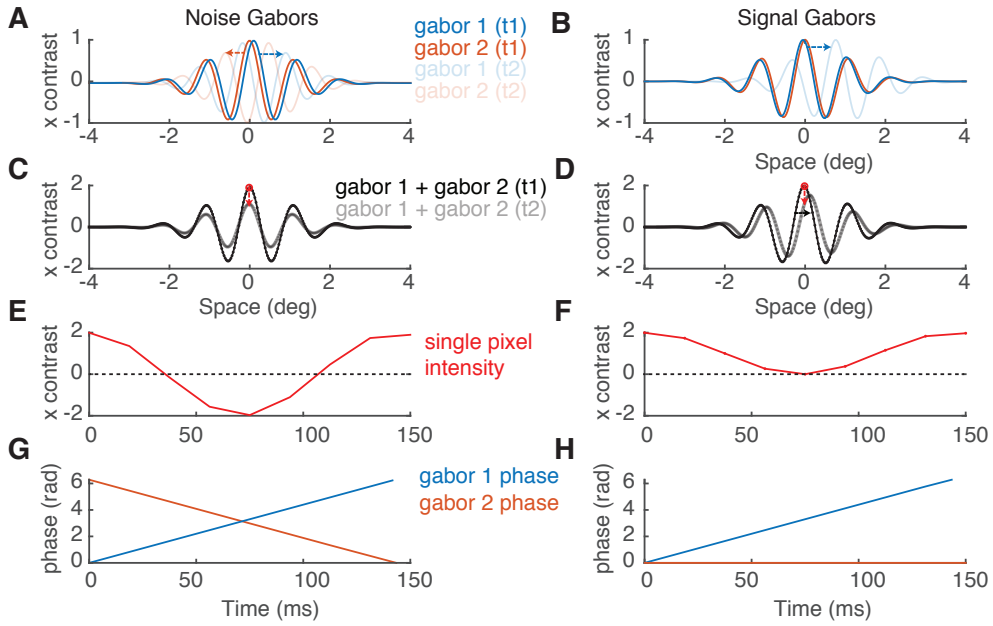

Figure 2.5: Implementation of signal and noise in the Gabor stimulus (**A**) To implement the signal and noise in a manner that supported a coherent percept of motion, we implemented each Gabor in the grid as the sum of two superimposed Gabors with equal spatial frequency and orientation. At any time, the fraction of Gabors that are selected to be "noise" undergo counterphase flicker. This is implemented by having each of the two Gabors drift in opposite directions at equal Temporal frequencies. (**B**) The "signal" Gabors undergo drift plus flicker. This is implemented by freezing one of the two component Gabors and letting the other drift. (**C**) Spatial slice of the pixel intensity of the stimulus at one Gabor location. For the noise Gabors undergoing counterphase flicker, the phase does not change and the amplitude merely changes from frame 1 (black) to frame 2 (gray). The red dot represents a single pixel intensity, which is examined in more detail in E. (**D**) Same as D except for the signal Gabors. Both the amplitude and the phase change over frames. (**E**) The magnitude of the red pixel in C plotted over time. The pixel reverses polarity at the temporal frequency of the flicker. (**F**) Same as E, but for signal Gabors. The pulsing Gabors flicker at 1/2 the temporal frequency of E such that motion information is available only when the Gabor element has positive contrast. (**G,H**) Phase of each component Gabor for the noise and signal Gabors respectively.

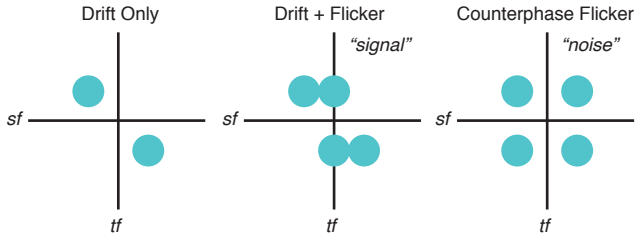

Figure 2.6: Schematic of Fourier components of the Gabor stimulus. (left) Leftward drifting Gabor depicted in the Fourier domain. (middle) Depiction of the signal Gabors for left motion in the Fourier domain. (right) The noise Gabors undergo counterphase flicker which has equal and opposite left and right motion energy.

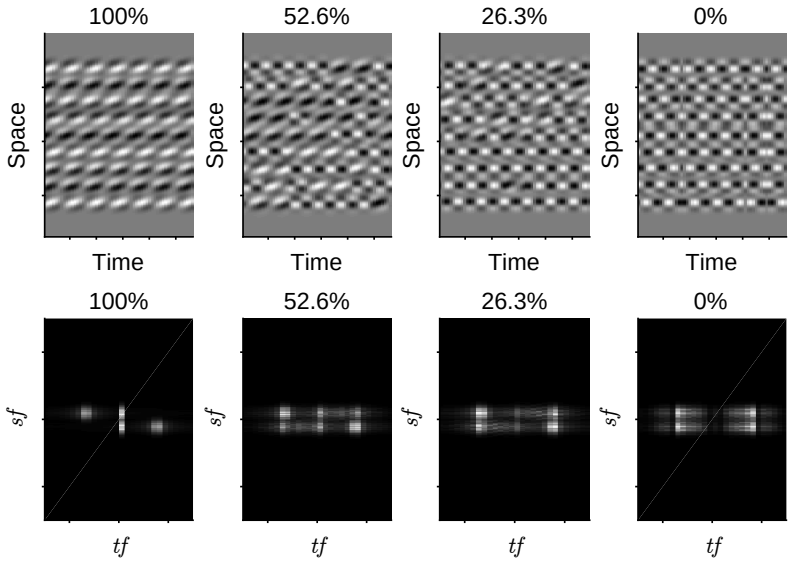

Figure 2.7: Gabor pulse stimulus in the Fourier Domain. (Top row) Space time slice of the Gabor-pulse stimulus at different motion strengths with signal Gabors drifting to the left. Stimulus strength decreases from from left to right. The pulsatile delivery of oriented structure is clearly visible in the 100% signal strength case. (Bottom row) Gabor motion from the corresponding space-time plots viewed in the Fourier domain. The oriented structure becomes more symmetric as the motion strength is decreased (from left to right)

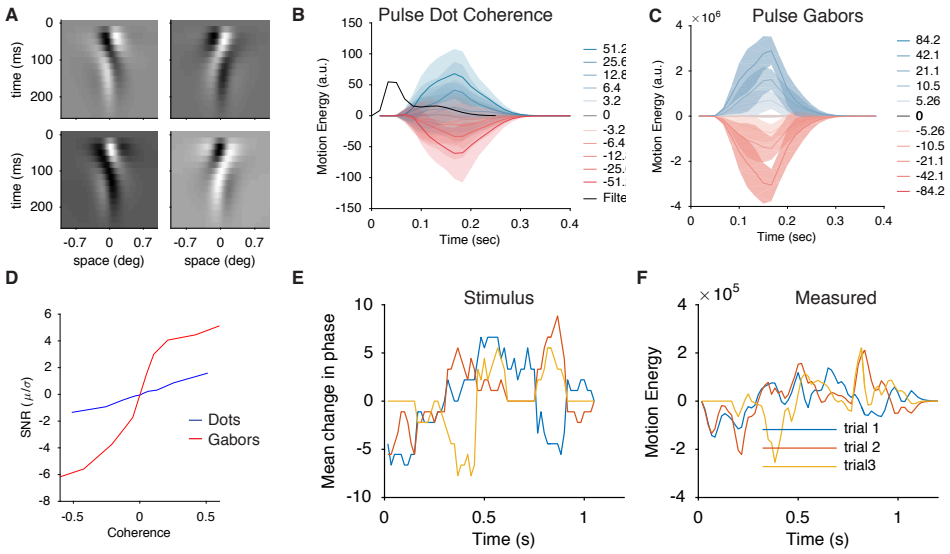

Figure 2.8: (**A**) Example space-time oriented filters that make up the motion energy computation. These filters are identical to the ones from (Kiani et al. 2008). (**B**) Motion Energy of the of the random dot stimulus used by (Britten et al. 1992). The trial-by-trial variability in motion energy is large given a particular motion strength (indicated by the separate colors). Error fill area is standard deviation of motion energy. The black trace is the impulse response of the motion energy filters from A. (**C**) Output of motion energy filters for the Gabor stimulus as a function of fraction of drifting elements. This is the same plot as B, but for the Gabors. (**D**) Ratio of the mean output of motion energy filters to the standard deviation across trials for a given stimulus strength. "Coherence" refers to the fraction of drifting elements in both cases. The experimenter has substantially more control over the motion energy manipulating the fraction of drifting Gabors over the fraction of drifting dots. (**E**) Mean change in Gabor phase for three trials averaged across space. (**F**) Measured motion energy averaged across space for the same three trials in E.

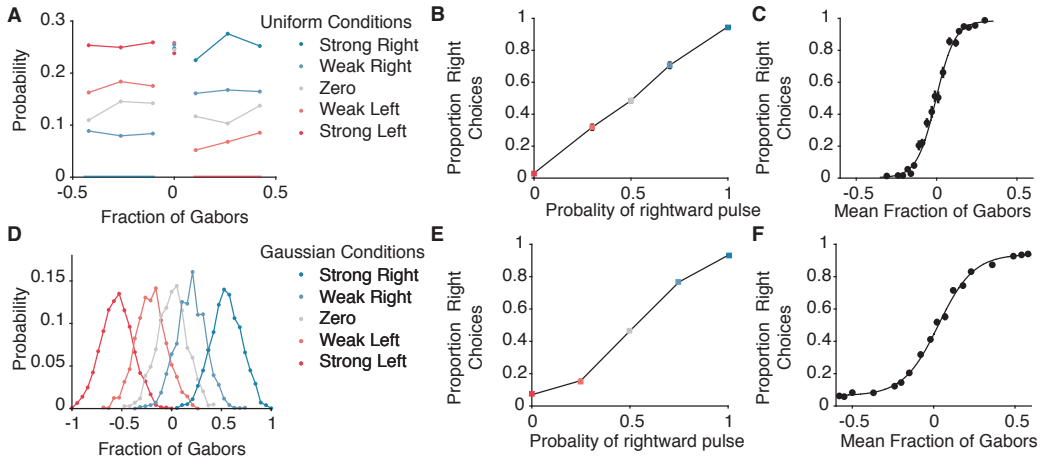

Figure 2.9: (**A**) Motion strength was manipulated by changing the probability of a rightward pulse. The different colors represent the different conditions with dark blue resulting in a rightward pulse with probability=1, although the strength of those pulses was uniformly distributed across several levels. The gray distribution represents the reverse correlation trials where all directions and strengths are equally likely. (**B**) Psychometric function for stimulus conditions shown in A. The probability the monkey chooses right as a function of the probability that an individual pulse was to the right (pulse strength ignored). (**C**) Psychometric function showing the probability of choosing right as a function of the net motion that was shown (by averaging the signed pulse strengths). (**D**) Alternate implementation of stimulus strength. Pulse strengths were drawn from Gaussian distributions with different means. This biased pulses towards rightward or leftward motion. (**E**) Monkey's choices as a function of stimulus conditions shown in D. (**F**) Proportion right choices as a function of the net motion strength that was shown for the stimulus conditions shown in D.

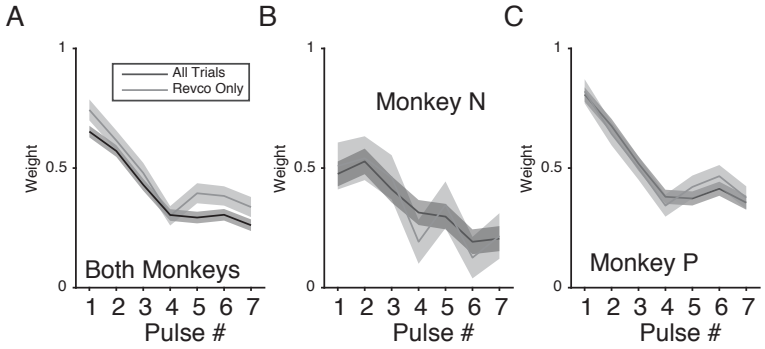

Figure 2.10: (**A**) Psychophysical Kernels for measured using logistic regression for both monkeys averaged together calculated using all trials or zero-expected motion trials only. (**B,C**) Psychophysical kernel for monkey N and P plotted separately. Both monkeys showed a general tendency to weigh early pulses more than later ones.

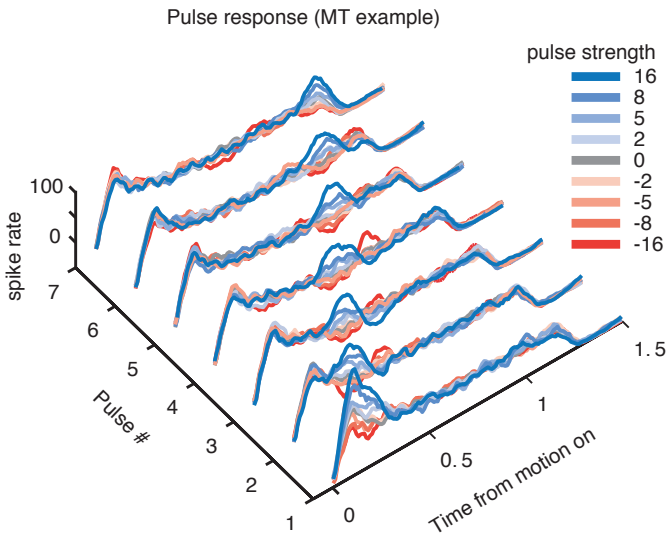

Figure 2.11: Example MT neuron responses to the motion strength at each pulse. The plot depicts the PSTH for an example MT neuron aligned motion onset sorted by the motion strength at each pulse. The x-axis is the time from motion onset. The y-axis is the pulse number that is conditioned on for the corresponding PSTH. It is clear from this plot that conditioning on motion strengths that were present at pulse 1 affected the spike rate of MT only during the following 150ms and did not have any effect after. The clear effect of each pulse can be seen.

Chapter 3

Signal and noise in MT and LIP

The middle temporal (MT) and lateral intraparietal (LIP) areas are thought to play complimentary roles in perceptual decision-making, where MT represents instantaneous motion evidence and LIP represents evidence accumulation towards a decision threshold. Here we used simultaneous multi-area recordings to analyze the flow of signal and noise across this putative circuit. We found that the time-varying representation of motion in MT could explain the observed time course of motion-dependent responses in LIP. However, to explain LIP's choice-dependence, it was necessary to incorporate a large ramping term that did not depend on motion. Additionally, we found no evidence of feedforward coupling between MT and LIP, but instead found task-modulated feedback. These results suggest that although LIP's motion-driven responses are sculpted by the dynamics of MT responses, the isolated contribution of motion integration is a small component of LIP responses, which appear to feed back to MT more than they integrate MT.

3.1 Introduction

Area MT plays a critical role in representing the motion information used for direction-discrimination (Britten et al. 1996, Salzman et al. 1990, Ditterich et al. 2003). Neurons in LIP have spike rates that reflect the time course of decision formation (Roitman & Shadlen 2002, Gold & Shadlen 2007). These lines of work have been synthesized in the form of two stage computational models, in which MT represents the instantaneous motion evidence and LIP integrates MT's output, forming a neural correlate of the decision variable (Shadlen & Newsome 1996, Mazurek et al. 2003, Shadlen & Newsome 2001, Gold & Shadlen 2007, Beck et al. 2008, Wong et al. 2008, Wimmer et al. 2015). In these models, decisions are made when LIP's representation hits a bound, which constitutes the requisite amount of evidence in favor of one direction over the other. Although these models provide parsimonious accounts of both decision-making behavior and the average neural responses in LIP, this framework has been built on single-neuron recordings performed in the two areas at different times and often in different versions of the task.

To more directly investigate the roles of these two areas, we recorded in both areas simultaneously during performance of a motion discrimination task. We then used descriptive statistical models of single trial neural activity to characterize the motion-driven response (signal) and trial-by-trial variability (noise) in both areas. This characterization allowed us to test three aspects of the MT-LIP accumulation-to-bound model. The first relates to the representation of signal in MT and the signal transformation between MT and LIP.

In particular, the motion signals coming from MT are assumed to be flat over time, and the strongly time-varying representation of the integrated motion signal in LIP is thought to be a signature of bounded accumulation (Mazurek et al. 2003). However, MT neurons are known to adapt to motion direction over fast timescales (Priebe et al. 2002) and have time-varying temporal integration (Cook 2004, Bair & Movshon 2004). It thus remains an open question whether these time-varying dynamics occur in MT during decision-making, and whether they are sufficient to account for LIP's time-varying responses to motion (Huk & Shadlen 2005).

The second prediction is that the entirety of LIP's coherence- and direction- dependent ramping should be explained based on the integration of the signals coming from MT. Models of LIP typically attempt to explain LIP based on the time-integrated differential output coming from MT (Mazurek et al. 2003), but prior work has not been able to clearly distinguish motion-driven responses from decision-related ramping (Park et al. 2014). The third prediction relates to the trial-by-trial variability that cannot be explained by the stimulus and task: if LIP directly integrates the noisy motion evidence coming from MT, then fluctuations in MT responses should precede corresponding fluctuations in LIP, with a time course similar to the propagation of signal between the areas.

Although LIP was originally chosen for study because of anatomical projections from MT to LIP, the latencies and flexible stimulus-response mappings inherent to the dots task are good reasons to believe that the MT-

LIP relationship is more distant (Shadlen & Newsome 1996). But the nature and importance of intervening stages has not been investigated or included in computational models: No direct paired measurements have been made in this paradigm, so it is unknown whether feed-forward activity is measurable at all–or whether LIP instead influences MT in a feedback manner, as has been observed in other paradigms (Herrington & Assad 2010, Saalmann et al. 2007, Siegel et al. 2015).

Our recordings revealed that MT neurons responded more strongly to motion early in the trial, and that this early weighting in MT was sufficient to explain the early weighting in LIP. We were able to parsimoniously account for MT responses with a simple model that represented the contrast and direction components of the stimulus along with a standard linear-nonlinear mapping between this feedforward visual filtering and spiking output. This accurate account of MT's early weighting was in turn sufficient to explain the strongly time-varying component of stimulus weighting in LIP—implying that a substantial part of LIP's early weighting need not result from bounded integration, but may simply be inherited from the time-varying output of MT. However, LIP's responses were not completely described by the mere integration of MT output, and instead required the addition of a ramping signal that signified the eventual choice on that trial, but which did not reflect the isolated signature of the time-varying motion.

We then analyzed the noise correlations within and between MT and LIP populations by including directional dependencies (i.e., functional connec-

tivity) between neurons within a generalized linear model (GLM) framework (Stevenson & Kording 2010). Consistent with observations in other visual and motor areas (Stevenson et al. 2012), within-area coupling was strongly predictive of single trial spikes in both MT and LIP. In contrast, feed-forward coupling was extraordinarily weak, and we did not find strong functional coupling from MT to LIP. Instead, we found that feedback coupling from LIP to MT was robust and significantly larger, particularly during the period of the trials in which the monkeys were most strongly weighing the motion stimulus.

Taken together, these results expand our understanding of the functional properties of MT and LIP, as well as the link between them. Specifically, they reveal that the time-varying weighting of sensory evidence begins in MT, that LIP's responses are explained by a modest amount of motion integration combined with a distinct choice-dependent ramp, and that it is easier to find feedback instead of feedforward interactions between LIP and MT. Our characterizations of the flow of signal and noise between these areas will require expanded conceptions of how MT signals are passed on to LIP, as well as exploration of the computational role of feedback from LIP to MT.

3.2 Materials and Methods

3.2.1 Stimulus Apparatus

All stimuli were presented using the Pychophysics Toolbox with Matlab (The Mathworks) using a Datapixx I/O box (Vpixx) for precise temporal registration. Monkey's sat in a primate chair (Crist Instruments) and faced a 55

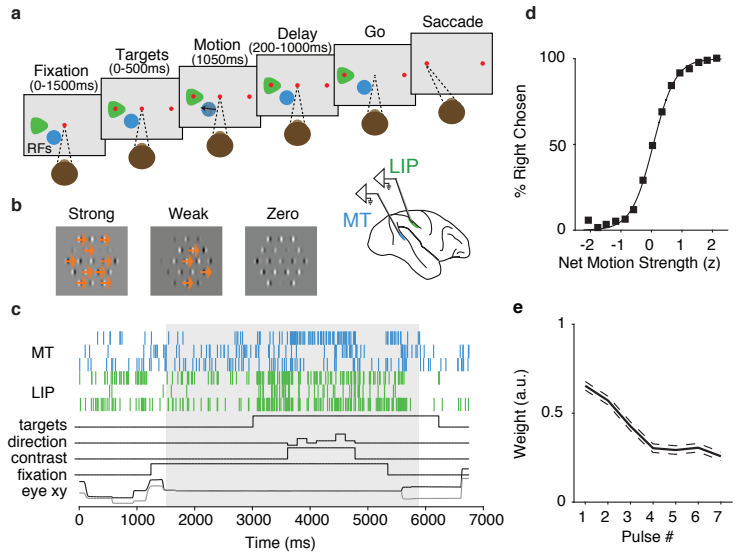

Figure 3.1: Experimental design: Motion discrimination task, basic psychophysical performance, and explanation of simultaneous physiology **a** Monkeys indicate their choice about the net direction of motion with an eye movement. After obtaining fixation, two targets appear. One is placed in an LIP RF (green). After a variable duration, motion is presented for 1050ms in the RF of MT neurons (blue). The monkey must wait for the fixation point to dim before making a saccade to one of the two choice targets. Timings of experimenter controlled task variables were jittered according to a 500ms-wide uniform distribution. **b** The motion strength at any given time was manipulated by changing the proportion of drifting vs. flickering Gabor elements. Each 1050ms motion stimulus presentation was separated into 7, 150-ms-long, motion "pulses"; each pulse could have a different motion strength. **c** Example trial: spikes recorded from MT (blue ticks) and LIP (green ticks) simultaneously during on a sample trial. The gray box indicates the region of time on each trial that was analyzed within the GLM. **d** Average psychometric function: Percent right chosen as a function of the net motion strength on each trial. The net motion strength was computed as the average pulse strength divided by the standard deviation over al possible pulse strengths on that session (n=22,838 trials). **e** Psychophysical kernel shows early weighting: The contribution of each pulse to the choice was measured with logistic regression.

inch LCD (LG) display (resolution = 1920 x 1080p, refresh rate = 60Hz, background luminance = 26.49 cd/m^2) that was corrected to have a linear gamma function. Monkeys viewed the stimulus from a distance of 118cm such that the screen subtended 100 degrees of visual angle. Eye position was tracked using an Eyelink eye tracker (SR Research), sampled at 1kHz. Reward was delivered through a computer controlled solenoid.

3.2.2 Preparation and Electrophysiology

Data were recorded from two adult rhesus macaque monkeys (one male and one female, referred to as P and N hereafter), aged 14 and 10, weighing 10 and 7.7kg, respectively. All procedures were performed in accordance with US National Institutes of Health guidelines and Institutional Animal Care and Use Committee at The University of Texas at Austin. Both N and P had standard surgery for implantation of a head-holder (Meister, Hennig & Huk 2013). Monkey P had a cilux chamber (Crist Instruments) placed over left V1 (L17,P17) for a posterior approach to MT and a separate chamber over right LIP (L12,P5). Monkey N had a custom titanium chamber placed dorsally over posterior parietal to access both MT and LIP (L9,P2). Extracellular recordings were accomplished using a combination of single electrodes (glass-coated tungsten; Alpha Omega) (8 sessions) and multisite linear-electrode arrays (U-probe or V-probe; Plexon; 35 sessions). Both areas were targeted using cranial landmarks or structural MRI. MT and LIP were identified us-

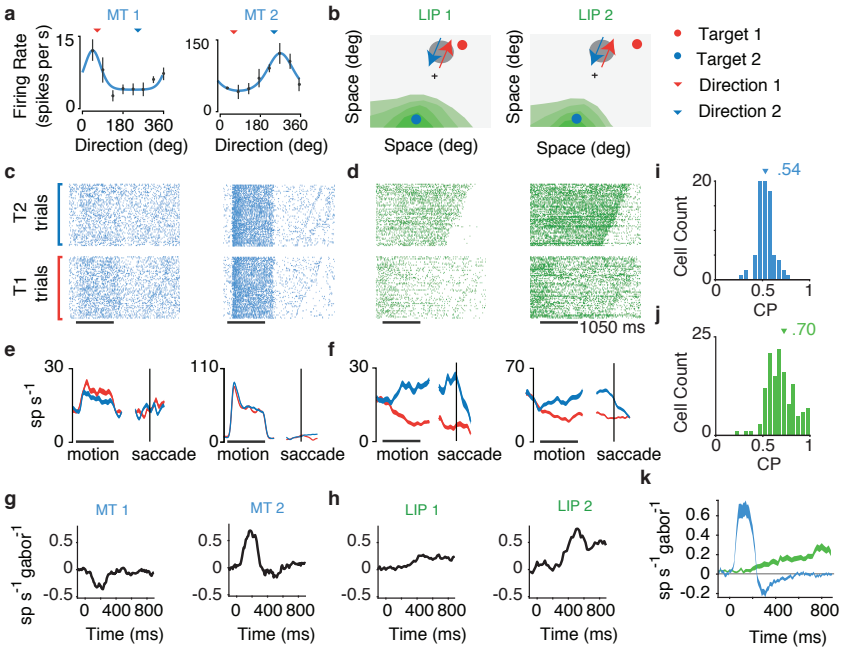

Figure 3.2: Simultaneous recordings example session**a** Tuning curves for two MT neurons. The red and blue arrows indicate the two possible directions of motion in the discrimination task. Blue lines are von Mises fits. **b** Response fields of two LIP (green) neurons recorded simultaneously with the MT neurons in a. The LIP response field maps were measured during a delayed saccade task. Contour lines represent 60% to 90% of the peak response in increments of 10%. **c,d** Spike rasters for MT (blue) and LIP (green) aligned to motion onset and sorted by the time of saccade are shown for each choice. **e,f** Choice-sorted PSTHs for the corresponding MT (left) and LIP (right) neurons aligned to motion onset and time of saccade. Width is standard error of the mean. **g,h** Pulse-triggered average (PTA) for the two example MT and two LIP neurons for pulses in the direction of target 2. **i** Choice probability for MT (blue) calculated using frozen repeats trials. **j** CP for LIP (green) calculated the same trial-type and window as in i **k** Population average PTA for well targeted MT (blue; n=112) and LIP (green; n=115) shows the vastly different dynamics of motion responses in the two areas. Width of the curves reflects the standard error across neurons.

ing electrode depths, sulcal anatomy (identified with gray/white boundaries during recording) and functional mapping. Functionally, MT was identified based on receptive field size and a preponderance of directionally selective cells (Albright 1984). LIP was identified by spatially selective visual and saccadic activity with delay period activity during a memory-guided saccade task (Gnadt & Andersen 1988)

Electrophysiological recording methods were as follows. In monkey P, neural signals were amplified, bandpass filtered (0.25-8000 Hz), and digitized at 40 kHz (12-bit resolution) using a MAP server (Plexon). In monkey N, amplification and filtering were identical, however signals were digitized at 20kHz (12-bit resolution). In monkey P, initial spike sorting was performed offline using standard clustering algorithms on each channel separately (Plexon Offline Sorter). In monkey N, signals were high-pass filtered at 500Hz, down-sampled to 12kHz and clustered across 5 channels using a mixture of Gaussians (Ecker, Berens, Keliris, Bethge, Logothetis & Tolias 2010). In both monkeys, sorts were refined using maximum a posteriori estimation under a model that the multi-electrode voltage was the linear superposition of Gaussian white noise and the spike trains convolved with their associated multi-channel waveforms (Pillow et al. 2008, Pillow, Shlens, Chichilnisky & Simoncelli 2013). Neurons were included if they did not violate a refractory period and if their spike change during pre and post binary pursuit was less than 15% (Pillow et al. 2013). We found this criterion reflects a combination of single and multi-unit clusters.

Recording stability for each unit was assessed by comparing the spike rate across the experiment to a fitted line. Units were excluded if the largest region of stability was less than 100 trials. For the remaining units, the window of analysis was restricted to the largest region where all units were stable during the Gabor task (range 127 trials to 774 trials; median 426). For choice probability and PSTH analyses, units were included if they had an absolute SNR (d' for the two directions) greater than .2 (Supplemental Figure 1). This yielded 112 MT and 115 LIP neurons. All units were included in the analysis of coupling and we found no systematic dependence on SNR.

3.2.3 Gabor stimulus

The stimulus consisted of a hexagonal grid (5-7 degrees across, scaled by eccentricity) of 19 Gabor patches (0.9 cyc/deg, σ = 0.1 x eccentricity). The spatial frequency was selected to roughly match the peak selectivity of MT neurons (Bair & Movshon 2004). The inter-element spacing and spatial standard deviation of each Gabor element were scaled by 10% of the eccentricity of the center of the aperture to match the average RF size of a V1 neuron at that eccentricity (Van Essen et al. 1984). This ensured that all of the Gabors were non-overlapping, and spaced by their standard deviations. All motion was presented by varying the phase of the sinewave carrier of each Gabor. All positions and Gaussian-envelopes were fixed across the experiment. The temporal frequency of the Gabors was 7Hz (Monkey P) or 5Hz (Monkey N), yielding velocities of 7.778 and 5.55 degrees per second respectively. Sub-

jects were trained to report the net direction of motion in a field of drifting and flickering Gabor elements with an eye movement to one of two saccade targets.

Each trial's motion stimulus consisted of seven consecutive motion pulses, each lasting 9 or 10 video frames (150ms or 166ms), with no interruptions or gaps between the pulses. The strength of each pulse, (X_i), was set by a draw from a Gaussian rounded to the nearest integer value: $X_i \sim \mathcal{N}(\mu, \nu)$, where μ and ν were fixed on each trial. On pulse i, $|X_i|$, Gabors were randomly assigned to pulse and all would drift their carrier cosine-wave in the same direction (sign(X_i)) at their specified temporal frequency. The remaining Gabors underwent a counter-phase flicker. The initial phase of each Gabor was assigned randomly to minimize grouping of flicker. The difficulty on each trial was modulated by manipulating both μ, and σ. The monkey was rewarded based on the empirical stimulus, not the stimulus distribution. That is, for motion discriminated on a horizontal axis, the monkey was rewarded for making a choice to the target on the right if the sum of the seven pulses was greater than zero, and for making a saccade to the target on the left if the sum was less than zero. On trials that summed to exactly zero, the monkey was rewarded at random with probability 0.5. 10% of trials consisted of a fixed, frozen seed. Across all stimulus strength, the average expected performance if the monkey was using only one pulse is 75% ($\pm$2%) correct. Monkeys typically exceeded that average with 80% ($\pm$1.2%) correct. The average % correct on the zero-expected motion trials if the monkey was using only one pulse was

51% (±2.2%) correct . Monkeys averaged 64% (±2.4%) correct on these trials. Thus, it is unlikely that monkeys based their choices on single pulses. (For a detailed description of the stimulus and task, see chapter 2)

3.2.4 MT and LIP mapping

After hand-mapping the retinotopic location and direction selectivity of MT using drifting dot stimuli, MT maps were refined and quantified using a pair of protocols. For 59 of the MT neurons, we used a dynamic flow field to measure the direction preference and spatial RF (Mineault, Khawaja, Butts & Pack 2012, **?**). Spatial velocity fields were estimated using the spike-triggered average velocity at all spatial locations:

$$RF_{xy} = \frac{1}{N}\sum_{i=1}^{T} y(i)(V_x(i), V_y(i))$$

where $V_x(i)$ and $V_y(i)$ are the horizontal and vertical velocities at each location, i, that the dots in hyperflow were sampled from and y is a vector of spikes. This allowed us to measure the direction preference at each spatial location in the RF.

For 122 MT neurons, we measured the tuning function by presenting drifting 100% coherence dots in 12 evenly spaced directions and calculating the average spike rate in each direction. Tuning was estimated by least-squares fitting of a von Mises function to the spike rate:

$$f(\theta) = r_{min} + (r_{max} - r_{min}) \exp\left(-\beta(1 - \cos(\theta - \theta_{pref})\right)$$

where r_{min} and r_{max} are the minimum and maximum firing rate, respectively, β is the bandwidth, θ is the stimulus direction and θ_{pref} is the preferred direction of the neuron. 28 MT neurons were mapped using both methods.

LIP was mapped using a memory-guided saccade task (Gnadt & Andersen 1988). LIP response fields were estimated by counting spikes between target onset and saccade and using linear regression between the spatial location of the target and the spike rate on each trial.

Behavior

To measure the contribution of each pulse to the monkey's choice on each trial, we used logistic regression, where the probability of the monkey's choice across the dataset is given by:

$$p(\mathbf{Y}|\mathbf{X}, \mathrm{w}) = \frac{\exp(Y^T \mathbf{X}\mathrm{w})}{1 + \exp(\mathbf{X}\mathrm{w})}$$

Where $\mathbf{Y} \in \{0, 1\}$ is a vector of the choice on each trial, $\mathbf{X}$ is a matrix of the seven pulses on each trial, augmented by a column of ones to capture the bias, and w is the seven pulse weights plus a bias term. This model was fit using maximum likelihood. Fit results are plotted in Figure 3.1, error bars were derived from the matrix of partial second derivatives. The psychometric function in Figure 3.1 uses the same likelihood, but has a single stimulus weight for the sum of the pulses on each trial.

Neural Analysis

To measure the relationship between the time-varying pulse strength and the spike rate, we measured the cross-correlation between pulses and the spike rate. The pulse-triggered average (PTA) effectively measures the excess spike rate that would result from a pulse at a particular time of particular strength. To compute the PTA we binned the pulse stimulus and spike counts at 10ms resolutions. Let $x(t)$ denote the stimulus at the tth bin and $y(t)$ the spike rate. All trials are concatenated such that the stimulus vector, $\vec{x}$, is size $T \times 1$ and is zero everywhere except at the time of pulse onsets. For a pulse at time t, $x(t)$ is the number of Gabors pulsing with $x(t) > 0$ for pulses in the preferred direction and $x(t) < 0$ for the anti-preferred direction. To compute a PTA over n lags from each pulse onset, we built a design matrix, X, of size $T \times n$, where $\mathrm{X}(i, j)$ is the stimulus $\vec{x}$ at the ith bin, at j lags ($x(i + j)$). The PTA can then be estimated with ordinary least squares (OLS)

$$\mathrm{PTA} = (\mathrm{X}^T\mathrm{X})^{-1}(\mathrm{X}^T\mathrm{y}) \tag{3.1}$$

where y is the vector of spike counts divided by the bin size. To compute the PTA separately for each of the seven pulses we built a design matrix for each pulse and concatenated them $\mathrm{X} = [\mathrm{X}_1, \mathrm{X}_2, \ldots, \mathrm{X}_7]$ and used the same OLS estimation procedure. To visualize the PTAs, responses were smoothed with a 25ms gaussian kernel.

We noted that two sources of slow, non-directional autocorrelation in the spike trains could substantially bias the estimates of the PTA. The first

is the motion onset response. Both MT and LIP exhibited large fluctuations in spike rate that resulted from the onset of the stimulus. The second was the large premotor buildup in LIP, which had progressively larger biases on pulses later in motion viewing. To correct for these components we subtracted off the average spike rate aligned to motion onset from the binned spike rates in MT and then estimated the PTA using the residual rates. To correct for premotor/choice dependent components of the LIP firing rate, we subtracted off the average rate for each choice depending on what choice the animal made that rial. Figure 3.2g,h,k shows the uncorrected PTA for example neurons and population average. Figure 3.3d,e shows the PTA computed separately for each pulse corrected for motion onset. Figure 3.4d,e shows the PTA corrected for choice. In all cases, we used the same analysis to compare model and data.

PSTHs were smoothed with a Gaussian filter (25ms). Trial motion strengths were z-scored and binned into three quantiles.

Encoding Model

We modeled single trial spike trains as with a Poisson point process in the form of GLM (Truccolo et al. 2005, Pillow, Paninski, Uzzell, Simoncelli & Chichilnisky 2005). We discretized time in bins of duration Δ =10ms. The log-likelihood of the response, $\mathbf{r}$, of a single neuron is (up to an additive constant)

$$L(\mathbf{r}|\lambda) = \sum_t \mathbf{r}(t) \log(\Delta\lambda(t)) - \Delta\lambda(t)$$

where the conditional intensity (instantaneous spike rate), λ at time t is given by

$$\lambda(t) = \exp(\mathbf{k} \cdot \mathbf{x}(t) + \mathbf{h} \cdot \mathbf{r}(t-1) + \mathbf{c} \cdot \mathbf{s}(t) + \mu)$$

where $\mathbf{k}$ are weights on the stimulus covariates, $\mathbf{x}$, $\mathbf{h}$ is the post-spike weights that integrate the neuron's own spiking history, $\mathbf{r}(t-1)$, $\mathbf{c}$ are coupling weights on simultaneously recorded spikes $\mathbf{s}$, and μ is a constant offset to capture the neuron's baseline firing rate. $\mathbf{k}$ comprises of a set of n_i weights for each of the m stimulus covariates and $\mathbf{k} \cdot \mathbf{x}$ is shorthand for $\sum_{i=1}^{m} \sum_{j=1}^{n_i} \mathbf{k}_{i,j} f_j(\mathbf{x}_i(t-\tau : t))$, where f_j are nonlinearly scaled cosine functions (Pillow et al. 2008).

To avoid overfitting, weights were fit with maximum a posteriori estimation of θ, where $\theta = \{\mathbf{k}, \mathbf{h}, \mathbf{c}\}$ and penalized with a regularizing term $\alpha(\|\mathbf{k}\|_2 + \|\mathbf{h}\|_2 + \|\mathbf{c}\|_2)$. α was fit by cross-validation on the training set.

To fit the dependence of LIP responses on MT's transformation of the stimulus, we simulated MT rates using the average filters for contrast and direction from our population. We simulated the MT response and a hypothetical anti-neuron response by convolving the stimulus with recovered filters and exponentiating their output. For the anti-neuron simulation, we flipped the sign of the direction filter, but kept the contrast filter identical (Figure 3.3a). We used these simulated rates in place of the contrast and direction of the stimulus to recover LIP's "MT-preferred" and "MT-antipreferred" kernels (Figure 3.4a).

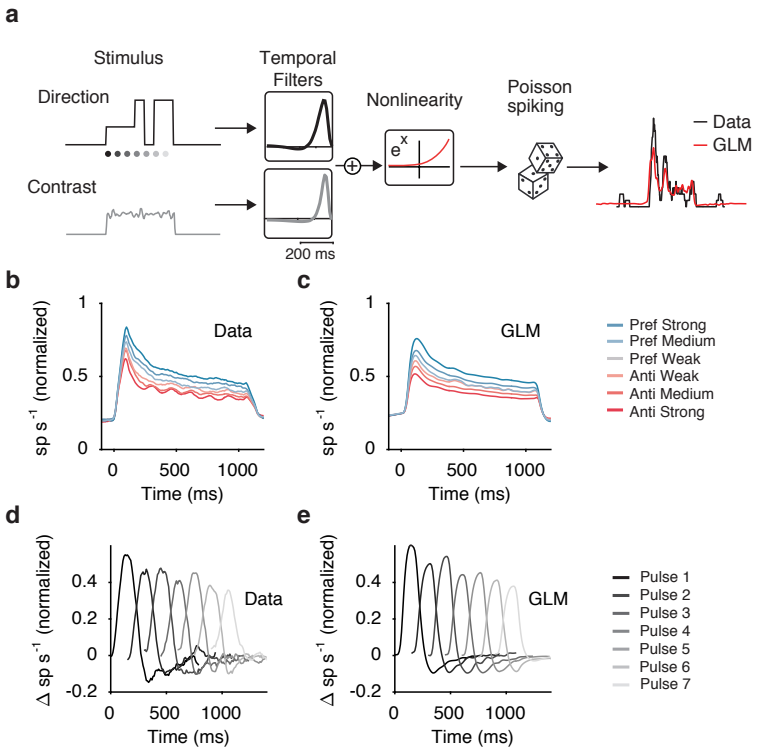

Figure 3.3: MT has strong time-varying responses to motion which are well-described by a GLM **a** Schematic of modeling approach. The contrast and direction of each Gabor are summed spatially and fed into a GLM as a temporal signal. The recovered average temporal filters for contrast and direction show brief integration of visual inputs. The outputs of these linear filters are summed and then passed through an exponential nonlinearity to generate the rate of a Poisson distribution that controls the probability of spiking. Example prediction shows binned measured spike trains smoothed by a 50ms boxcar compared to a predicted rate. **b** Population PSTH for MT aligned to motion on, and sorted by the net strength and direction of the motion stimulus. Spike trains were smoothed with a 25ms Gaussian kernel and binned at 10ms. The PSTH for each cell was normalized by the max response before averaging. **c** Same as in b, but for rates predicted by the GLM for withheld data. **d** Response to each of the seven motion pulses for the MT population. These pulse-triggered averages characterize the change in spike rate for unit motion strength at each of the 7 pulse onset times. **e** Model responses to the seven pulses.

To compare the effects of different parameterizations of the stimulus, we fixed specific $\mathbf{k}_i$ to zero and retrained the model. We used the same procedure to compare inter and intra-areal coupling.

Model Evaluation

To evaluate the GLM we used 5-fold cross-validation. The test-likelihood was computed by subtracting the log-likelihood of a homogeneous Poisson process from log-likelihood of the model

$$LL = (L(\mathbf{r}|\lambda) - L(\mathbf{r}|\bar{\lambda}))/\sum_t \mathbf{r}(t)$$

with units of bits per spike. Goodness-of-fit was computed on test data by stitching across cross-validation folds to generate the PSTH. For coupling models, the model spike rate was estimated using spike input from the data.

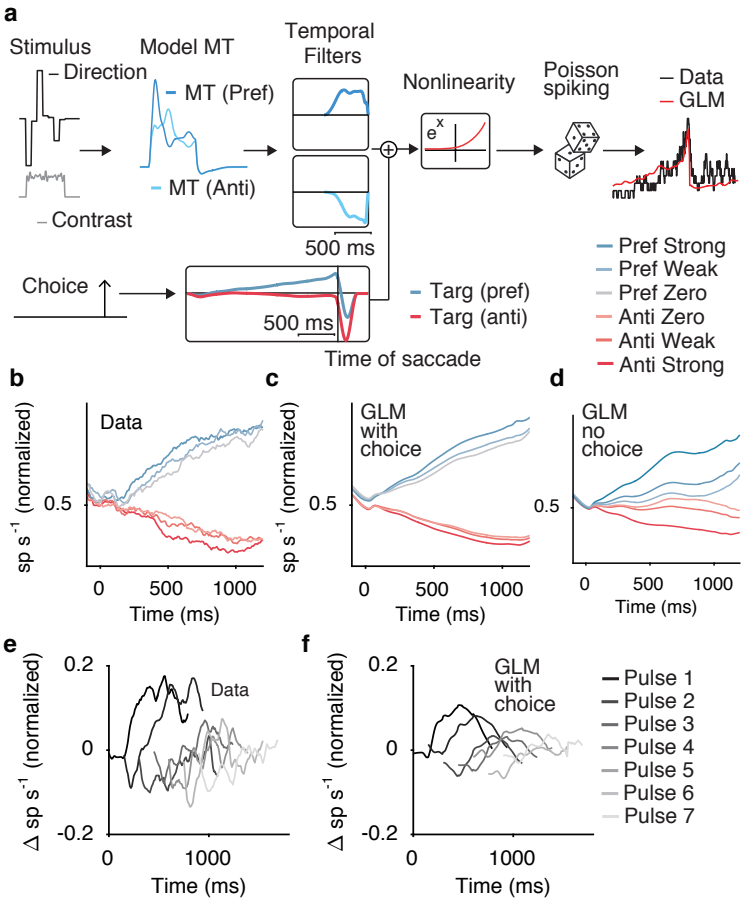

Figure 3.4: MT early weighting is sufficient to describe LIP early weighting. **a** Schematic of LIP model. Trial direction and contrast are used to simulate MT responses which are then fed into a GLM as a temporal signal. Anti-preferred MT response was simulated by flipping the sign of the direction filter in Figure 3.3a. The average measured temporal filters for the LIP population integrating MT in the preferred and anti-preferred direction. Model mechanics and example fit are identical to the description in Figure 3.3. **b** Motion strength dependent population PSTH for LIP aligned to motion on. Spike trains are smoothed with a 25ms Gaussian kernel and binned at 10ms. PSTH for each cell was normalized by the max response before averaging. **c** Same as in b, but for rates predicted by the GLM with included choice term (predictions were made to withheld data). **d** Model predictions without choice term. **e** Response to the seven pulses for LIP population. **e** Model responses to the seven pulses.

3.3 Results

Behavior and physiology in a reverse correlation motion discrimination task

MT and LIP responses have vastly different temporal dynamics, which are thought to support their distinct roles in decision making (Gold & Shadlen 2007). To characterize the response properties of both areas, as well as the stimulus-driven psychophysical performance of the monkeys, we developed a motion-discrimination task amenable to reverse correlation analysis. Similar to an often-used moving-dot direction-discrimination task, monkeys viewed a field of dynamic (flickering and drifting) elements (Gabor patches), and indicated their choice about the net direction of motion with an eye movement to one of two choice targets (Figure 3.1a). The strength of motion was controlled by manipulating the proportion of elements drifting in one direction vs. the other (Figure 3.1b). The time-course of the stimulus was determined by the motion contained in seven discrete 150 ms epochs ("motion pulses") (Figure 3.1c; "direction" trace). Decisions exhibited a conventional sigmoidal dependence on the net motion strength (i.e., the integral of the motion pulses; Figure 3.1d), and early pulses were weighted more strongly by the monkey than late pulses (Figure 3.1e). Similar overall performance and early temporal weighting has been observed in the classic moving-dot paradigm (Kiani et al. 2008, de Lafuente, Jazayeri & Shadlen 2015).

We recorded from 157 MT and 200 LIP neurons across 43 sessions. The example session shown in Figure 3.2 schematizes the general paired-recording

approach and illustrates the conventional response dynamics of MT and LIP neurons. Keeping with standard practice, we placed the motion stimulus in the receptive fields (RF) of MT neurons, and one of the choice targets in the response fields of LIP neurons (Figure 3.2a,b). MT neurons showed strong and directionally-selective responses during the motion epoch (Figure 3.2a,e), while LIP neurons had spike rates that ramped up or down depending on the choice (Figure 3.2f). In MT, small but significant correlations with choices that could not be explained by the stimulus (choice probabilities, CP) were 0.53 on average, as calculated by counting spikes between motion onset and go-signal on repetitions of identical trials (i.e, "frozen noise"). In LIP, the correlation with choice was much larger, with CP of 0.72 on average (using the same trial-types and counting window). Additionally we calculated a pulse-triggered average (PTA) that captures the change in spike rate that resulted from a pulse in the preferred direction of the cell. MT neurons exhibited PTAs that were brief and resembled a smoothed version of the 150ms pulse (Figure 3.2g,k). LIP neurons resembled long temporal integration of each pulse with a substantial delay. Figure 3.2(h,k) shows the PTA for example neurons and the population of MT and LIP cells in our sample.

Given that both the psychophysical behavior and physiological responses in MT and LIP were reconcilable with prior literature, we were then able to use our framework to precisely characterize the time course of motion integration in MT and LIP.

Motion responses in MT decrease over time

To understand how MT responds to visual motion signals during decision-making, we fit an encoding model of single-trial spike trains (Figure 3.3a). The encoding model describes the probability of a spike train as a Poisson generalized linear model (GLM) (Truccolo et al. 2005, Pillow et al. 2008, Park et al. 2014), which is defined by three stages: (1) a linear stage that filters each stimulus component; (2) an exponential nonlinearity that converts the summed filter outputs into a spike rate; and (3) conditionally Poisson spiking. In its simplest form, the GLM is a linear-nonlinear-Poisson (LNP) model with causal stimulus filters.

To describe MT responses, the "stimulus-to-MT" model contains two time-varying stimulus inputs: The first is the time-varying pulse strength; the second is the spatially averaged contrast (Figure 3.3a). This simple causal model reproduced the average stimulus-dependent responses for MT (Figure 3.3b,c), capturing 78% of the variance.

To describe the temporal dependence of MT responses on the motion pulses, we calculated a pulse-triggered average (PTA) separately for each of the seven pulses (Figure 3.3d). The PTA depicts the contribution to spike rate from motion in each of the seven epochs (see online methods). In MT, although all seven of the pulses exerted strong and fairly transient effects on spike rate, early pulses affected MT considerably more than later pulses, with the last pulse reaching only 54% of the magnitude (l_2-norm) of the first pulse.

We asked whether this dynamic sensory weighting in MT was captured by the "stimulus-to-MT" model, which contains static linear filters and a single output nonlinearity. The stimulus-to-MT model reproduced the temporal dependence of motion integration in MT (Figure 3.3e). The recovered filters demonstrate a potential mechanism for these early strong responses. At the onset of motion, the contrast of the stimulus jumps from uniform gray (0% Michelson contrast) to 25% contrast, and thus generates a strong onset transient independent of the directional content of the stimulus (similar effects would be expected using moving dots, which contain both a luminance and contrast transient (Britten et al. 1993)). This time-varying non-directional drive creates a gain term on the sensitivity to direction across time, as the exponential nonlinearity that follows these two filters effectively multiplies the contrast and direction responses together, (i.e., $\exp(a) \cdot \exp(b) = \exp(a + b)$). The precise form of the spiking output nonlinearity does not matter as long as it is well approximated by an exponential. As a result, this form of contrast gain scales the response, such that early motion pulses exert larger effects than late pulses (Figure 3.3e).

In summary, we observed time-varying motion responses in MT that were parsimoniously explained with causal temporal filtering and a standard static nonlinearity. Next we explored the consequences of this time-varying MT representation for the time-varying responses to motion often observed in LIP.

Signal transformations from MT to LIP

LIP neurons exhibited ramping average spike rates that depended on the choice and net direction (Figure 3.4b). Additionally, they exhibited time-varying motion responses with a strong decay in response across the seven pulses (Figure 3.4d). Specifically, the last pulse reached only 38% of the strength of the first pulse in LIP, an even stronger fall-off than observed in MT. This decrease in LIP responses to motion has been observed previously (Huk & Shadlen 2005), and in conjunction with the motion-dependent ramps, has been interpreted as evidence for LIP reflecting the bounded accumulation of MT activity (Wong et al. 2008). We extended our modeling framework to understand the signal transformations from MT to LIP, using the output of the "stimulus-to-MT" model as the temporal input to a GLM fit to LIP spike trains (Figure 3.4a).

To implement realistic MT input, we used the model fits from our MT population. We filtered the motion stimulus with the population average contrast and direction filter, and then exponentiated the sum to generate an MT spike rate on each trial. This simulation generates a single spike rate for each trial that represents the average expected response from the population of MT neurons we recorded from. Importantly, it captures the time-varying dynamics in motion responses that we observed in the data. We also simulated a hypothetical "anti-neuron" response, with opposite direction preference (Britten et al. 1992), implemented simply by flipping the sign of the direction filter while leaving the contrast filter the same. Thus, two simulated MT rates were

fed into the GLM as temporal signals.

We first compared the MT-to-LIP model to a "stimulus-to-LIP" model, which used the same parameterization as the stimulus-to-MT model but was fit to LIP (i.e., it took the motion stimulus as input, as opposed to MT's response to the stimulus). The MT-to-LIP model's inclusion of realistic MT input provided a better account of LIP (p ¡ 0.001; sign test). We used this MT-to-LIP model to recover temporal kernels for the MT-to-LIP transformation, estimating how much temporal integration LIP reflected when operating upon realistic MT outputs. These MT-LIP integration filters had time constants ($\tau = 174 \pm 7$ms) significantly shorter than the stimulus referenced filters from the stimulus-to-LIP model ($\tau = 250 \pm 9$ms; t-test $p < 0.001$), reflecting the fact that the MT stage itself performs some degree of temporal integration.

This motion-based GLM did not provide complete fits to the average responses in LIP (Figure 3.4e,f). Specifically, no model based solely on integrated motion signals (modeled either as the stimulus or as the MT output) could capture the relatively steep slopes of the ramps for low coherence. To better account for the full constellation of motion- and choice- dependent ramps evident in averaged LIP activity, we had to include a variable in addition to the visual motion drive, conceived of as a "choice" term for choices (saccades) to the preferred target and anti-preferred target (Park et al. 2014). A schematic of the "MT-to-LIP" model with choice terms included is depicted in Figure 3.4a. The independent time-varying nature of our stimulus allowed us to separate choice dependence and motion dependence in LIP spike rates.

Figure 3.4d demonstrates that LIP spike rates are not solely proportional to an MT integrator. Similar failures of integrator models of LIP are present in (Mazurek et al. 2003) (Figure 5 and 7).

The MT-to-LIP model (with choice terms included) explained 73% of the variance of the PSTH on average, and it reproduced the strong early weighting in LIP (Figure 3.4e). (In contrast, the stimulus-to-LIP model failed to reproduce the early weighting, regardless of whether a choice term was included). Thus, MT's time-varying weighting was a necessary component to reproduce LIP's early weighting without invoking nonlinear weighting mechanisms.

The need for added choice terms in the MT-to-LIP model draws attention to the relatively small effect of motion in LIP. Even without correcting for strong choice-correlated premotor buildup in LIP that biases the estimates of the PTA (online methods), LIP responses are only minimally driven by the motion (Figure 3.2k). Given the fact that the pulse-driven component of the LIP response was small in both absolute and relative terms, we entertained the hypothesis that LIP might not be directly involved in integrating MT responses, and that instead the pulse responses we did observe were distant results of a decision process implemented elsewhere. To further investigate the relationship between MT and LIP, we turned to our simultaneous recordings from both areas to ask whether trial-by-trial fluctuations in MT activity were correlated with fluctuations in LIP.

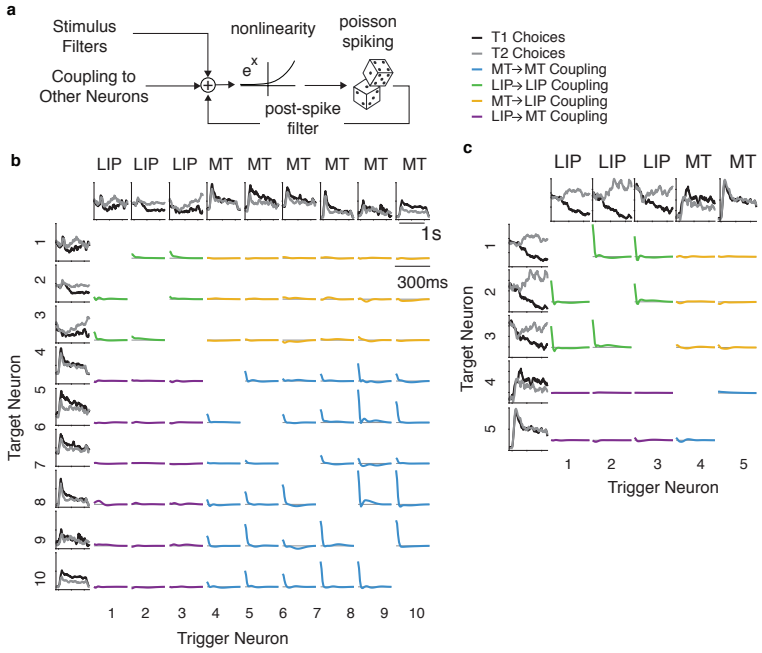

Figure 3.5: Coupling Example Sessions. **a** Schematic of fully-coupled MT-LIP model. The stimulus covariates and spike trains from simultaneously recorded neurons are the input to a GLM, where each covariate has its own temporal filter (temporal filters not shown). The number of filters per model scales with the number of simultaneously recorded neurons. **b** Example session coupling filters from the fully-coupled MT-LIP model. The insets along the left column and top row show the choice sorted PSTH. The other insets show the spike rate gain change for the neuron at each row (Target) that results from a spike by the neuron specified by the column (Trigger). This session illustrates the strong fine-timescale coupling that is common in area MT. All coupling insets are scaled to have the same y-axis. **c** Same as in b for the example session shown in Figure 3.2. This example session highlights strong intra-areal coupling in LIP

Trial-by-trial variability in MT and LIP is inconsistent with simple feedforward integration

Having described the activity of MT and LIP as a function of the visual stimulus (for MT) and the neural representation of the stimulus (for LIP), we

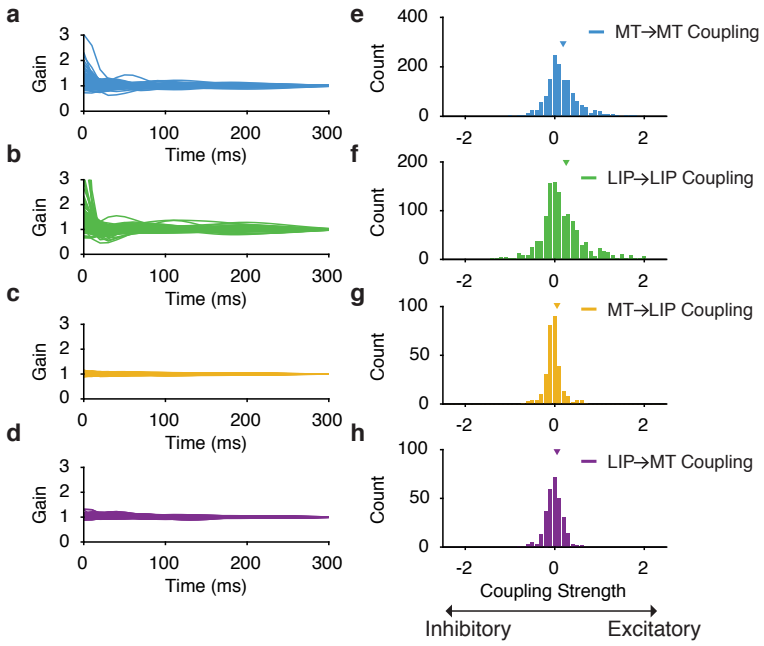

Figure 3.6: Recovered coupling filters across all simultaneously recorded neurons (Filters come from the fully-coupled model) **a** Recovered MT-MT coupling plotted as spike rate gain (by exponentiating the filters). This plots the multiplicative gain change in firing rate for an MT neuron in the 300ms following another MT neuron's spike (at time 0) **b** Same as in a except for LIP-LIP coupling. Similar to MT coupling, the strength of coupling was largest in the shortest lags. **c,d** Coupling filters for feedforward (LIP triggered on MT spikes) and feedback (MT triggered on LIP) **e,f,g,h** Net effect of coupling. Histogram of the sum of the coupling filters of each category before exponentiating. This measures whether the net effect of coupling is excitatory or inhibitory. MT-MT (blue) and LIP-LIP (green) coupling are largely excitatory and inter-areal coupling in the feedforward (yellow) or feedback (purple) direction were near zero on average.

then characterized how the responses of neurons in these areas depend on the trial-by-trial variability in the spiking responses of other neurons. The GLM can be extended to capture such dependencies by incorporating coupling terms,

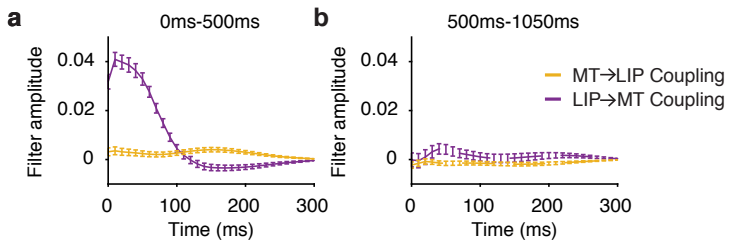

Figure 3.7: Feedforward and Feedback. **a** Average feedforward (yellow) and feedback (purple) coupling filters during the first 500ms of motion. Coupling filters were averaged across all 333 MT-LIP pairs and error bars signify the standard error. **b** Average feedforward and feedback coupling during the second 500ms of motion. Feedback (but not feedforward) coupling was modulated by the epoch analyzed.

which take spikes as input, and which characterize the temporal kernels that relate these spikes to the output of each neuron (Figure 3.5a). Figure 3.5b,c shows coupling analyses in the fully-coupled MT-LIP model applied to two example sessions in which we recorded from multiple units in MT and LIP simultaneously. The figure shows choice-sorted PSTHs and coupling within and between simultaneously-recorded MT and LIP neurons. Each subplot in the figure is the coupling filter that impacts the change in spike rate for the neuron shown on each row (left side), given a spike from the neuron depicted at the top of the columns (top). These coupling filters are similar in spirit to the positive lags of cross-correlations, except that they can be fit directionally and only measure variance that is not already explained by the stimulus and autocorrelation of individual neurons. Additionally, they also allow us to compare how much they explain spiking activity relative to other factors, such as

the stimulus (Okatan, Wilson & Brown 2005, Stevenson et al. 2008).

We successfully recorded from both areas with the requisite task geometry on 18 of the sessions, yielding 100 MT, 67 LIP neurons, supporting 333 MT-LIP pairs. Coupling terms capture both directions of possible interaction (1474 for within-MT, 1482 for within-LIP, and 666 for between MT and LIP). We validated the incorporation of these coupling terms within each area first, by adding intra-area coupling filters to the basic stimulus GLM fit. On average, the GLM with added intra-area coupling had 74% more bits per spike than the uncoupled model in MT and 139% more in LIP. These contributions were surprisingly strong. In fact, a "coupling only" model, which had no stimulus or task terms was often a better description of single trial responses than the stimulus. Over half of our MT cells (59%) and almost three-quarters of our LIP cells (69%), were better predicted by local connectivity alone than by the stimulus and task variables (Supplemental Figure 2). This effect was significant across the population for MT (sign test, $p = .0199$) and LIP (sign test, $p < 2.0 \times 10^{-8}$), and on average coupling contained 55% more bits/spike in MT and 120% more bits/spike in LIP. We then similarly analyzed the functional connectivity between MT and LIP. Across the population, the fit quality of the GLM with added inter-areal coupling was not significantly better than the uncoupled model in either the feedforward (p=0.6; sign test) or feedback (p=.98; sign test) direction.

To quantify the relative strengths of coupling within and across MT and LIP, we plotted the individual coupling filters and summarized their net

magnitudes (Figure 6). As was evident in the example sessions, MT-MT and LIP-LIP coupling kernels were large, and had shapes indicating that responses were driven most strongly by neighboring spikes within 10-20ms (Supplemental Figure 3), in a mostly excitatory manner (Figure 3.6e,f). The MT-LIP kernels were difficult to discern, and in contrast to the MT-MT and LIP-LIP coupling, did not improve the model's ability to predict responses, and they were negligible relative to the effects of the stimulus (Supplemental Figure 2). Although the statistical relationship between MT and LIP was minimal, we were able to systematically measure coupling filters that were small, but outside the distribution expected if the neurons were independent. A recent study identified small, but measurable, inter-areal correlations that were task modulated during decision-making (Tauste Campo, Martinez-Garcia, Nácher, Luna, Romo & Deco 2015). This study did not speak to the predictive power of this coupling, but we wondered whether the coupling we observed was similarly modulated by the behavior.

We tested for task-modulated inter-areal correlations by estimating coupling filters within distinct epochs of the trial. Because the monkey's choice depended more strongly on the first 2 or 3 pulses of motion than on the latter 4 (Figure 3.1e), we examined the MT-to-LIP and LIP-to-MT coupling terms in more detail, zooming in on just the spikes that occurred either early (first 500ms) or late (last 500ms) of the motion viewing period (Figure 7a). This revealed strong LIP-to-MT (feedback) coupling early during motion viewing, despite little if any MT-to-LIP (feedforward) relations at this time. Later in

motion viewing, there was little coupling in either direction (Figure 7b). Thus, the inter-areal coupling appears to be strongly time-dependent: during early phases of motion viewing– when the animal's behavior is most affected by the visual motion– components of the LIP response not explained by the stimuli and task ("noise") propagate back to MT; during later motion viewing– when the animal's behavior is less affected by motion– the areas are closer to independent (Supplemental Figure 4). And at no time in the trial, regardless of whether the animal appears to be using the stimulus or not, did we find impacts of MT on LIP in a manner consistent with LIP integrating MT's signal and noise in a relatively direct and feedforward manner.

Discussion

We characterized the stimulus dependence and functional connectivity of neurons in MT and LIP, two areas in the macaque brain that are thought to play important roles during sensory decision-making. Using a reverse-correlation psychophysical paradigm, paired multi-neuron recordings in both areas, and generalized linear model analysis, we performed a functional dissection of how neural activity in this circuit depended on stimuli, task performance, and activity in other neurons. Our characterizations revealed several surprising components of how both signal and noise propagate between MT and LIP.

First, we observed attenuating responses to motion not just in LIP, but also in MT. MT's response attenuation to motion could be explained with

feedforward mechanisms, in which constant response to directional motion is modulated by a decaying gain response to the visual contrast. Second, we found that LIP's time-varying motion response could be parsimoniously explained with a temporal integration filter that operates upon the time-varying MT input, combined with a distinct ramping term related to the impending choice. Third, a coupling analysis revealed that the trial-scale variability present in these areas was difficult to reconcile with LIP integrating MT directly. In fact, coupling was larger in the feedback direction, an effect that was most prevalent during the time period in which the animal's behavior most strongly depended on the visual motion.

We interpret these results as follows. MT's representation of visual motion likely limits task performance (Newsome & Pare 1988), and its time-varying responses likely contribute to the time-varying nature of both LIP responses and psychophysical performance. Although our GLM analysis considered the impact of the stimulus on MT directly, we note that of course the direction and contrast components of MT responses reflect a cascade of computations that start in the retina and pass through several stages of earlier thalamic and cortical processing, although the decaying responses may be mediated by circuit mechanisms within MT (Priebe et al. 2002). Although the small visual-motion driven component of LIP's response can be parsimoniously explained in terms of temporal integration of the MT output, it appears unlikely that direct feedforward integration is an accurate description of the functional link between MT and LIP. The required addition of a choice-related

ramping signal suggests that LIP may be receiving a substantial premotor or decision formation signal in addition to the integrated sensory signals that have received primary focus.

In some ways, our functional connectivity results may simply recapitulate anatomical connections, which are dense within areas and sparse between areas (Markov et al. 2014). It is possible that by subsampling small populations of MT and LIP neurons, we were not able to resolve feedforward connectivity that indeed exists anatomically (Ungerleider & Desimone 1986). However, the fact that we detected feedback but no feedforward coupling suggests that individual spikes in MT do not have a large influence on LIP spiking probability in addition to what the average motion signal is carrying. As such, we prefer the interpretation that LIP's temporally-integrated representation of MT's motion representation, despite involving only simple computations to transform it from MT input, is more likely to reflect substantial intervening processing that washes out the contributions of individual MT neurons.

The notion of intervening processing between MT and LIP is actually not a new one (Shadlen & Newsome 1996). In fact, comparisons across separate studies of the two areas during the classical moving dots task reveals a very significant latency difference (in response to the visual motion stimulus) between the areas, on order of 100 ms. Given that the latency of MT responses to visual motion are approximately 100 ms, a simple consideration of timing suggests that the distance from the retina to MT is similar to the distance between MT and LIP. The flexible mapping between visual motion (which

drives MT neurons) and saccadic choice targets (used to drive LIP neurons) is also consistent with a remote link between the two areas. In the standard direction-discrimination paradigm, the visual stimulus is placed within the RF of MT neurons, and the choice targets are placed elsewhere, in the RF of LIP neurons. The relation between the motion stimulus and the saccadic choice targets is not fixed or necessary, and animals can associate saccades to arbitrary locations in response to particular directions. This flexible mapping requires a routing stage to intervene between the two areas, and thus the lack of measurable noise correlations is different than investigations that typically focus on measuring inter-areal co-fluctuations between neurons with overlapping receptive fields (Shadlen & Kiani 2013).

Although our analyses did not need to explicitly model "top down" factors like attention or decision formation, it is certainly possible that they also play a role. The time-varying response we observed in MT could reflect gain changes driven by attention (Cook 2004, Ghose & Bearl 2010), and the time-varying response we observed in LIP could reflect bounded accumulation. But it is certainly interesting that simple known mechanisms explain much of the time-varying response dynamics in both areas. It has previously been assumed that the time course of MT's motion representation could be assumed to be flat, because a comparator step (i.e., which compares motion signals for one direction over another) would effectively "subtract off" any temporal dynamics (Mazurek et al. 2003, Ditterich et al. 2003, Wong et al. 2008, Law & Gold 2008, Wimmer et al. 2015). This in fact would only work for addi-

tive effects, and would not compensate for the (multiplicative) gain effect on direction representation we characterized in MT.

Our analysis of LIP opens some large questions for future consideration. There appears to be a substantial component of LIP responses that are not well-explained as the temporal integration of MT, and instead appear to be more directly related to the impending choice (Park et al. 2014). Furthermore, our analysis has not explained how or where the significant temporal integration reflected in LIP is performed. Finally, the propagation of noise in LIP to subsequent MT responses was a surprise and its functional interpretation will require new experiments. In summary, these straightforward techniques (simultaneous recordings of multiple neurons in multiple areas, coupled generalized linear models, and an integrated reverse-correlation framework) have provided the basis for a considerably more detailed understanding of the decision making circuit. This integrated set of approaches is applicable both to other parts of this circuit, and can also be applied to other neural circuits and their relations to cognitive and perceptual processes.

Chapter 4

Decoding motion direction from populations of MT neurons

Motion discrimination is a classic model system for probing computations and circuits underlying perceptual decisions. Despite a long history of studying the sensitivity of single neurons, little is known about how direction can be read out from the activity of neural populations. We recorded from ensembles of MT neurons while monkeys performed a motion-discrimination task. We compared the performance of a simple, neurally plausible, decoder to the psychophysical performance and to the sensitivity of single neurons. We found that the population was more accurate than the best single neurons and performed at least as well as the monkey at our task. We also found that the joint response patterns of neurons was not needed to compute the optimal weight pattern. MT populations were most sensitive to the stimulus immediately following motion onset, which corresponded to psychophysical weights of the monkeys. Finally, we compared choice probability of individual neurons to the performance of the population for decoding choice. The population decoded choice better than the best single neurons, however, choice probability, which assumes a hypothetical "anti-neuron" was often higher than the accuracy of the population decoder. These results provide empirical groundwork

for extending single neuron studies of perception to the population level.

4.1 Introduction

A large body of work has focused on the sensitivity of single neurons in MT to the direction of motion, and their relationship to the organism's choice (Britten et al. 1992, Britten et al. 1996, Parker & Newsome 1998, Cohen & Newsome 2009, Price & Born 2010). To make a decision about the direction of motion, an organism likely integrates over large populations of correlated MT neurons (Shadlen et al. 1996), where the particular structure of interneuronal correlations can impair or improve decoding performance (Averbeck, Latham & Pouget 2006, Ecker et al. 2011, Moreno-Bote et al. 2014). It remains unknown, how much information is available in a population of MT neurons and how complicated the decoder needs to be to perform well at the tasks used to study motion-perception.

Here we study the activity of up to 21 MT neurons, recorded simultaneously while macaques discriminated the net direction of motion in a noise stimulus. We apply a simple, neurally plausible, decoder to read out of the direction or the choice of the animal on single trials. Population decoding methods have proven useful in understanding the information available in populations of neurons in motor cortex (Georgopoulos et al. 1986), primary visual cortex (Graf et al. 2011, Berens et al. 2012, Chen et al. 2006), as well as the dynamics of decision-making in frontal cortex (Kiani et al. 2014) and oculomotor planning in the parietal lobe (Graf & Andersen 2015).

We found that the population carried more information about direction than the best single neuron and was sufficient to explain the monkey's behavior even though the single neurons were not. The decoder did not need to know the full joint statistics of the population to perform as well as a decoder that treated the neurons as independent. The sensitivity of the population was greatest at the beginning and the optimal temporal weighting strategy preferentially weighs spikes immediately following motion onset, yet a fixed temporal decoder reached 95% of the performance of a more sophisticated temporal decoder. Finally, we examined the amount of information about choice in the population. We found that the population contained more information about the choice than the single neurons, yet this was dependent on whether we were able to record from neurons with oppositely tuned neurons. Taken together, these results suggest that a simple population code is all that is required to perform coarse direction-discrimination tasks using MT neurons.

4.2 Materials and Methods

4.2.1 Electrophysiological recordings

Recordings were performed in one male (monkey P) and one female (monkey N) rhesus monkey (macaca mulatta) using linear electrode arrays (Plexon Uprobe/Vprobe). All procedures were performed in accordance with US National Institutes of Health guidelines and Institutional Animal Care and Use Committee at the University of Texas at Austin. Monkey P had a cilux chamber (Crist Instruments) placed at stereotaxic coordinates L17P17

for an approach through left V1. Monkey N had a custom titanium chamber positioned dorsally at L9P2 for an approach. MT was identified physiologically by depth, sulcal anatomy (using gray/white boundaries), and functionally by a preponderance of directionally selective neurons. We performed 20 recordings, but focus on 10 sessions where we recorded at least 7 neurons simultaneously (median: 10 neurons).

4.2.2 Spike Sorting

In monkey P, spike sorting was performed by hand refinement of a standard clustering algorithm (Plexon Offline Sorter v3). Single unit isolation quality was established using SNR (Kelly, Smith, Samonds, Kohn, Bonds, Movshon & Lee 2007). In monkey N, spike sorting was performed by fitting a mixture of Gaussians model to clipped waveforms in a reduced dimensional space (Tolias, Ecker, Siapas, Hoenselaar, Keliris & Logothetis 2007). In both monkeys, sorting was refined by maximum aposteriori estimation of a model where the multi-electrode voltage was the linear superposition of Gaussian white noise and the spike waveforms (Pillow et al. 2008, Pillow et al. 2013). We included all units that had no refractory period violations and spike rates that did not change by more than 10% after refinement algorithms. We found this was largely single units, but also likely included some multiunit clusters.

4.2.3 Stimulus Apparatus and Task

Stimuli were presented using Psychophysics Toolbox. The display LCD had a resolution of 1920 x 1080 pixels and a refresh rate of 60Hz and was corrected to have a linear gamma function. Monkeys viewed the stimulus from a distance of 118cm such that the screen subtended 100 degrees of visual angle.

Monkeys were trained to discriminate the net direction of motion in a field of flickering and drifting Gabor patches. On each trial, the motion strength varied across seven 150ms long epochs (pulses). The strength and direction of each pulse was varied by changing the proportion of Gabors that were drifting. The stimulus is described in detail in Chapter 2.

4.2.4 Preferred direction and tuning functions

MT was mapped using two separate protocols. We used a dynamic flow field to measure the direction preference and spatial RF (Mineault et al. 2012, Cui et al. 2013). Alternatively, we measured the tuning function of an MT cell, by presenting drifting 100% coherence dots in 12 evenly spaced directions and calculating the average spike rate in each direction. The preferred direction was estimated by least-squares fitting of a von-mises function to the spike rate:

$$f(\theta) = r_{min} + (r_{max} - r_{min}) \exp\left(-\beta(1 - \cos(\theta - \theta_{pref}))\right) \tag{4.1}$$

where r_{min} and r_{max} are the minimum and maximum firing rate, respectively, β is the bandwidth, θ is the stimulus direction and θ_{pref} is the preferred direction

of the neuron. In figures 2 and 5, the θ is plotted relative to the direction of the discrimination stimulus.

4.2.5 Population Decoder

We evaluated the population level representation of motion-direction using regularized logistic regression (Bishop 2006). The probability that the direction, y, on any trial y_i was right given the decoding weights, $\mathbf{w}$, and neural response, $\mathbf{r}$, is

$$p(y = \text{right}|\mathbf{w}, \mathbf{r}) = \frac{1}{(1 + \exp(\mathbf{rw}))} \tag{4.2}$$

We estimated the weights using L2 regularization via the glmnet toolbox (Friedman, Hastie & Tibshirani 2010):

$$\hat{\mathbf{w}}(t) = \arg\max_{\mathbf{w}(t)} y^T(\mathbf{r}(t)\mathbf{w}(t)) - \ln(1 + \exp(\mathbf{r}(t)\mathbf{w}(t))) + \lambda||\mathbf{w}(t)||_2 \tag{4.3}$$

where $\mathbf{r}(t)$ is a matrix of spike counts on each trial at time bin t augmented by a column of ones to capture a bias term, $\mathbf{w}(t)$ is a vector of weights (one for each neuron and one for the bias), y is a vector of the direction on each trial (1 or right, 0 for left). λ was chosen using 10-fold cross validation. The classification accuracy was evaluated on the test-set.

In some cases we made modifications to the decoder: To compare the fixed decoder to an instantaneous decoder, we took the average spike rate during the motion stimulus to train $\mathbf{w}_{\text{fixed}}$. To evaluate the population level representation of choice, we re-trained weights to maximize the quantity p(c—$\mathbf{w}$,$\mathbf{r}$), where c is a vector of the monkey's choices on each trial. The *correlation-blind*

(CB) decoder was estimated by shuffling the trial identity for each neuron within each condition for the training set. The CB decoder was evaluated on data that was not shuffled.

4.2.6 Choice Probability

Choice probability (CP) is a measure of the predictive relationship between the neural responses and the monkey's choice independent of the stimulus (Celebrini & Newsome 1994, Britten et al. 1996). CP is defined as the area under a receiver operating characteristic (ROC) curve from the pair of response distributions for each choice (Britten et al. 1996). CP is often computed on *zero coherence* trials, which have no expected motion, but have fluctuations in the instantaneous motion strength. Here, unless otherwise specified, we compute CP and population level choice decoders on trials that have zero *expected* motion, but do contain instantaneous fluctuations that vary from trial to trial.

4.2.7 Neurometric Performance

We evaluated the performance of single neurons at different stimulus strengths by evaluating the accuracy of a linear classifier trained to discriminate the net direction of the stimulus using only the spikes from the neuron. The percent correct of a linear classifier for a 1D decision variable is $PC = \Phi(\frac{d'}{2})$, where Φ is the cumulative normal distribution (Duda et al, 2000) and d' is the difference of the means of the response distributions for

the two directions divided by the square-root of the sum of the two variances:

$$d' = \frac{\mu(A) - \mu(B)}{\sqrt{\nu(A) + \nu(B)}}, \tag{4.4}$$

We diverged from classic estimation protocols for neurometric functions that typically use the area under the ROC curve to quantify percent correct (Britten et al. 1992, Uka & DeAngelis 2004) because in this task, which only has one stimulus presentation per trial, the area under the ROC requires the assumption of a hypothetical "anti-neuron" to be interpreted as the percent correct (see Discussion). Note: this interpretation is not required for 2AFC tasks which display both the "signal absent" and "signal present" versions of the stimulus on each trial (Green & Swets 1966). Both our discrimination task and the classic "dots" task fit display only one stimulus presentation on each trial, thus the assumption of an "anti-neuron" is required to interpret the area under the ROC curve in terms of accuracy of an ideal observer. We compare this assumption directly in the domain of choice probability in figures 8 and 9.

4.2.8 Psychophysical and neuronal threshold

To quantify psychophysical and neuronal thresholds, we fit a cumulative Weibull function to the accuracy of the monkey or neuron.

$$\text{p(correct)} = 1 - .5 \exp\left(-(\frac{s}{\alpha})^{\beta}\right), \tag{4.5}$$

where s denotes the net motion strength, α is the threshold on motion strength (at the 82% level), and β is the slope of the function. We used the fitted values

of α for comparisons of neuronal, population and psychophysical *threshold*.

4.2.9 Psychophysical Kernel

To measure the contribution of each pulse to the monkey's choice on each trial, we used logistic regression, where the probability of the monkey's choice across the dataset is given by:

$$p(\mathbf{Y}|\mathbf{X}, \mathrm{w}) = \frac{\exp(Y^T \mathbf{X}\mathrm{w})}{1 + \exp(\mathbf{X}\mathrm{w})} \tag{4.6}$$

Where $\mathbf{Y} \in \{0, 1\}$ is a vector of the choice on each trial, $\mathbf{X}$ is a matrix of the seven pulses on each trial, augmented by a column of ones to capture the bias, and w is the seven pulse weights plus a bias term. This model was fit using maximum likelihood. Fit results are plotted in Figure 4.1, and error bars were derived from the matrix of partial second derivatives.

4.3 Results

We measured the activity of up to 21 simultaneously recorded MT neurons while monkeys performed a motion-discrimination task (Figure 4.1a). On each trial, the monkey indicated his or her choice about the net direction of motion with an eye movement to one of two targets. The single units in our population have responses during motion that are strongly dependent on the net motion strength during the motion stimulus (Figure 4.1b). The sensitivity of neurons with responses like these have been studied extensively in single unit or cell pair recordings during a similar motion-discrimination paradigm

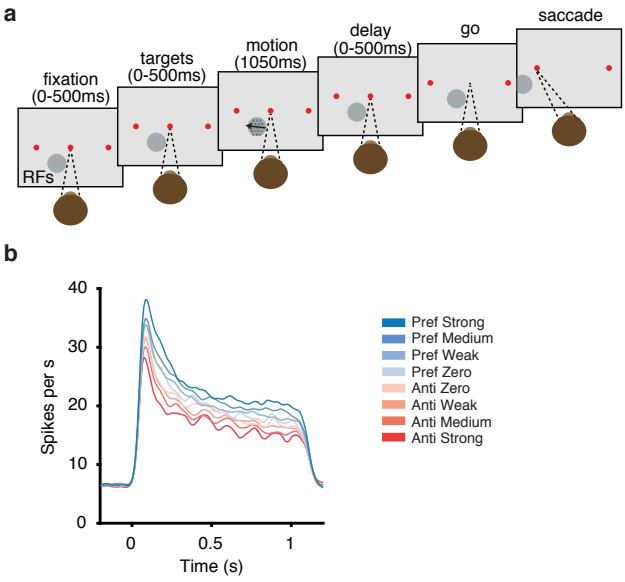

Figure 4.1: Motion-discrimination task and average single neuron responses. (**a**) After obtaining fixation, the monkey holds steady fixation while viewing a 1.05 second long motion stimulus and then waits for a go signal before indicating his or her choice about the net direction of motion with an eye movement to one of the two saccade targets. (**b**) The average response of single MT neurons depends on the net direction and motion strength of the stimulus.

(Britten et al, 1992; Britten et al, 1996; Zohary et al, 1994; Bair et al, 2001, Cohen and Newsome, 2008).

Here, we used a population decoding approach (Georgopoulos et al. 1986, Berens et al. 2012) to study the representation of motion and choice in joint activity patterns of simultaneously recorded units. We used logistic regression in 50ms time bins to decode direction or choice because it is easily fit to data (Friedman et al. 2010), it is biophysically plausible (Schwartz, Pillow,

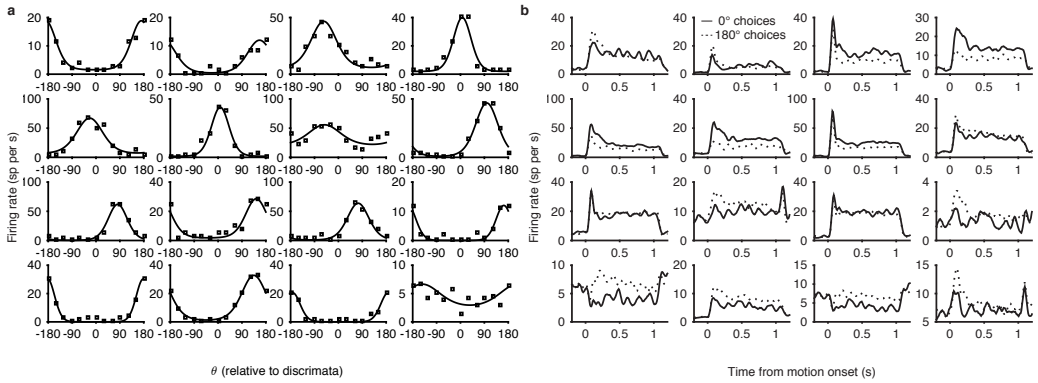

Figure 4.2: Example simultaneously recorded neuron tuning functions and responses during motion-discrimination. (**a**) Firing rate as a function of direction for 16 simultaneously recorded MT neurons. Points indicate the measured firing rate and lines are fits from a von-mises function (see methods) (**b**) Average choice sorted PSTHs for the same neurons as in (a)

Rust & Simoncelli 2006, Berens et al. 2012), and it has been recently used in a similar paradigm to measure single-trial activity (Kiani et al. 2014). This decoder is similar to previously proposed pooling mechanisms for decoding motion direction from MT (Shadlen et al. 1996, Cohen & Newsome 2009), where the sign of the weights indicates a neuron's membership in a different pool and the magnitude of the weigh indicates each neuron's contribution to its respective pool.

4.3.1 Population decoder is better than best single neuron

A large proportion of MT neurons are directionally selective when recording with single electrodes (Albright 1984), and we found a similar preponderance of directionally selective cells in our array recordings. Figure 4.2a shows the responses of 16 simultaneously recorded neurons to different di-

rections of motion. These same cells were responsive in a direction-selective manner during the motion-discrimination task (Figure 4.2b).

Previous comparisons of the performance of single neurons to the behavior of a monkey on a similar motion-discrimination task found that, given 2 seconds of viewing duration, single neurons can out perform the monkey. However, when viewing duration is dictated by the monkey in a response time paradigm, the monkey's performance is significantly better than the single neurons (Britten et al. 1992, Cohen & Newsome 2009). This is likely because the monkey does not use all of the stimulus to form decisions (Huk & Shadlen 2005, Uka & DeAngelis 2003, Kiani et al. 2008).

We compared single neurons in our sample to the performance of the monkey and to the performance of the population decoder. To relate to previous work, we compared neurometric and psychometric performance. Figure 4.3a-d shows four example sessions psychometric function (black) compared to the population decoder (red) and the best single neuron from that session (gray).

Since our recordings sample MT neurons in the vicinity of the probe, we do not only sample neurons that are perfectly targeted by the stimulus (Figure 5a shows neuron sensitivity as a function of relative preferred direction). Thus, we compared neurometric and psychometric performance in two ways: First, we compared the ratio of the total accuracy of each single unit to the monkey and the total accuracy of the decoder to the monkey (Figure 4.4c). The geometric mean of the distribution of single neuron ratios was significantly lower

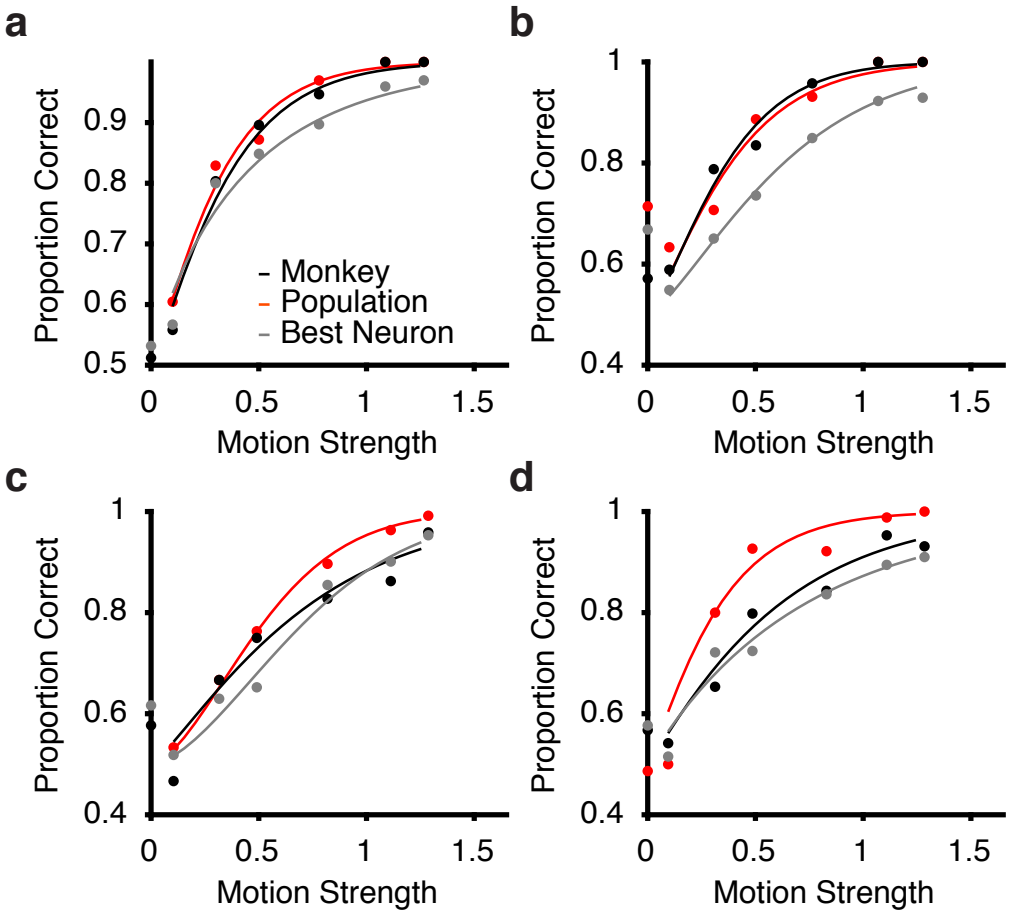

Figure 4.3: Example population neurometric functions and psychometric functions **(a,b,c,d)** Example sessions psychometric function (black) and respective neurometric functions for the population decoder (red) and the best single neuron (gray)

than 1 (0.76; p=1.3956e-71, t-test) meaning that the monkey performed better than the average unit. This is not surprising, as we recorded from many neurons that were not optimally targeted by the direction of the discrimination stimulus. We further analyzed a subset of "elite" neurons that were suffi-

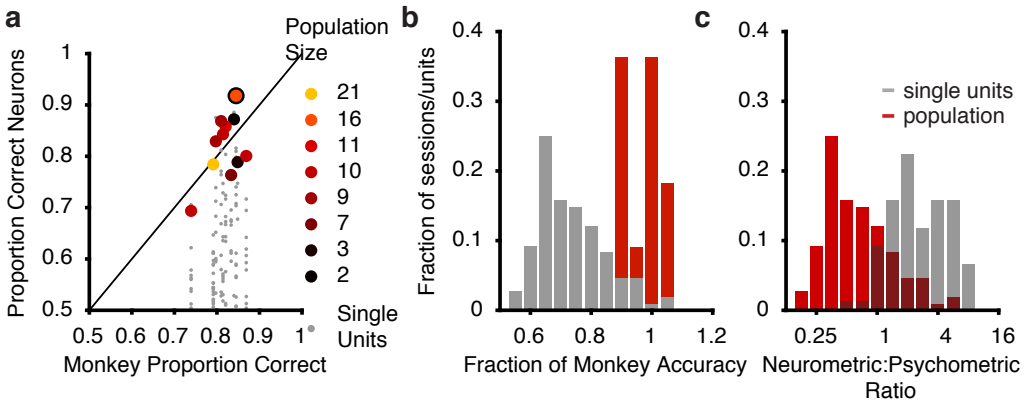

Figure 4.4: Comparison of neural decoder to psychophysical performance (**a**) Proportion correct of the monkey plotted against the proportion correct for the population decoder (oranges) and single neurons (gray points). The example session from (A) is circled in black.(**b**) Fraction of the monkey's accuracy (proportion correct) achieved by single units (gray) and by the population decoder (red)(**c**) ratio of the neurometric:psychometric threshold at the 82% level.

ciently well-targeted by the discrimination stimulus (n=67) to perform better than 85% correct at strong motion strengths. We then calculated the ratio of the threshold for the neurometric and psychometric functions. Here ratios greater than 1 indicate that the neuron performed worse than the monkey (see methods). Even with this subset of neurons, the geometric mean of the distribution was significantly larger than 1 (2.1325, p= 1.5259e-12). This number is similar to previously reported neurometric-psychometric ratios (Cohen & Newsome 2009). We also compared the performance of the population decoder to the monkey. The geometric mean of the distribution of the decoder ratio for the 10 sessions with 7 or more neurons was not significantly different than the monkey's performance (1.08; p=.3277 t-test), meaning the monkey

did not do better than the population decoder and the decoder did not do better than the monkey on average (5 sessions were greater than 1 and 5 sessions were less than 1). 3 single neurons outperformed the monkey (6% of the elite group), thus we further compared the population decoder to the single units that were recorded on the same day to see if the population performed better than the best single neuron.

On each session, the population decoder performed better than the average of the single units for that day (Figure 4.5a). This result is trivial. In theory, the population decoder should have a lower bound at the performance of the best single neuron, since the weights of all other neurons could just be set to zero to achieve this result. We found that this was mostly true and the population performed as well as if not better than the best single neuron (Figure 4.5b). In general, the population decoder was significantly better than the respective best single unit (p=2.3526e-04, t-test). The performance of the population decoder depended strongly on the best single unit, but also depended on the size of population (linear model: bestNeuron: .94, p=8.402e-11; number of neurons: .0065, p= 0.00012157). These results confirm that MT populations are sufficiently sensitive to explain the monkey's performance and that (with small numbers) pooling from more neurons improves performance. This improvement was often relatively small over the best single neuron, which could be explained by noise correlations between neurons or because of the low sensitivity of other neurons in our sample. Thus, we asked the decoder needs to know the correlation structure by comparing a decoder that assumes the

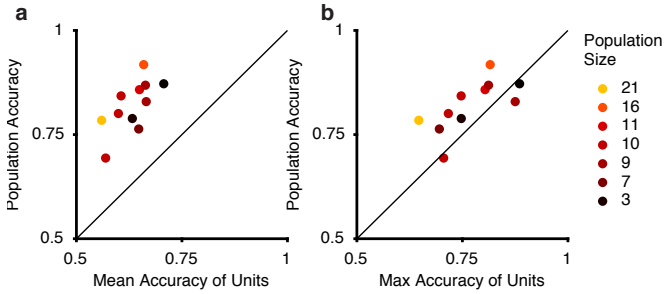

Figure 4.5: Population decoder performs better than single units (**a**) Accuracy of the population decoder plotted against the mean accuracy of the units from each session. (**b**) Accuracy of the population decoder plotted against the accuracy of the best single neuron from each session.

neurons have independent noise to one that was trained on the real patterns of activity.

4.3.2 Knowledge of the correlation structure is not required to decode direction

Noise correlations are widespread in cortex (Cohen & Kohn 2011) and these correlations between neurons can improve or limit sensory encoding depending on their structure (Averbeck et al. 2006, Ecker et al. 2011, Moreno-Bote et al. 2014). Previous studies have reported contradictory results decoding from ensembles of V1 neurons. Recordings from anesthetized monkey using random subsets of 20 neurons found that correlation blind decoders performed worse that a decoder that was sensitive to the true joint distribution of spiking activity (Graf et al. 2011). Contrary to this, another study recording from V1, but in awake-fixating monkeys, found that it was not necessary to know the full neural response distribution an a characterization of the individ-

ual stimulus-response properties of neurons was sufficient (Berens et al. 2012). A possible difference in these two studies is the magnitude of pairwise correlations that were present in the data. The second study had noise correlations that were an order of magnitude smaller than is often reported from V1 (Ecker et al. 2010, Cohen & Kohn 2011). We analyzed 800 cell pairs from our dataset and found that noise correlations were largely positive (Figure 5c). The mean noise correlation was significantly larger than zero (.10; p=3.3758e-39, t-test). We recorded from many neurons with different tuning functions (Figure 5a preferred direction on x-axis), thus noise correlations structure in high-dimensions could carry additional information about the stimulus direction.

We compared single neuron sensitivity to the decoding weights we measured, and then compared a correlation-blind decoder to our population decoder. Figure 5a shows the single neuron sensitivity as a function of offset in preferred direction from the stimulus axis. Unsurprisingly, neurons that were well targeted by the stimulus (tunings near 0 or 180) had d-prime values that were significantly different than 0 (after adjusting for direction: mean=.54; p=4.8271e-11, t-test) and neurons that were orthogonal to the task did not (mean=-0.05; p=0.5111, t-test). We found that this relationship was well described by a cosine function (r^2=.57). We found a similar pattern in the decoding weights for each neuron (Figure 5b), but with less of a dependence on cosine of the angle between the stimulus direction and the preferred direction of the single neuron ($r^2 = .33$). To compare the performance of a correlation-blind decoder to the full decoder, we used logistic regression, trained on shuffled data

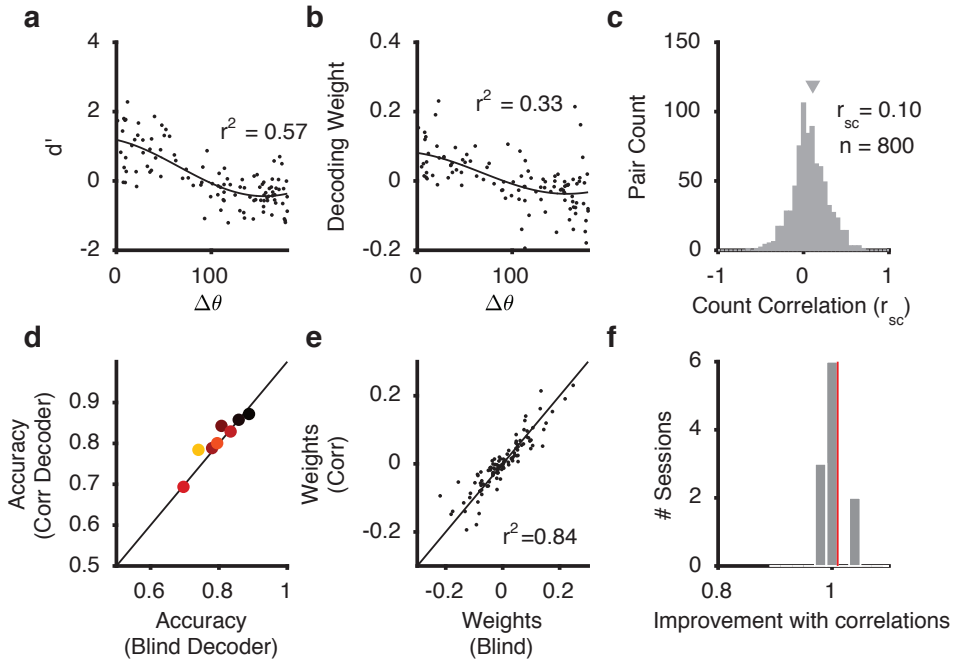

Figure 4.6: Correlation-Blind decoder performs as well as full population decoder(**a**) Points are the sensitivity of single neurons (d') plotted as a function of the angle between their preferred direction and the stimulus direction. Black line is a cosine fit which explains 46% of the variance. (**b**) Individual neuron weights, as trained by the population decoder and cosine fit (same as in (a))(**c**) Pairwise noise correlation measured on repeat trials for 800 MT pairs.(**d**) Comparison of the accuracy of a correlation-blind decoder to decoder trained on the full response distribution. Colormap is the same as in Figure 4(**e**) Correlation between individual neuron weights for the correlation-blind decoder and the full decoder.(**f**) Ratio of the performance of the full decoder over the performance of the correlation-blind decoder.

(see methods) and tested on the real data. The correlation-blind decoders performance was strongly correlated with performance of the full decoder (Figure 5d; ρ=.992, p=1.5424e-20). The recovered weights for the correlation-blind decoder were also strongly correlated with the full decoder weights (Figure 5e;

ρ=0.9359, p=4.1339e-77). We compared the performance of the correlation-blind decoder to the full decoder (Figure 5f). The correlation-blind decoder achieved 98% if the accuracy of the full decoder on average. This amounts to a difference in accuracy of less than 1% (-0.008; p=0.006, t-test). Thus, despite positive pairwise noise-correlations, the read-out mechanism need not know the correlation structure to reach the full decoder performance on this task. We next asked how direction could be decoded over time and how complicated the temporal structure of the weights needs to be.

4.3.3 Population is most sensitive during the transient phase

We evaluated the temporal information available in the population by decoding from the instantaneous spike rate in a 50ms sliding window. For each time bin we trained new weights and evaluated the performance of those weights on test data (see materials and methods). We found that weights were flat before motion onset, and began to diverge 60ms after motion onset (Figure 6a,b). Once they diverged from 0, they had a systematic structure that depended on preferred direction of the neuron (Figure 6b,c). This structure was maintained across the entire motion epoch (Figure 6b) and was very similar to the cosine dependence in the weights that were trained on the entire motion epoch (Figure 5b, 6c). We compared the performance of the instantaneous decoder to a decoder with fixed temporal weights (Figure 6d). Both decoders had a similar shape over time, although the instantaneous decoder had a marked advantage outside of the motion epoch in that it could fit the

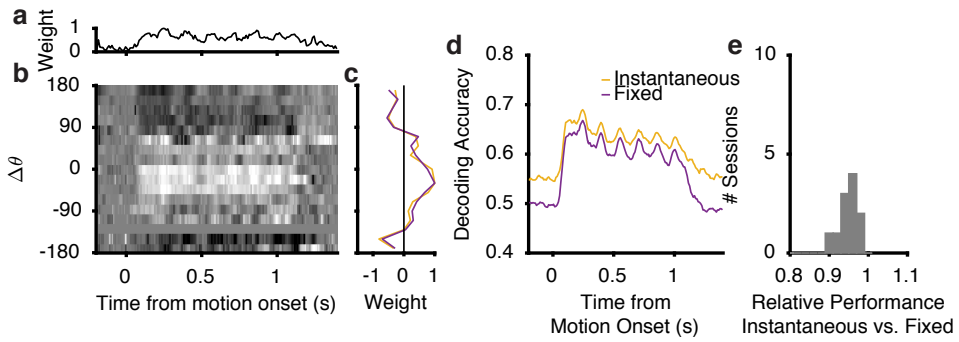

Figure 4.7: Comparison of instantaneous decoder to fixed temporal weights(**a**) average absolute value of the instantaneous decoding weights over time (normalized to a maximum of 1)(**b**) Average instantaneous decoding weights sorted by preferred direction of the neuron (relative to the stimulus) and plotted for each time bin.(**c**) There is a close correspondence between the shape of the marginal instantaneous weights (yellow) and the fixed weights (purple). The marginal of the instantaneous weights was calculated by averaging over the motion epoch (from 0.1 to 1.1 seconds)(**d**) The accuracy of net-direction decoding of the instantaneous decoder plotted over time (yellow) and compared to the accuracy of a fixed decoder (purple) averaged across all sessions(**e**) the ratio of the fixed decoder to the instantaneous decoder. Mean of the distribution is .96

monkey's bias (Figure 6d).

We compared the performance of the two decoders by averaging their accuracy during the motion epoch (Figure 5e). In general, the fixed decoder did slightly worse than the instantaneous decoder (p=8.0544e-38, t-test), achieving 96% of the performance of the instantaneous decoder, which amounts to 2% correct worse on average. We noticed that although this difference was sustained throughout the motion epoch, both decoders did seemed to perform slightly better during the transient phase of the spiking response (Figure 6d). This is not due to the stimulus, which is equally informative about the net

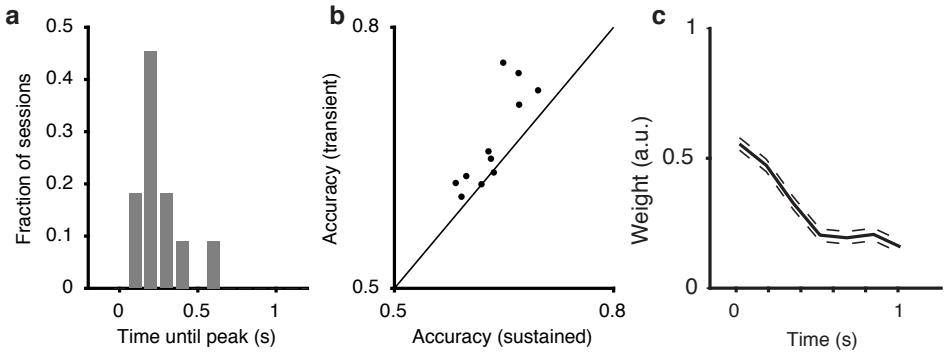

Figure 4.8: Peak decoding performance happens early in the motion epoch (**a**) Fraction of sessions that reach their peak decoding performance at the time bin on the x-axis. The mean peak performance is at 285ms. (**b**) Comparison of the average decoding accuracy during the transient (100-300ms) and the sustained period that follows (300-1000ms). (**c**) Average psychophysical weighting of the monkeys.

direction over time. Across our sessions, the peak performance was reached, on average, 285ms after motion onset, and 80% of sessions reached peak performance within the first 400ms (Figure 7a). We averaged performance during the early transient phase (100-300ms) and compared it to the performance during the sustained period (300-1000ms). Figure 7b shows the comparison of the transient phase to the sustained phase. The population was clearly more sensitive early in motion viewing.

4.3.4 Decoding choice: Listening to a single neuron vs. listening to a population

In neuroscience, choice probability (CP) is a popular metric for measuring how predictive a single neuron's activity is of the choice on each trial. Introduced by (Britten et al. 1996), the primary appeal of CP over a decod-

ing framework, like we've used in the rest of this paper, is that is quantifies the relationship between neuron activity and choice independent of the overall probability of the choice, by integrating over all possible criterion levels (Green & Swets 1966). In practice, CP is computed by taking the area under the receiver-operating-characteristic (ROC) curve for the distribution of spike counts for each choice outcome (Britten et al. 1996, Green & Swets 1966). This value can be interpreted as the percent correct one could predict the organism's choice given spikes from the neuron under study and spikes from a hypothetical "anti-neuron" with identical response properties except that it has the opposite preferred direction. In our datasets, we often recorded from neurons with opposite direction preferences (ie. real neuron anti-neuron pairs).

Figure 4.9a illustrates the classic signal detection theory approach to measuring sensitivity. If there are two states of the world, "right" and "left", then there are two distributions that describe the probability of a response given each of the two states. If the observer is presented with one stimulus draw (randomly selected from either distribution) on each trial, then over trials he must learn how to place his criterion so as to maximize accuracy. It can be shown that if the two states are equally likely a priori, then the optimal criterion should be set where the two distributions cross (i.e. where the likelihood-ratio is 1). The setting of the criterion directly affects the proportion of correct identifications of the stimulus (Hits) and the proportion of false alarms, which can be visualized with an ROC curve (Figure 4.9B). The criterion shown in A is illustrated on the ROC curve as the open circle. The

performance of the subject is also directly related to these two quantities

$$p(\text{Correct}) = \frac{1}{2}\int_{c}^{\infty} p(r|\text{right})dr + \frac{1}{2}\int_{-\infty}^{c} p(r|\text{left})dr \tag{4.7}$$

assuming left and right are equally likely, where c if the criterion. This quantity is equal to the cyan shaded area in figure 4.9B. The quantity on the left of the equation is just the probability of a hit and the quantity on the right is 1 - p(FA). By carving up the area in figure 4.9B, it is easy to see that the quantity in the cyan are is equal to the percent correct of an observer given a fixed criterion.

If the observer is given two observations on each trial, one from each state of the world, (which is referred to as a two-alternative force choice task (2AFC)), then no learning of the criterion is required. This is because the subject simply needs to compare the two samples to each other. For example, if the monkey in our study has only two MT neurons, one that prefers right motion and one with equal and opposite tuning that prefers left, then his response should align with whichever neuron fired more. The ROC curve give us insight into how this works. The first sample effectively sets the criterion for the second sample. If the second sample is larger, then it is likely that it came from the "right" distribution. Thus, to measure the percent correct in a 2AFC task, one must integrate over all possible criterion which corresponds to the gray shaded area under the ROC curve.

The area under the ROC curve maps onto the percent correct the monkey would achieve with a neuron anti-neuron pair. It has a square-root of 2

improvement over the performance with a single neuron. That improvement most directly results from he information gained by being able to set the criterion on each trial according to one of the samples. This is equivalent to gaining two independent samples of each trial. Needless to say, choice probability does not equal the percent correct the monkey would achieve if decoded one neuron. This theoretical relationship is plotted as the red line in figure 4.9d. Our data closely corresponded to this theoretical relationship (as they should). Thus, to fairly compare the information in our population to the information in a single neuron, rather than assume a hypothetical "anti-population", we compared the performance of single neurons directly.

Just as with the stimulus decoding above, we compared the population decoder to single neurons. The population had more information about the subject's choice than the best single neuron (Figure 4.10b. The population did not perform better than the best single neuron anti-neuron pair (Figure 4.10d.

4.4 Discussion

Here we analyzed the performance of a simple population decoder that used single MT neurons to perform a coarse direction-discrimination task. We found that the population decoder is sufficient to explain the monkey's behavior even though the single neurons are not. The full joint statistics of neural responses were not helpful for decoding over a much simpler, correlation-blind decoder. This differed from the results of (Pillow et al. 2008, Graf et al. 2011), which both found that the joint statistics carried information about

the stimulus. In the light of those studies, our result is somewhat surprising. The only other study that similarly found no improvement with correlations (Berens et al. 2012) had an order of magnitude lower noise correlations that we observed in our MT population. We believe this is largely due to the task complexity. Our study decoded only two conditions, whereas the others had multiple stimulus orientations (Graf et al. 2011, Berens et al. 2012) or decoded the full stimulus in pixel space (Pillow et al. 2008).

We also found that the population of MT neurons is most sensitive early in the motion epoch, immediately following stimulus onset. This may result from individual neuron signal to noise (Churchland, Yu, Cunningham, Sugrue, Cohen, Corrado, Newsome, Clark, Hosseini, Scott, Bradley, Smith, Kohn, Movshon, Armstrong, Moore, Chang, Snyder, Lisberger, Priebe, Finn, Ferster, Ryu, Santhanam, Sahani & Shenoy 2010). It is possible that this property makes startegies that integrate the beginning of the stimulus (such as accumulation to bound) more advantage than ones that weigh later parts of the stimulus. The monkeys both used the beginning of the motion stimulus to inform their choices as well. It is possible that they are sensitive to the sensitivity of their neurons and are weighing them over time in proportion to the their reliability, much like a cue-combination task (Ernst & Banks 2002). The relationship is purely correlative here and could go in either direction: simple sensory adaptation (Priebe et al. 2002) causes early weights or because the monkey is "paying attention" (Treue & Maunsell 1996) early makes the population more sensitive. Future work could focus on biasing the monkey's

strategy to be late by manipulating aspects of the stimulus statistics.

Finally, we showed that the population has more info about choice than single neurons, but CP over-estimates the info available in a single neuron. Recordings from many neurons in neighboring columns with opposite direction-selectivity can constrain this relationship with empirical measurements. Overall, it is still likely that the tasks are too simple. Taken together, these results reenforce the idea that population decoding methods are a powerful tool to generalize beyond results from single neurons.

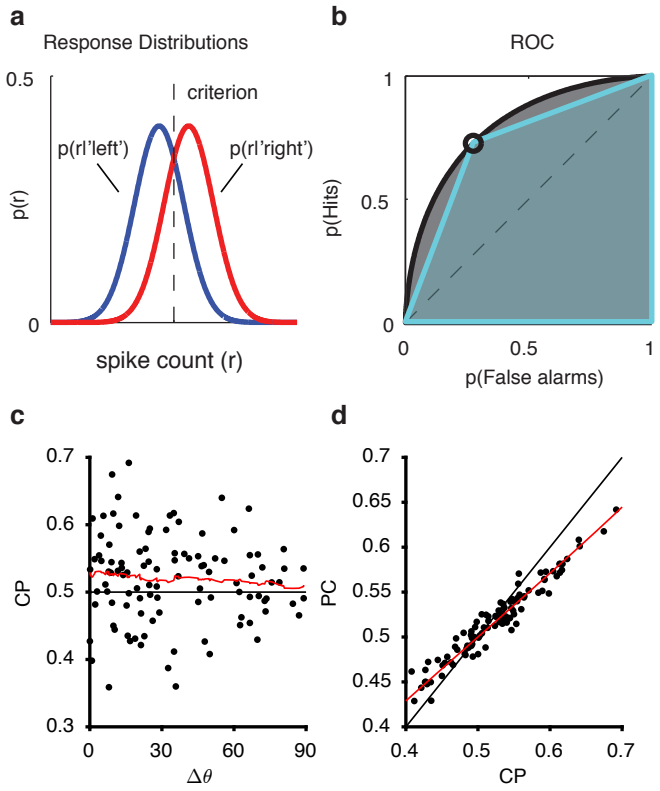

Figure 4.9: What does the hypothetical "anti-neuron" add? (**a**) hypothetical response distributions for the two choices. If the two distributions intersect at only one point (ie. the log-likelihood ratio is monotonic), and the probability of each response is equal, the optimal readout criterion is placed at the intersection. (**b**) Receiver Operating Characteristic curve (black) for the distributions in (a) plots the probability of falsely reporting right vs the probability of correctly reporting 'right' at all criterion levels. Black circle indicates the point corresponding to the ML decision rule. Choice probability (area under the black curve) measures accuracy based on the response of a neuron/anti-neuron pair. As expected, CP is greater than the readout probability (area under cyan curve), which is the accuracy of the ML decoder based on the response of a single neuron. (**c**) Measured CP of single neurons as a function of their offset in preferred direction from the stimulus direction.(**d**) the theoretical relationship between percent correct of the single neuron ML decoder and Choice probability (red) and measured empirically on single neurons (black point)

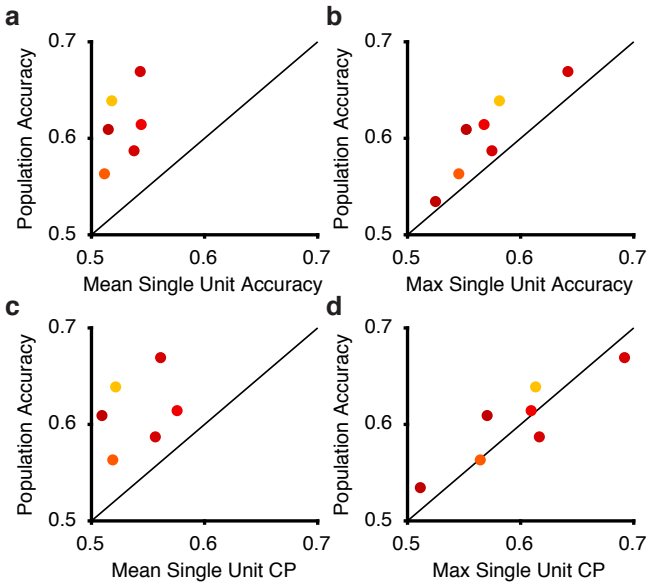

Figure 4.10: Single neuron and population information about choice(**a**) Population accuracy about choice compared the the mean of the single units from each corresponding session.(**b**) The population had more information about the monkey's choice than the most informative single neuron. (**c**) Comparison of the population decoder to the average choice probability from each session. The populations exceeded the average CP(**d**) Comparison of the population decoder to the maximum choice probability from each session. The population only performed as well as the best single neuron by this metric. Thus, the hypothetical anti-neuron often had more information than the neurons in our recorded populations.

Chapter 5

Discussion

A large body of work has suggested that the lateral intraparietal area (LIP) is involved in the accumulation of sensory evidence that is represented in the middle temporal area (MT) to subserve decisions about motion. In this thesis, I have described my efforts to probe this circuit using descriptive statistical models, large-scale recording techniques, and causal manipulations.

There are two main parts to the central body of work described here. In the first part (chapter 3), I use a unified statistical framework to measure the signal transformations from the stimulus to MT, from MT to LIP, and to measure how trial-by-trial variability is shared across neurons. I found that the representation of signal in MT contained non-trivial temporal dynamics, where the responses to motion were stronger early in the stimulus than later. LIP neurons contained a signature of motion integration, which was multiplexed on top of choice-dependent ramps, and could be explained with temporally integrated average MT responses. Thus, the simple signal transformation between MT and LIP that has been proposed in the past (integration) was not sufficient to explain the strong ramping activity in LIP. Additionally, trial-by-trial variability was not shared between the two areas and LIP activity did not

depend on MT. In the second part (chapter 4), I use a decoding approach to measure the information available in small populations of MT neurons.

5.0.1 A unified framework for studying neural and behavioral responses

A hallmark of this thesis is the use of a unified statistical encoding framework for understanding the computations at multiple levels in the cortical hierarchy. The model in question, a Generalized Linear Model (GLM), was able to describe the response properties of single MT and LIP neurons, as well as small neural ensembles. Additionally, a GLM was used to understand the psychophysical weighting of the subjects. The GLM is flexible and tractable, yet in my opinion, its key strength is interpretability. The stimulus filters in chapter 3 can be thought of as the temporal receptive field of each neuron. The coupling filters reflect the shared input and local connectivity in groups of neurons. Importantly, the GLM allowed for the direct comparison of different hypotheses about the connectivity within and between MT and LIP. In particular, I showed that local cortical activity was more predictive than the stimulus for both MT and LIP. This strongly contrasted with inter-areal functional connectivity, which contained no additional explanatory information about single trial activity in either area.

5.0.2 Signal transformations and interareal correlations

The lack of measurable feedforward coupling from MT to LIP was somewhat disappointing. At first glance, the lack of trial-by-trial correlation be-

tween MT and LIP seems at odds with the logic of the task and the presence of an integrated motion signal in LIP, which strongly suggest that activity that is present in MT does appear later in LIP. However, in may ways the lack of correlations is not all that surprising.

What could cause this lack of inter-areal correlation? It is possible that this result simply recapitulates what is known from the anatomy: that connections between areas are sparse (Markov et al. 2014). Additionally, inter-areal correlations follow specific laminar dependent patterns with ascending (feedforward) pathways projecting from superficial layers to layer IV and descending (feedback) projecting from deep layers (V, VI) to superficial and deep layers (Felleman & Van Essen 1991). Here, although we were recording with linear electrode arrays, MT and LIP are deep within sulci and thus we do not know the layer we are recording from. It is therefore possible that we simply have missed the anatomical connections that are known to exist. If this is all we have learned here, then there is still an interesting consequence, which is that we don't really understand how sparse inputs can shape responses across an entire network of neurons. It remains unknown how direct projections could be so weakly correlated. I believe it is likely that this dilution of inter-areal correlation occurs through the processing of many intermediate stages. There is a lot of reason a priori to believe that the relationship between MT and LIP is indirect: The monkey must flexibly map motion signals from one region of the visual field to targets that are in entirely separate retinotopic locations. It seems highly unlikely that the anatomical connections that exist between MT

and LIP can support this type of flexible mapping across each experimental session (Shadlen & Newsome 1996).

The decoding results from chapter 4 hint at one reason why MT and LIP might appear so closely related in their average responses, yet so distant in their trial-by-trial activity: If LIP is reflecting the decision rather than the integration of MT, then it will be robust to any small fluctuations in MT activity. In chapter 4, I found that a very simple decoder performed as well as more sophisticated ones. This is not entirely surprising, given that single neurons in MT are so sensitive, but it makes a very simple point with regard to decision-making paradigms. It suggests that a neural decision variable could easily be robust to fluctuations in activity across MT neurons. That is, the probability that a stimulus is moving to the right, might saturate (at 1 or 0) with very little time and few neurons, and thus activity in the decision stage no longer can depend on fluctuations in MT (because it is saturated at 1).

5.0.3 MT-LIP accumulation model

More broadly speaking, the work in this thesis suggests the burgeoning field of cognitive neuroscience has been using a model to understand higher cognition that fails to describe the data at every stage. The model fails to describe MT sensitivity and choice probability (Cohen & Newsome 2009). Simple integration of MT over estimates coherence dependence and underestimates choice dependence (Mazurek et al. 2003) (and Chapter 3). Trial-by-trial variability in LIP activity does not readily depend on spiking activity in MT (chapter 3).

LIP is not causally linked to the choice behavior (Appendix A) and single trial dynamics are not well described by bounded accumulation (Appendix B).

Extensions of this model that describe realistic time-varying responsiveness to direction in MT (chapter 3) and sensitivity to direction (chapter 4) may reconcile the failure of the accumulator model to capture choice-probability and sensitivity in MT during short duration stimuli, however, the lack of a causal role in LIP cannot be reconciled so easily. Of course, choice-dependent ramps are present in many different areas of the brain (Shadlen & Newsome 1996, Shadlen & Kim 1999, Horwitz et al. 2004, Ding & Gold 2011). However, many brain areas have substantial proportions of directionally selective neurons (besides MT) (Lennie 1998) yet inactivating MT has profound effects on performance (Newsome & Pare 1988)(Appendix A).

5.0.4 Future directions

It seems quite likely that the neural representation of a decision variable exists at the level of populations of neurons. Neurons throughout the parietal and frontal lobes show mixed selectivity to decision relevant and irrelevant signals (Meister et al. 2013, Fusi, Miller & Rigotti 2016). These types of responses, which seem complex at the single neuron level, can results from simple, flexible computations at the population level (Barak, Sussillo, Romo, Tsodyks & Abbott 2013, Fusi et al. 2016). It remains unknown how the sensory representation, in MT for example, is read out by higher brain areas. Future experiments may be able to take advantage of recent advances in ge-

netic tools to trace the MT projection neurons *in vivo* and more directly test these hypotheses (Belmonte, Callaway, Churchland, Caddick, Feng, Homanics, Lee, Leopold, Miller, Mitchell, Mitalipov, Moutri, Movshon, Okano, Reynolds, Ringach, Sejnowski, Silva, Strick, Wu & Zhang 2015).

Appendices

Appendix A

Dissociated functional significance of decision-related activity across the primate dorsal stream

Here I describe an experiment that was performed in collaboration with a fellow graduate student, Leor Katz. This work has been submitted for publication, Katz LN, Yates JLY, Pillow JW, Huk AC. For a more detailed description of the experiment and results, I highly recommend reading Leor's dissertation.

A.1 Summary

During decision-making, neurons in multiple brain regions exhibit responses that are correlated with decisions (Britten et al. 1996, Shadlen & Newsome 2001, Gu, DeAngelis & Angelaki 2007, Ding & Gold 2013, Liu, Gu, DeAngelis & Angelaki 2013, Hanks, Kopec, Brunton, Duan, Erlich & Brody 2015). However, whether or not various forms of decision-related activity are causally related to decision-making remains uncertain (Nienborg & Cumming 2010, Cohen & Kohn 2011, Pitkow, Liu, Angelaki, DeAngelis & Pouget 2015). Here we test the functional significance of decision-related ac-

tivity by recording and reversibly inactivating the lateral intraparietal (LIP) and middle temporal (MT) areas of rhesus macaques performing a motion direction discrimination task. Neurons in area LIP exhibited firing rate patterns that directly resemble the evidence accumulation process posited to govern decision making (Shadlen & Newsome 2001, Brunton, Botvinick & Brody 2013), with strong correlations between their response fluctuations and the animal's choices.

Neurons in area MT, in contrast, exhibited weak correlations between their response fluctuations and animal choices, and had firing rate patterns consistent with their sensory role in motion encoding (Britten et al. 1996). The behavioral impact of electrophysiological inactivation of each area was inversely related to their degree of decision-related activity: while inactivation of neurons in MT profoundly impaired psychophysical performance, inactivation in LIP exerted no measurable impact on decision-making performance, despite having inactivated the very clusters that exhibit strong decision-related activity.

Although LIP inactivation did not impair psychophysical behavior, it did influence spatial selection and oculomotor metrics in a free-choice control task. The unaltered performance in the decision-making task was stable over trials and sessions, ruling out several forms of compensation, and was robust to changes in stimulus type and task geometry. Thus, decision-related signals in LIP may not be necessary for computing perceptual decisions. If they are, then downstream "read out" mechanisms must be more flexible and/or different

than traditionally assumed. More broadly, our findings reveal a dissociation between decision correlation and causation, showing that even strong neuron-decision correlations may reflect secondary or epiphenomenal signals, which do not necessarily constitute a computational crux for task performance.

A.2 Methods

A.2.1 Monkey preparation

We performed electrophysiological recordings and reversible inactivations in the middle temporal (MT) and the lateral intraparietal (LIP) cortices of two rhesus macaques (subject N and subject P), aged 10 and 14 years, weighing 7.7 and 10 kg, respectively. Subject N had a single custom-machined titanium chamber that enabled access to both MT and LIP on the right hemisphere, guided by MRI. Subject P had a cilux chamber (Crist Instruments) over the right LIP and another over the left MT. Standard surgical procedures were applied (Meister et al. 2013). All experimental protocols were approved by The University of Texas Institutional Animal Care and Use Committee and in accordance with National Institute of Health standards for care and use of laboratory animals.

The subject sat comfortably while head-posted in a primate chair (Crist Instruments), facing a linearized 55 inch LCD (LG) monitor (resolution = 1920 x 1080p, refresh rate = 60Hz, background luminance = 26.49 cd/m2) at a distance of 118cm, in a dark room. Eye position was recorded using an Eyelink eye tracker (SR Research), sampled at 1 kHz. A solenoid-operated reward

system was used to deliver liquid reward to the monkey. Stimuli were generated by using the Psychophysics Toolbox (Brainard 1997) in MATLAB (The MathWorks), and task events and neural responses were recorded (Plexon) using a Datapixx I/O box (Vpixx) for precise temporal registration. All of these systems were integrated using the PLDAPS system developed in our lab (Eastman & Huk 2012).

A.2.2 General procedure and experimental design

Recording sessions in either MT or LIP began by lowering an electrode to the known location of the area based on previous mapping and recording sessions. Anatomical identification (MR guided in monkey N; previously established in monkey P (Meister et al. 2013)) was followed by functional identification (mapping receptive/response fields (RF) of MT and LIP neurons, detailed below). Inactivations of either area began by lowering both a cannula and multichannel electrode to the region of interest, collaterally, at least 1mm apart. The electrode was used to (i) confirm that the cannula is within the target cortex, (ii) to record electrophysiological responses to relevant task events pre-infusion, and (iii) to confirm the electrophysiological silencing of neurons during and after the infusion. Thus, while it is not feasible to precisely measure the inactivated proportion of an area, we do confirm the silencing of a large swath (>1mm radius), on every session (detailed in Inactivation Protocol, below).

MT inactivation was predicted to disrupt motion perception within a

specific region of contralateral space, consistent with MT retinotopic organization (Newsome & Pare 1988, Chowdhury & DeAngelis 2008). The behavioral consequence of MT inactivation was measured by comparing psychophysical performance in the direction-discrimination task, before and after muscimol infusion, within the same experimental session, with the motion stimulus placed inside the inactivated region of space. LIP inactivation was predicted to disrupt spatial selection to contralateral space more generally (Wardak, Olivier & Duhamel 2004, Balan & Gottlieb 2009, Wilke, Kagan & Andersen 2012, Erlich et al. 2015), noting that LIP RF are large and that the topographic organization is less precise than in earlier visual areas (Patel, Shulman, Baker, Akbudak, Snyder, Snyder & Corbetta 2010). The behavioral consequence of LIP inactivation was measured by comparing the proportion of contralateral choices in a double-target memory-guided "free-choice" task, before and after muscimol infusion, within the same session. To measure the impact of LIP inactivation in the direction-discrimination task, we compared psychophysical performance between a pair of sessions, baseline and treatment, in which the treatment session was a muscimol, saline, or sham treatment. The paired sessions took place at the same time of day and after a similar number of tasks and trials, either 1 day apart (n = 28) or 2-3 days apart (n = 6), to minimize the impact of within-session fatigue or motivation on behavior. Behavioral data for the muscimol treatment sessions were collected 15 - 30 minutes after infusion end, and typically completed within 150 minutes.

A.2.3 Direction discrimination task

The principal task employed in all session types was a motion direction discrimination task. Subjects were required to discriminate the net direction of a motion stimulus and communicate their decision with an eye movement to one of two targets. The sequence of task events is presented in Fig. 1a. The timing of each event was randomly jittered from trial to trial (Fig. A.1 B). A trial began with the appearance of a fixation point. Once the monkey acquired fixation and held for 400 - 1200ms (uniform distribution), two targets appeared and remained visible until the end of the trial. 200 - 1000ms after target onset, the motion stimulus was presented at an eccentricity of 5 - 7° for 1050ms. The fixation point was extinguished 200 - 1000ms after motion offset, and the subject was required to shift its gaze towards one of the two targets within 600ms (saccade end points within 3° of the target location were accepted).

We used a reverse-correlation motion stimulus inspired by the classic moving dots stimulus (Newsome & Pare 1988) in which motion was in either one direction or the opposite, with varying motion strength. The motion stimulus consisted of 19 non-overlapping Gabor elements arranged in a hexagonal grid (5-7° across, scaled by eccentricity). The individual elements were set to approximate the RF size of a V1 neuron and in total, the grid approximated the RF size of an MT neuron. Motion was presented by varying the phase of the sine-wave carrier of the Gabors. Each Gabor underwent a sinusoidal contrast modulation with independent random phase to prevent pop-out ef-

fects of individual drifting elements. Gabor spatial frequency (0.9 cycles/$^\circ$, sigma = 0.1 x eccentricity) and temporal frequency (7Hz for monkey N, 5Hz for money P, yielding velocities of 7.77 and 5.55 $^\circ$ /s, respectively) were selected to match the approximate sensitivity of MT neurons.

Each trial consisted of seven consecutive motion pulses lasting 150ms each (9 video frames), producing a pulse sequence of 1050ms in duration. On any given pulse X_i, a number of Gabors would drift their carrier sine-waves in unison to produce motion (signal Gabors), and the remaining would counter-phase flicker (noise Gabors). Signal Gabors on pulse X_i were assigned at random within the grid and all signal Gabors drifted in the same direction.

Motion strength was defined as the proportion of signal Gabors out of the total, the value of which was drawn from a Gaussian distribution, $X_i \sim N(\mu_k, \sigma)$ and rounded to the nearest integer, where μ_k was set to one of five values: -50%, -12%, 0%, 12%, and 50% (negative sign indicates motion in the opposite direction), and σ was set to 15%. Thus, while each pulse within a sequence could take on any value (or sign) from distribution $N(\mu_k, \sigma)$, the expectation of a sequence would be μ_k. Motion strength was then z scored over all sessions, for each monkey separately.

On the motion strength axis, we use positive values to indicate motion towards the hemifield contralateral to the LIP under study, and negative values to indicate motion towards the hemifield ipsilateral to the LIP understudy. We use the term "Proportion choices" to refer to the proportion of choices towards the contralateral target. For consistency, we maintain this convention

throughout the paper, such that even on MT inactivations sessions, psychometric performance is evaluated in relation to the LIP under study.

The monkey was rewarded for selecting the target consistent with the sign of the pulse sequence sum, independent of the distribution k from which they were drawn. On trials that summed to exactly zero, the monkey was rewarded at random. 10% of trials consisted of a frozen random seed, generating identical pulse sequences. In addition to the direction discrimination task described here, we performed a subset of experiments (n = 2) using the classical moving dots stimulus (Newsome & Pare 1988) (Fig. A.7).

A.2.4 Free choice task

A free choice task was used to measure spatial bias to one target over another and confirm a behavioral consequence of LIP inactivation (Wilke et al. 2012, Erlich et al. 2015). The sequence of events within the free-choice task is illustrated in Fig. A.6 A and B. Trials began with the appearance of a central fixation point. At a random time after acquiring fixation (500 - 900ms), two targets were simultaneously flashed for a brief 200ms. Subjects were required to maintain fixation until the fixation point disappeared (600 to 3,000ms after target flash), and then saccade to either of the remembered locations of the two targets. On every trial, target position was determined independently from one another and at random, drawn from a 2D Gaussian with a mean of either [-12, 0] (left target) or [12, 0] (right), and a standard deviation of 2 - 4° for x and 3 - 5° for y position. Means and standard deviations were sometimes

adjusted online to better position the distributions within the LIP RF (when recorded) or LIP inactivated field (when inactivated).

A trial was successfully completed when the monkey's saccade entered a circular window (unobservable to the monkey) around either target and held for 300-500ms (window radius scaled by 0.35° x eccentricity, minimum: 3). Successfully completed free-choices were rewarded on 70% of trials irrespective of the target chosen for monkey N, and 100% of trials for monkey P. Monkey N also performed memory-guided saccades to single targets (30% of trials, randomly interleaved) that appeared randomly in space (uniform distribution), and were rewarded 100% of the time. The adjustments in subject N's task were performed to prevent a spatial bias and decrease feedback reliability that may otherwise influence the subject. Overall performance and inactivation effects were similar between monkeys despite subtle differences in task parameters.

A.2.5 Behavioral analysis

All analyses were performed in Matlab (The Mathworks). Responses in the direction discrimination task were analyzed with a maximum likelihood fit of a two parameter logistic function (Wichmann & Hill 2001) assuming a Bernoulli distribution of binary choices, in which the probability of a contralateral choice is P and ipsilateral choice is 1 - P, where P is given by:

$$P = \frac{1}{1 + e^{-\beta(x-\alpha)}} \tag{A.1}$$

where x is the motion strength value (z-scored over all sessions for each monkey separately; positive values indicate rightward motion), α is the logistic function shift parameter (reflecting the midpoint of the function, i.e., bias, in units of motion strength), and β is the slope (i.e., sensitivity, in units of log-odds per motion strength). Error estimates on the parameters were estimated from the hessian numerically. A four-parameter model including sub-perfect response rates for the top and bottom asymptotes (Erlich et al. 2015) was also considered, but did not confer any advantage over the two-parameter model nor change analysis results, and so we focus on the simpler 2-parameter fit (data not shown). The first 10 - 30 trials of every session were excluded from analysis because motion strength was maximal to "warm up" the animal. Median session length for all baseline and treatment sessions was 409 trials. Sessions were excluded from analysis if the animal either completed less than 250 trials or performed poorly (lapse rate $> 10\%$). For inactivation sessions, all sessions were included regardless of performance. A single inactivation session in monkey P was aborted due to a leak in the infusion system, and was not included in the analysis.

Animal strategy in the direction discrimination task (Figure A.5) was measured by computing psychophysical weights via logistic regression, where the probability of the binary choice Y 0,1 on every trial is given by

$$P(Y|w, X) \;=\; e^{YXw} \;/\; (1 + e^{Xw})$$

where X is a matrix of the seven pulse values on each trial, augmented

by a column of ones to capture the bias term, and w is a vector of the monkey's weights. w was estimated via maximum likelihood estimation using Matlab's glmfit function.

In the free-choice task, spatial bias was computed as the proportion of choices to the target contralateral to the LIP under study. Saccade onset and offset were detected in every task by identifying the time at which eye velocity exceeded 30 °/sec (onset) and returned below 50 °/sec (offset). We only analyzed saccades on trials where the task was completed successfully (i.e. no broken fixations and no saccades outside of the target windows). Saccades were analyzed for reaction time, amplitude, duration, and error amplitude (i.e. distance of saccadic end point from saccadic target). Saccadic reaction times less than 100ms from the go signal were excluded to ensure that only task relevant saccades are analyzed.

A.2.6 Neuronal recordings

Recordings were performed in areas MT and LIP with either single-channel glass coated tungsten electrodes (Alpha Omega) or multi-electrode arrays (Plexon U or V Probe). Neuronal signals were amplified, bandpass filtered, digitized, and saved (Plexon MAP server). Neural waveforms passing a manually-set threshold were isolated for online mapping of their receptive fields (both MT and LIP) and directional tuning (MT).

MT RF locations were hand mapped using drifting dot stimuli in a circular aperture. Once the retinotopic location was identified, direction pref-

erence and selectivity were measured using drifting dot stimuli at 100% coherence in 12 directions. LIP RF locations were mapped with a memory-guided delayed saccade task (Gnadt & Andersen 1988).

In monkey P, offline spike sorting was performed by hand refinement of a standard clustering algorithm (Plexon Offline Sorter v3). Single unit isolation quality was established using SNR (Kelly et al. 2007). In monkey N, spike sorting was performed by fitting a mixture of Gaussians model to clipped waveforms in a reduced dimensional space (Tolias et al. 2007). In both monkeys, sorting was refined by maximum a posteriori estimation of a model, where the multi-electrode voltage was the linear superposition of Gaussian white noise and the spike waveforms (Pillow et al. 2008, Pillow et al. 2013).

A.2.7 Neuronal Analysis

Peri-stimulus time histograms (PSTHs) were computed by aligning spike times to events (motion onset or saccade time), binned at 10ms resolution, and smoothed with a Gaussian kernel with standard deviation of 25ms. Trial motion strengths were binned into three groups (low, medium, high), where "low" was strengths between 0 and 0.25, "medium" was between 0.25 and 1, and "high" was anything greater than 1. We averaged spike rates separately for the three motion strengths for each choice. The buildup rate analysis (Fig. A.2, inset) was performed according to Lafuente et al. (de Lafuente et al. 2015)

A.2.8 Choice Probability

Choice probability (CP) is a metric used to measure the predictive relationship between neural responses and choice, independent of stimulus strength. It is defined as the area under the receiver operating characteristic curve (ROC) for a pair of spiking response distributions sorted by choice (Celebrini & Newsome 1994, Britten et al. 1996). We quantified CP using trials that had zero expected motion and were repeated with identical random seeds (i.e. had no stimulus variation, "frozen noise"). Sometimes more than one random seed was repeated in a session, in which case we calculated the spiking response distributions for each seed separately, subtracted the mean, and then combined them, similar to an analysis known as Grand Choice Probability (Britten et al. 1996). Neurons with >25 "frozen" repeats were included (90/94 MT cells, 96/113 LIP cells), and significance testing against the null (i.e. CP=0.5) was performed using a Student t test. To compare to previous literature, in MT, we counted spikes over a window from motion onset to 200ms after motion offset (before the go signal). In LIP, we counted spikes over a 400ms window counting backwards from the 100ms before the saccade.

A.2.9 Infusion Protocol

Infusions were performed by lowering an infusion cannula into grid locations that had previously yielded the largest number of selective cells during the recording phase of the study. The cannula (31-32 gauge) was lowered alongside a multi-electrode array, at least 1mm away (Fig. A.3 B). The two

were lowered to target cortical areas where functional identification took place (mapping). Infusion was then performed, and electrophysiological silencing was confirmed on the recording electrodes, typically within 15 minutes of infusion start.

Infusions were performed with a syringe pump (Harvard Apparatus) through a single and direct line to the cannula (constant rate of 0.1-0.4μl/min, 15-30 minutes), in agreement with infusion parameters proposed by Noudoost and Moore (Noudoost & Moore 2011). We delivered 6.66-8μg/μl muscimol (in phosphate buffered saline) at volumes of 5-12 μl (mean 7.4μl), netting a total mass of 40-80μg (mean 56.4μg). This protocol was chosen to match the very high end of ranges used previously in order to maximize the probability of neural inactivation. Infusions were typically made at multiple depths within a single cannula track. On 5 of the 21 main LIP inactivation sessions, more than one cannulae were lowered. Cannluae were left in situ for at least 15 minutes after infusion end. Saline infusions followed the same protocol and included both a cannula and multi-electrode array. Sham infusions included only a multi-electrode array but followed similar timings, including the operation of the syringe pump with no syringe attached.

A.2.10 Spatial and temporal extent of Inactivation

Previous analyses of the spatial extent of muscimol inactivation have estimated the functional silencing to cover a spherical radius of roughly 2-3mm (Martin 1991, Arikan, Blake, Erinjeri, Woolsey, Giraud & Highstein

2002, Liu, Yttri & Snyder 2010, Yttri, Liu & Snyder 2013). The study most comparable to ours, Liu et al. (Liu et al. 2010), co-infused muscimol and Manganese (Mn) into LIP of awake macaques and imaged the spread. They also estimated a cortical silencing of approximately 2-3mm in radius, in line with the linear dependence of volume distribution (mm^3) on infusion volume (μl) (Heiss, Walbridge, Asthagiri & Lonser 2010).

In our experiments, lowering both a multi-electrode array and infusion cannula collaterally (Fig. A.3 B) enables direct confirmation of neural silencing at known distances from the cannula tip. This places a lower bound on the spatial extent of functional inactivation. Although our standard protocol placed the multi-electrode array 1mm away from the cannula tip, we sometimes lowered a second array, 2 or 3mm away. On these sessions too, we observed silencing on most recording channels. Taken together, we conservatively estimate neural inactivation in LIP to span a radius of at least 2.5mm, silencing large swaths of LIP while primarily targeting its ventral portion (Lewis & Van Essen 2000, Liu et al. 2010).

On a few occasions, residual firing persisted despite near-complete silencing of electrophysiological activity (example shown in Fig. A.3 B, voltage traces, channels 5 and 6). We tested the selectivity of residual firing with the appropriate mapping task (motion for MT, memory guided saccades for LIP) and found that these spikes did not respond selectively, indicating that these residual spikes likely emanate from afferent fibers terminating within the inactivated area (Chapman, Zahs & Stryker 1991)

Previous LIP inactivation studies found no evidence to support within-session compensation that manifests behaviorally (Wardak et al. 2004, Balan & Gottlieb 2009, Liu et al. 2010, Yttri et al. 2013, Kubanek, Li & Snyder 2015), but see Wilke et al. (Wilke et al. 2012) In fact, studies that report the temporal effect of LIP inactivation find an increase in the lesion's impact over time, not a decrease (Wardak et al. 2004, Kubanek et al. 2015). Regardless, we measured the time course of psychophysical performance within a session, and also measured for compensation on longer time scales, across sessions, to explore the possibility of increasing behavioral robustness to inactivation that might develop over time.

A.3 Results

We investigated the functional significance of decision-related activity by recording and inactivating neural activity in two well-studied cortical areas, MT and LIP, while rhesus monkeys performed a challenging direction discrimination task. On each trial, the monkey maintained stable visual fixation while discriminating the net direction of motion, and then made a saccade to one of two choice targets to communicate their choice A.1. For electrophysiological recordings in MT, we placed the motion stimulus in the receptive field of the neurons and aligned it to the preferred direction of one or more MT neurons on the multi-electrode array. For LIP, we placed one of the two targets in the response field of the neurons, and the other target on the contralateral side of the visual field.

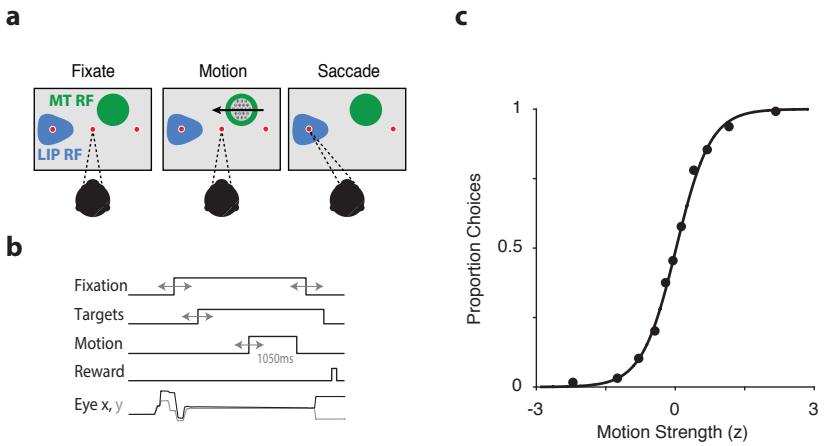

Figure A.1: **A.** Monkeys were trained to discriminate the direction of visual motion and communicate their decision with a saccadic eye movement to one of two choice targets. For MT recordings, motion was placed in the MT receptive field (RF) (green patch). For LIP recordings, one of the saccade targets was placed in the LIP RF (blue patch). **B.** Sequence of task events. Gray arrows indicate temporal jitter. **C.** Psychophysical performance in the task. The proportion of choices (y-axis) made to the target contralateral to the LIP under study, as a function of motion strength (x-axis), where positive motion strength values represent motion towards the target contralateral to the LIP under study.

A.3.1 MT and LIP present canonical electrophysiological responses during direction discrimination

We recorded 157 MT neurons and 200 LIP neurons with either single electrodes or multi-electrode linear arrays. MT neurons that were well-targeted by the stimulus (n = 94) had average firing rates that depended on its motion strength and direction (Fig. A.2, A). As expected in this area, responses increased sharply with motion onset and maintained a robust firing rate throughout motion viewing (Britten et al. 1993). The average responses of well-targeted LIP neurons (n = 113) were also consistent with classical observations (Shadlen & Newsome 2001, Huk & Shadlen 2005), exhibiting ramp-like increases or decreases in firing rate whose slopes were proportional to motion strength, the primary physiological characteristic that has implicated LIP in reflecting the accumulation of evidence over time (Fig. A.2, B).

We further quantified the decision-related activity of MT and LIP using choice probability (Britten et al. 1996) (CP), a measure of correlation between neural activity and choice behavior, independent of stimulus-driven responses. MT neurons were weakly but reliably correlated with the animal's choice on a trial-by-trial basis (mean CP = 0.54, p = 1e-5; Fig. A.2, C). LIP neurons were more strongly correlated with choices (mean CP = 0.70, p = 1e-21; Fig. A.2, D). Thus, the stimulus-dependent responses and choice probability in MT were consistent with its well-established role in representing the motion stimulus, and the response patterns in LIP resembled the temporal accumulation of motion signals. Together, these properties have given rise to a model where

LIP neurons either integrate, or reflect the integration of, motion evidence from area MT in favor of a decision (Mazurek et al. 2003, Gold & Shadlen 2007).

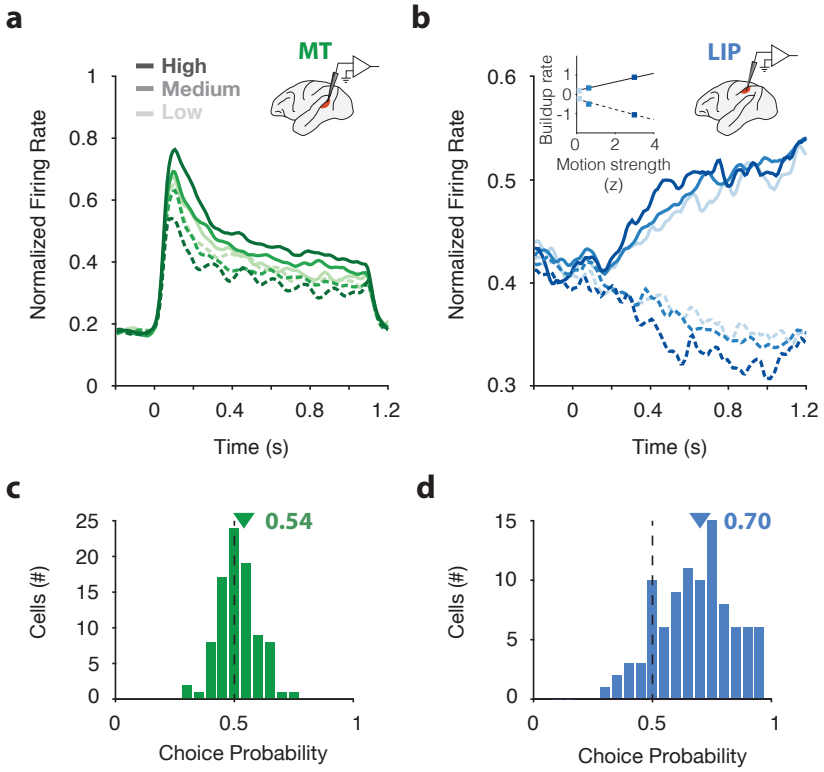

Figure A.2: **A.** Average response of 94 MT neurons as a function of motion strength (low, medium, high, represented by shade) and direction (in and out of cell's preferred direction, solid and dashed lines, respectively), aligned to motion onset. **B.** Average response of 113 LIP neurons as a function of motion strength (same as in A) and direction (in and out of cell's RF, solid and dashed lines, respectively), aligned to motion onset. Inset graph shows LIP buildup rate as a function of motion strength (z-scored) during putative integration, for choices in and out of cell's RF, solid and dashed linear fits, respectively. **C.** Choice probability for 90 MT neurons computed during the motion epoch. Triangle indicates mean, 0.54. **D.** Choice probability for 96 LIP neurons computed during the motion epoch. Triangle indicates mean, 0.70. Only neurons with >25 repeats of identical stimuli were included in the choice probability analysis.

A.3.2 Inactivation in area MT, but not LIP, influences psychophysical behavior

Having confirmed the neurophysiological properties of areas MT and LIP and their differential degrees of correlations with choices, we tested their respective causal contributions by performing reversible inactivations in each area and evaluating the impacts on psychophysical performance (hypothesized outcomes shown in Fig. A.3, A). We infused muscimol, a GABA-A agonist which hyperpolarizes cell bodies but not fibers of passage (Hess & Murata 1974) into either MT or LIP, at least 1mm away from a multi-electrode array Fig. A.3, B). The injection cannula was targeted to locations that had yielded the largest number of canonical MT or LIP units during recording sessions. The multi-electrode array was used to confirm standard physiological properties prior to infusion and post-infusion neural silencing, performed on every inactivation session. Silencing was typically observed across all recording channels of the array (Fig. A.3, B) and estimated to span a spherical volume of 2.5mm radius (see Methods).

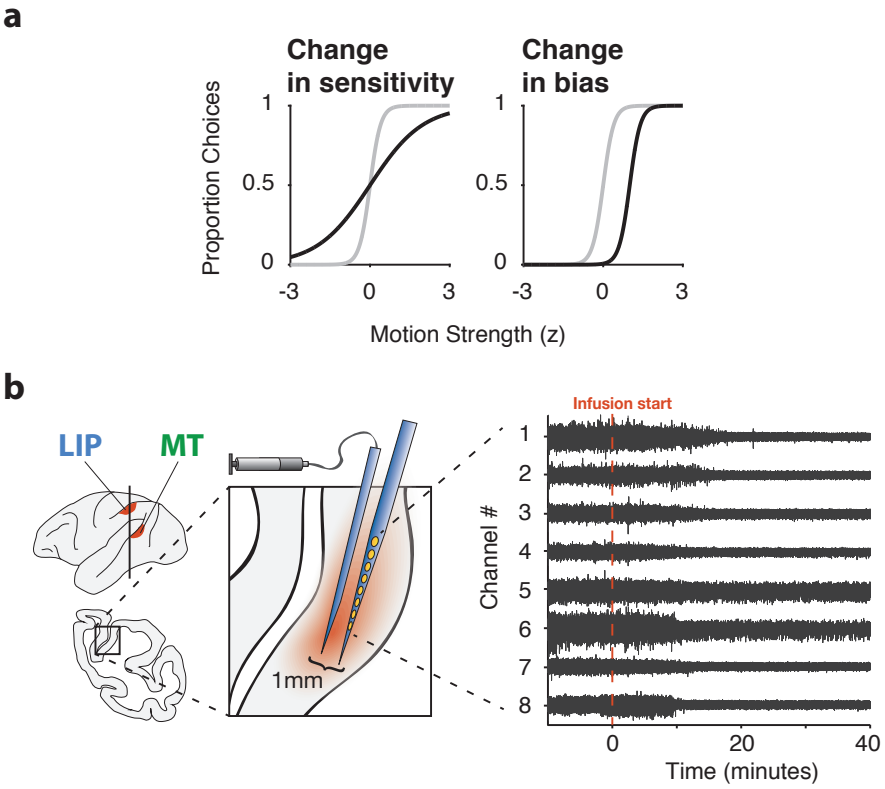

Figure A.3: **A.** Potential consequences of inactivation that would be captured by changes in logistic model fits to the dependence of choices on motion strength and direction. Left, decreased psychophysical sensitivity would be indicated by a decrease in slope. Right, increased psychophysical bias would be captured by a shifted midpoint. Positive values in the x-axis, z-scored motion strength, refer to motion towards the target contralateral to the LIP under study. Appropriately, the y-axis refers to the proportion of contralateral target choices. This convention is maintained throughout. **B.** Schematic of the inactivation protocol. Left, A multi-electrode array was lowered alongside the cannula to identify target cortex, verify neural selectivity prior to infusion, and confirm neural silencing after. Right, continuous voltage traces from an example inactivation session.

Inactivations in area MT exerted large effects on psychophysical performance. The motion stimulus was placed within a region of visual space retinotopically matched to the inactivated population of MT neurons (Fig. A.4, A). MT inactivations (n = 6) had a large and consistent impact on direction discrimination sensitivity (68.5% reduction from baseline, t(5) = -9.7, p ¡ 0.002, paired t test). When the motion stimulus was moved outside the inactivated region and into the non-inactivated hemifield within the same session (n = 3), psychophysical performance was restored to pre-infusion levels, indicating spatial specificity consistent with the retinotopic organization of MT, and confirming that the effects were not due to general changes in arousal or vigilance. These severe and specific impairments in direction discrimination performance were consistent with prior causal perturbations (Newsome & Pare 1988, Chowdhury & DeAngelis 2008).

In contrast, inactivations in area LIP (n = 21) did not exert compelling or substantial effects on psychophysical performance (Fig. A.4, B). In these experiments, we placed one choice target in the inactivated region of visual space, in line with previous electrophysiological investigations of LIP that place a choice target (as opposed to the visual motion stimulus) in the RF of the neurons to elicit the area's canonical decision-related responses. Although we performed large inactivations in locations where LIP electrophysiology had mirrored the accumulation of evidence and demonstrated strong decision-related activity, we did not detect significant changes in either the animal's sensitivity or bias, as indicated by statistically-indistinguishable dif-

ferences in the slope (3.7% reduction from baseline, $t(20) = -1.4$, $p = 0.16$, paired t test) or midpoint (-0.4% shift, $t(20) = -0.08$, $p = 0.93$, paired t test) of the psychometric functions. Saline and sham control experiments showed similar patterns to the main baseline vs. muscimol treatment comparison, considering either the effect size on average, or on individual session pairs. Thus, while the impact of MT inactivation on sensitivity was substantial, an effect of LIP inactivation was not clearly identifiable using our techniques and task (Fig. A.4, C).

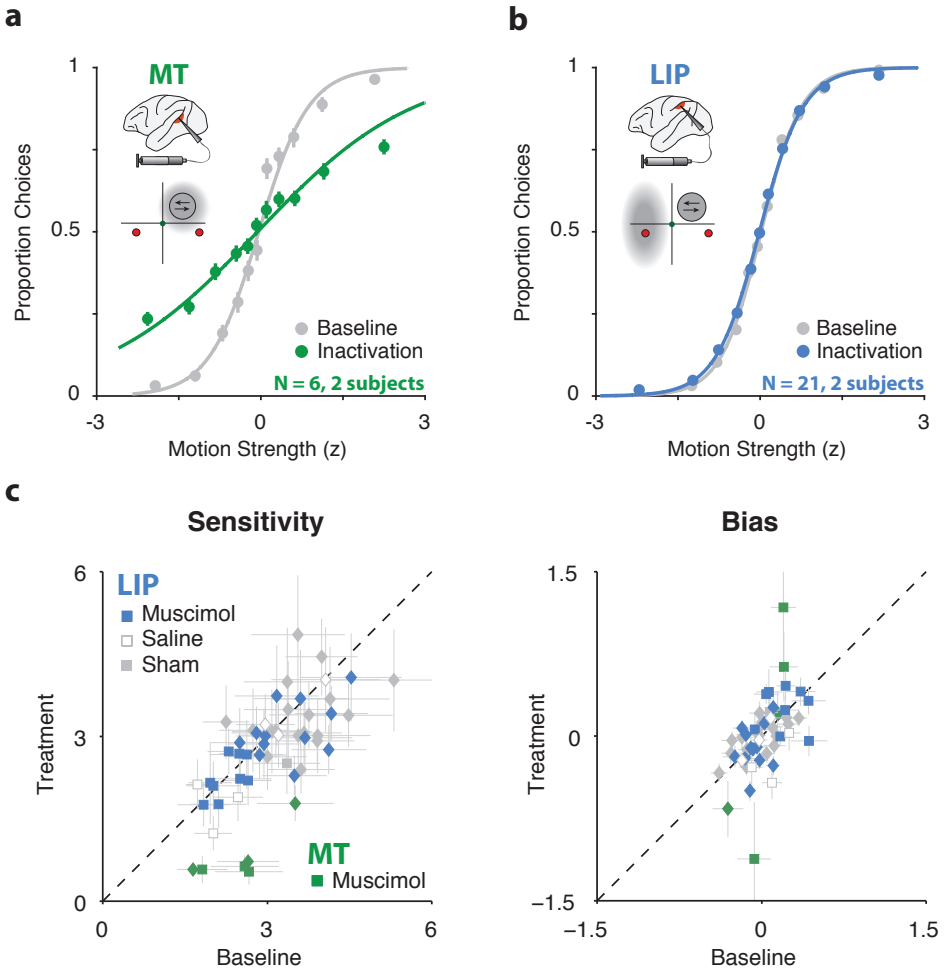

Figure A.4: Psychophysical data for averaged pairs of baseline and muscimol treatment sessions in MT (**A**), and LIP (**B**). Insets illustrate the brain region inactivated (top) and the corresponding experimental geometry (bottom), along with the estimated inactivated field (gray cloud). Error bars on points show ±1 SEM across all sessions. **C.** The distribution of psychometric function parameters, slope (left) and shift (right), reflecting sensitivity and bias, respectively, for baseline (x-axis) and treatment (y-axis) session pairs for MT inactivations (green symbols) and LIP inactivations (blue symbols), as well as LIP saline and sham experiments (gray open and filled symbols, respectively), for monkey N (diamonds) and monkey P (squares). Error bars show 95% confidence intervals for individual sessions.

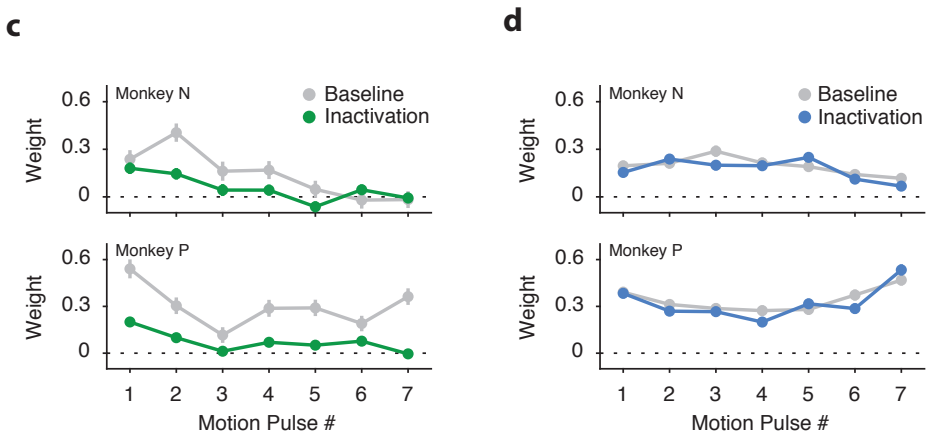

Figure A.5: Psychophysical weighting, estimated via reverse correlation. Y-axis indicates how much the subject weighed each of the motion stimulus pulses (logistic regression) for all baseline and inactivation session pairs in MT (**A**) and in LIP (**B**), for monkey N (top) and monkey P (bottom).

We also assessed whether inactivation affected the timing or strategy of evidence integration (Kiani et al. 2008, Raposo et al. 2014, Erlich et al. 2015). For example, if LIP supports the temporal integration of motion evidence, inactivation could alter the strategy to reflect "leakier" integration that might still support the same overall performance. Contrary to this possibility, psychophysical weighting of the motion stimulus (estimated via reverse correlation) was unaffected by inactivation (Fig. A.5). Although the two monkeys exhibited slightly different baseline weighting strategies, inactivation did not lead to a greater reliance on late information, nor did it clearly exert other idiosyncratic effects on the psychophysical weighting. Inactivations in area MT reduced the weighting of motion approximately evenly over time.

A.3.3 Inactivation in LIP disrupts behavior in a control task

Although inactivation in LIP had no measurable effect on direction discrimination, it did exert measurable effects on a "free-choice" control task, which was performed on every inactivation session (Fig. A.6). Inactivation of LIP biased choices away from the contralateral hemifield (8.88% reduction from baseline on average, $t(33) = 3.4$, $p = 0.001$, paired t test), (Fig. A.7), consistent with previous reports in monkeys (Wardak et al. 2004, Balan & Gottlieb 2009, Wilke et al. 2012), rodents (Erlich et al. 2015), and parietal lesions in humans (Kerkhoff 2001). Thus, our standard electrophysiological confirmation of LIP inactivation was complemented by a behavioral consequence in this free-choice control task. In addition to exerting a spatial bias, LIP inactivation caused an increase in endpoint error of saccades made to the hemifield contralateral to the inactivation (0.36° on average, $t(33) = 4.4$,$p < 0.0001$, Fig. A.7).

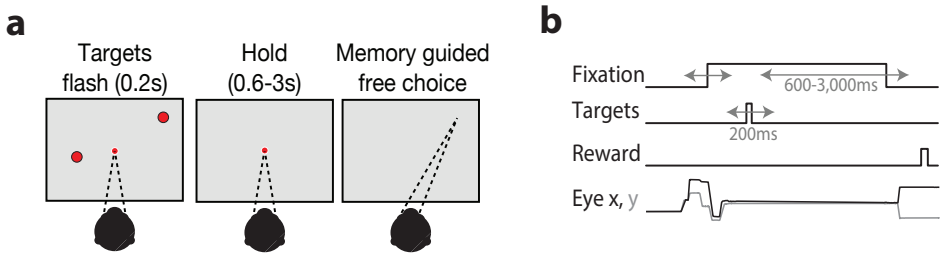

Figure A.6: Design of the free-choice control task. **A.** The "free-choice" task. Following a 200ms long presentation of two targets at random locations in space, monkeys were required to hold fixation for another 600-3,000ms, and then to move their eyes to the remembered location of either target. **B.** Task timing. Events in the task were presented in sequence and were jittered in time (gray arrows).

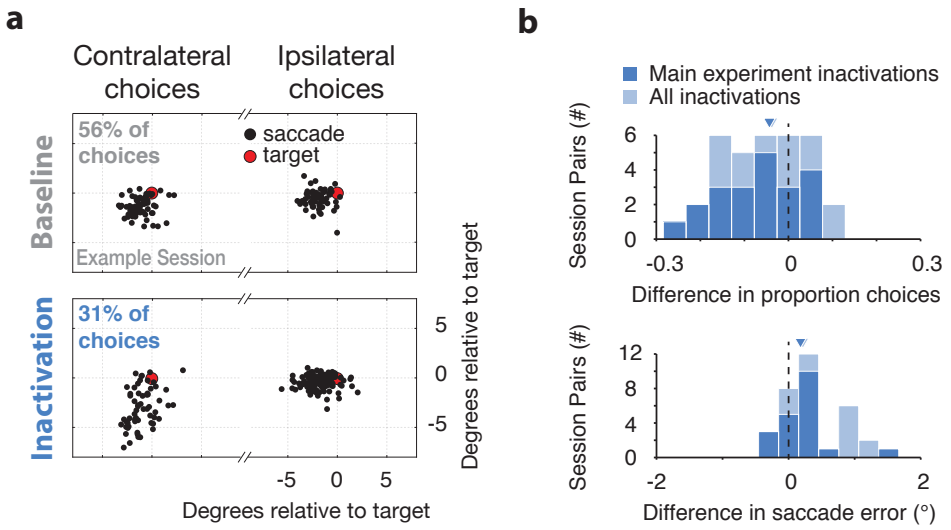

Figure A.7: Performance in the free-choice task following LIP inactivation. **A.** The effect of LIP inactivation on choice bias and saccade accuracy in the free-choice task, example session. Four panels show data from an example baseline/inactivation pair: saccade landing points (black dots) have been aligned to target position (red dot) for contralateral (left) and ipsilateral target choices (right), during baseline (top) and inactivation (bottom). Percent contralateral choices within a session are noted as text in the top left. **B.** The effect of LIP inactivation on choice bias and saccade accuracy in the free-choice task, over all sessions. Histograms show baseline/inactivation differences in proportion contralateral choices (top) and saccade error (bottom), where positive numbers indicate an increase in metric following inactivation. Dark bars indicate sessions that took place on the same days as the main direction discrimination experiment ("Main experiment inactivations", n=21); dark triangle indicates the median difference. Light bars include additional sessions that took place on other days ("All inactivations", n=34); light triangle indicates median difference (may be hard to discern on plot due to similarity in value).

No systematic change was detected in other free-choice oculomotor metrics (reaction time, peak velocity, or duration), and no change in any oculomotor metric was detected during the direction discrimination task. Despite observing a muscimol-induced effect in the free-choice task, effect magnitude in the free-choice task was not predictive of effect magnitude in the direction discrimination task, nor was there a dose-response relationship between muscimol mass and behavioral performance, suggesting that our large muscimol administrations were likely operating within a "ceiling" regime.

A.3.4 Compensation over time or between hemispheres is unlikely

Because muscimol inactivations require comparisons across relatively long time scales, it remains logically possible that LIP normally plays a critical role in decision-making, but that other areas are processing information in parallel (de Lafuente et al. 2015) and are able to quickly compensate when it is artificially inactivated. Although other techniques with faster time scales will allow for more direct tests of this possibility, we did not observe changes indicative of compensation either within a session or over sessions (data not shown).

To test for reliance or compensation involving the LIP in the non-inactivated hemisphere, we performed experiments with both choice targets placed within the contralateral hemifield, and again did not observe clear changes in behavioral performance (Fig. A.7, A). We also found no disruption of choice behavior using a moving-dot stimulus identical to that used

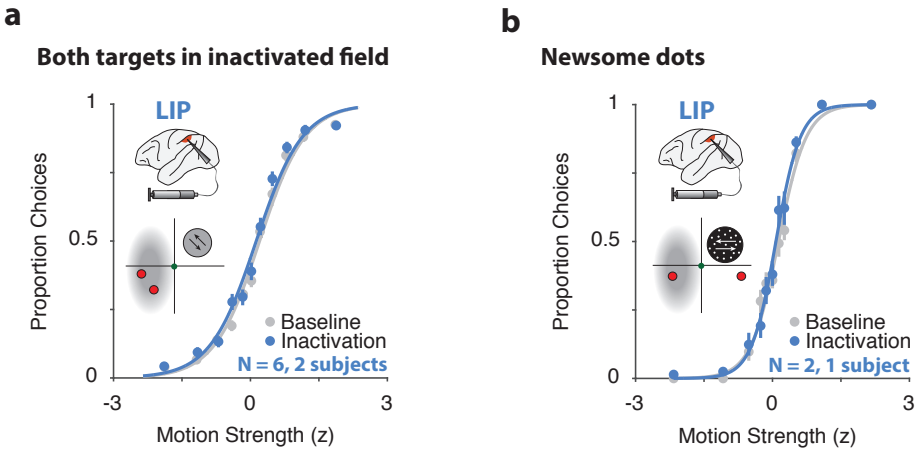

Figure A.8: **A.** Psychophysical data for pairs of baseline and muscimol treatment in LIP, when both choice targets were placed within the inactivated field. Inset presents stimulus geometry and estimated inactivated field. **B.**, Same format as A, for data collected when the motion stimulus was a random dot kinetogram ("Newsome dots", at motion strengths of 0, 3.2, 6.4, 12.8 25.6 and 51.2% coherence, z scored).

in the classical studies of LIP function during decision making (Newsome & Pare 1988, Shadlen & Newsome 2001) (Fig. A.8, B)

A.4 Discussion

Our results reveal a dissociation between decision-related activity in LIP and the causal role of such signals in decision-making. Instead, decision-related signals in LIP may be a result of feedback signal flow (Crowe, Goodwin, Blackman, Sakellaridi, Sponheim, MacDonald & Chafee 2013), or perhaps an emergent phenomenon driven by extensive training (Sarma, Masse, Wang & Freedman 2016). Although one prior study observed subtle effects of LIP microstimulation in a reaction time direction discrimination taskHanks:2006jt, such electrical perturbations can produce orthodromic (and antidromic) activation of connected areas, and their observed effects are reconcilable with multiple alternatives to evidence accumulation (Hanks et al. 2015).

Alternatively, it remains possible that LIP does contribute to decision-making, but does so in a nonessential manner in conjunction with associated brain regions. Indeed, a growing body of work has observed decision-related activity in other brain areas (Ding & Gold 2013, Gu et al. 2007, Liu et al. 2013, Hanks et al. 2015), consistent with the prospect of LIP playing a minor and/or nonessential role in decision-making. In fact, our results mirror findings made in rodent posterior parietal cortex, where despite electrophysiological correlates of evidence accumulation, inactivation did not yield clear evidence of a critical role (Erlich et al. 2015). Taken together, decision-related activity is likely represented broadly across the brain, and may be "read out" by a flexible process to support behavior (Pitkow et al. 2015, Siegel et al. 2015). Our results call for a broader consideration of both decision-making circuitry

and the mechanisms for reading out decision-related activity— regardless of whether decisions are instantiated, or merely reflected, in a particular brain area.

Appendix B

Single-trial Spike Trains in Parietal Cortex Reveal Discrete Steps During Decision-making

Neurons in the macaque lateral intraparietal (LIP) area exhibit firing rates that appear to ramp upwards or downwards during decision-making. These ramps are commonly assumed to reflect the gradual accumulation of evidence towards a decision threshold. However, the ramping in trial-averaged responses could instead arise from instantaneous jumps at different times on different trials. We examine single-trial responses in LIP using statistical methods for fitting and comparing latent dynamical spike train models. We compare models with latent spike rates governed by either continuous diffusion-to-bound dynamics or discrete "stepping" dynamics. Roughly three-quarters of the choice-selective neurons recorded in LIP are better described by the stepping model. Moreover, the inferred steps carry more information about the animal's choice than spike counts. This work has been published in *S*cience Latimer, Yates, Meister, Huk & Pillow (2015) [1] I was involved in experimental design, development of the generative models for LIP spike trains, and writing

[1]Latimer, K. W., Yates, J. L., Meister, M. L. R., Huk, A. C. & Pillow, J. W. (2015), 'NEURONAL MODELING. Single-trial spike trains in parietal cortex reveal discrete steps during decision-making.', Science 349(6244), 184?187.

of the paper. The statistical inference methods are described in Latimer, Huk & Pillow (2015).

B.1 Introduction

Neurons in the macaque lateral intraparietal (LIP) area exhibit firing rates that appear to ramp upwards or downwards during decision-making. These ramps are commonly assumed to reflect the gradual accumulation of evidence towards a decision threshold. However, the ramping in trial-averaged responses could instead arise from instantaneous jumps at different times on different trials. We examined single-trial responses in LIP using statistical methods for fitting and comparing latent dynamical spike train models. We compared models with latent spike rates governed by either continuous diffusion-to-bound dynamics or discrete "stepping" dynamics. Roughly three-quarters of the choice-selective neurons we recorded were better described by the stepping model. Moreover, the inferred steps carried more information about the animal's choice than spike counts. (Brunton et al. 2013) Ramping responses have been observed in a variety of brain areas during decision-making, and have been widely interpreted as the neural implementation of evidence accumulation for forming decisions (Mazurek et al. 2003, Gold & Shadlen 2007, Kiani et al. 2008, Kiani & Shadlen 2009, Shadlen & Kiani 2013). However, ramping can only be observed by averaging together responses from many trials (and often, many neurons), which obscures the dynamics governing responses on single trials. In particular, a discrete "stepping" pro-

cess (Miller & Katz 2010, Durstewitz & Deco 2008), in which the spike rate jumps stochastically from one rate to another at some time during each trial, can also create the appearance of ramping (Goldman 2015, Churchland, Kiani, Chaudhuri, Wang, Pouget & Shadlen 2011). Although decision-making at the behavioral level is well-described as an accumulation process (Ratcliff & Rouder 1998, Brunton et al. 2013), whether the brain computes decisions via a direct neural correlate (ramping) or a discrete implementation (stepping) remains a central, unresolved question in systems neuroscience.

We used advanced statistical methods to identify the single-trial dynamics governing spike trains in the lateral intraparietal (LIP) area of macaques performing a well-studied motion-discrimination task (Figure B.1) (Meister et al. 2013, Kiani et al. 2008). We formulated two spike train models with stochastic latent dynamics governing the spike rate: one defined by continuous ramping dynamics, and the other by discrete stepping dynamics (see supplementary methods for mathematical details). In the ramping model, also known as "diffusion-to-bound", the spike rate evolves according to a Gaussian random walk with linear drift (Figure B.1B). The slope of drift depends on the strength of sensory evidence, and each trial's trajectory continues until hitting an absorbing upper bound. Alternatively, in the stepping model, the latent spike rate jumps instantaneously from an initial "undecided" state to one of two discrete decision states during the trial (Figure B.1C). The probability of stepping up or stepping down and the timing of the step are determined by the strength of sensory evidence. For both models, we assumed spiking follows

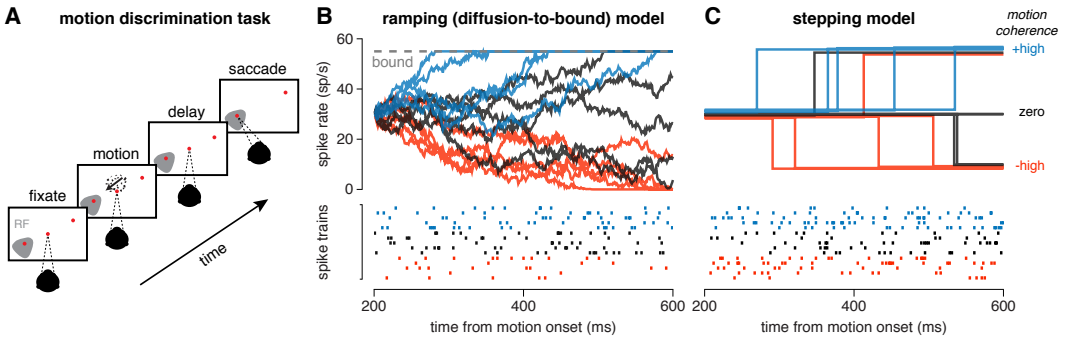

Figure B.1: **A** Schematic of moving-dot direction-discrimination task. The monkey views and discriminates the net direction of a motion stimulus of variable motion strength and duration, and indicates its choice by making a saccade to one of two choice targets 500 ms after motion offset. One choice target is in the response field of the neuron under study (RF; shaded patch on left); the other is outside it. **B** Ramping (diffusion-to-bound) model. Spike rate trajectories (solid traces) were sampled from a diffusion-to-bound process for each of three motion coherences (strong positive, zero, and strong negative). The model parameters include an initial spike rate, a slope for each coherence, noise variance, and an upper bound. We do not include a lower bound, consistent with the competing integrator (race) model of LIP (Shadlen & Kiani 2013). Spike trains (below) obey an inhomogeneous Poisson process for each spike rate trajectory. (**C**) Discrete stepping model. Spike rate trajectories (above) begin at an initial rate and jump "up" or "down" at a random time during each trial, and spike trains (below) are once again Poisson given the latent rate. The step times take a negative binomial distribution, which resembles the time-to-bound distribution under a diffusion model. Parameters include the spike rates for the three discrete states and two parameters governing the distribution over step timing and direction for each motion coherence. Both models were fit using the spike trains and coherences for each neuron, without access to the animal's choices.

an inhomogeneous Poisson process given the time-varying spike rate.

Both latent variable models are "doubly stochastic" in the sense that the probability of an observed spike train given the sensory stimulus depends on both the noisy trajectory of the latent spike rate and the Poisson variability

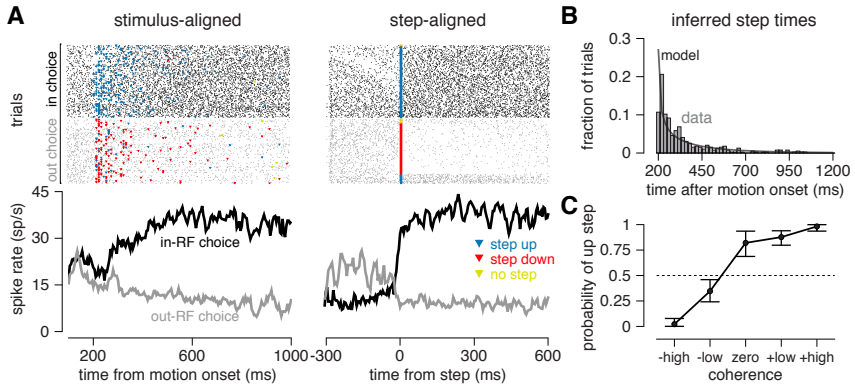

Figure B.2: Model-based analysis of spike responses from an example LIP neuron. **(A)** Spike rasters sorted by the monkey's choice in or out of the RF of the neuron under study (black="in-RF", gray="out-RF"), and their associated averages (PSTHs, below). Left: Conventional stimulus-aligned rasters with each trial aligned to the time of motion onset exhibit commonly-observed ramping in the PSTH. Blue and red triangles indicate the inferred time of an "up" or "down" step on each trial under the fitted stepping model. Yellow triangles indicate that no step was found during the trial, and are placed at the end of the trial segment we analyzed (200 ms after motion offset). Right: The same spike trains aligned to the inferred step time for each trial. Note that estimated step direction of the neuron does not always match the animal's decision on each trial. **(B)** The distribution of inferred step times shown in A (histogram), and the distribution over step times under the fitted parameters (black trace). **(C)** The probability of an "up" step, for each coherence level. Error bars indicate 95% credible intervals.

in the spiking process. Fitting such latent variable models requires integrating over all latent trajectories consistent with the observed spike trains, which is not analytically tractable. We therefore developed sampling-based Markov Chain Monte Carlo (MCMC) methods, which provide samples from the posterior distribution over model parameters and allow us to perform Bayesian model comparison.

B.2 Results

We focused on a population of 40 neurons with highly choice-selective responses that exhibited ramping in their average responses (Meister et al. 2013), typically increasing during trials in which the monkey eventually chose the target inside the response field (RF) of the neuron, and decreasing when the monkey chose the target outside the RF. We fit each neuron with both ramping and stepping models, using the spike train data from 200 ms after motion onset (Churchland, Kiani & Shadlen 2008) until 200 ms after motion offset (300 ms before the monkey received the go signal). Figure B.2 shows the raster of spike trains from an example LIP neuron plotted in two different ways: first, aligned to the time of motion stimulus onset (left); and second, aligned to the step time inferred under the stepping model (right). The traditional raster and peri-stimulus time histogram (PSTH) at left show that the average response ramps upward or downward depending on choice, as expected. The step-aligned raster at right, however, shows that these data are also consistent with discrete step-like transitions with variable timing across trials. Additional panels show the distribution of step times inferred under the model (Figure B.2B), and the dependence of step direction ("up" or "down") on the motion signal (Figure B.2C). Discrete steps in the instantaneous spike rate could thus plausibly underlie the gradual ramping activity seen in stimulus-aligned and averaged LIP spike responses.

We applied the same analysis to the full set of LIP neurons and observed similar structure in step-aligned rasters. Figure B.3A shows population-

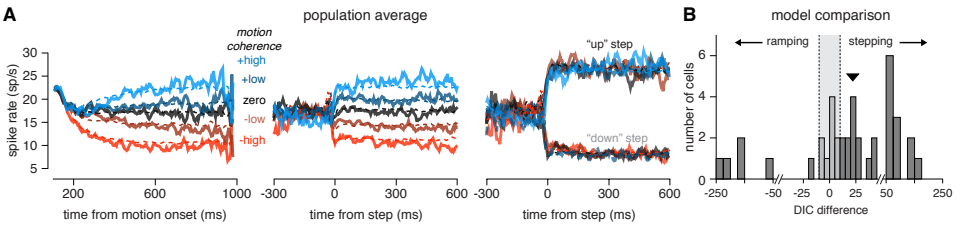

Figure B.3: **A** Population average PSTH sorted by motion coherence computed from spike trains: (left) aligned to motion onset and sorted by motion strength; (middle) aligned to step times inferred under the stepping model and sorted by motion strength; (right) aligned to step times and sorted by both motion strength and inferred step direction. Simulated results from the stepping model (dashed lines) provide a close match to the real data under all types of alignment and conditioning. **B** Quantitative model comparison using divergence information criterion (DIC) reveals a superior fit of the stepping model over the ramping model for the majority of cells (31 out of 40). A DIC difference greater than ± 10 (gray region) is commonly regarded as providing "strong" support for one model over the other. We found substantially more cells with strong evidence for stepping over ramping (25 cells vs. 6 cells; median DIC difference $= 22.1$, sign test $p < 0.001$).

averaged PSTHs computed from stimulus-aligned (left) and step-aligned responses, sorted by motion strength (middle), or motion strength and step direction (right). The middle and right plots show that spike rate is effectively constant when spike trains are aligned to the inferred step time on each trial. The gradient of step heights in the middle plot results from differential probabilities of stepping "up" or "down" as a function of motion strength over trials. The right plot confirms that the firing rate, once conditioned on stepping "up" or "down", is independent of motion strength. Furthermore, simulated spike responses, based on the fitted stepping models, resemble the real data under both kinds of alignment (dashed traces).

Although these analyses provide a visually compelling illustration of the plausibility of stepping dynamics in LIP, they do not by themselves definitively rule out the ramping model. Using our latent variable models, we can formally address this issue using statistical model comparison. Both models give a probability distribution over spike trains, and the model that better represents the data should place more probability mass over the observed spike trains. We compared the model fits using the deviance information criterion (DIC) (Spiegelhalter, Best, Carlin & van der Linde 2002) which integrates over the entire posterior distribution of model parameters given the data, thereby taking into account the uncertainty in the model fit as well as the number of parameters in each model.

The stepping model provided a superior account of LIP responses for 78% (31/40) of the cells compared to the ramping model (Figure B.3B). The stepping model therefore not only accounts for the ramp-like activity observed in averaged LIP responses, but its qualitative ability to reveal step times is bolstered by quantitative superiority in accounting for the statistical structure of spike trains for a majority of LIP neurons. The superiority was supported not just by DIC but also by other model comparison metrics, such as Bayes factor.

We subsequently examined how well the two models account for the time-varying mean and the variance of neural responses. Figure 4A shows the comparison for the mean responses (top row) and variance (bottom row) for the data (left column), stepping model (middle column), and ramping model

(right column). Although the models were fit to predict the spike responses on each trial, as opposed to these summary statistics, both models did an acceptable job of accounting for the mean response (fraction of variance in the PSTHs explained: stepping $R^2 = 0.94$, 95% credible interval:$[0.90, 0.94]$, ramping $R^2 = 0.78$ 95% CI: $[0.71, 0.79]$). This is consistent with the long-standing difficulty in distinguishing between these two mechanisms. However, the stepping model provided a more accurate fit to the variance of neural responses (stepping $R^2 = 0.40$, 95% CI:$[0.09, 0.45]$, ramping $R^2 = -0.49$, 95% CI: $[-0.86, -0.27]$). In particular, the stepping model captured the decreasing variance observed in trials with strong negative motion much better than the ramping model. (A similar result held for estimates of variance of the underlying spike rate).

Finally, the stepping model provides a platform for neural decoding, as the posterior distribution over steps can be used for reading out decisions from the spikes on a single trial. We first quantified decoding performance using choice probability (CP), a popular metric for quantifying the relationship between choice and a pair of spike counts. Aligned to motion onset, CP grows roughly linearly with time (Figure B.4B, left). However, the CP relative to the inferred step times (Figure B.4B, right) was consistent with an abrupt emergence of choice-related activity. We then compared classical CP with a model-based CP measure, which assumed that the direction of the neuron's step predicted the animal's choice. We reiterate that the model was fit to the spike trains without access to the animal's choices. The model-based CP

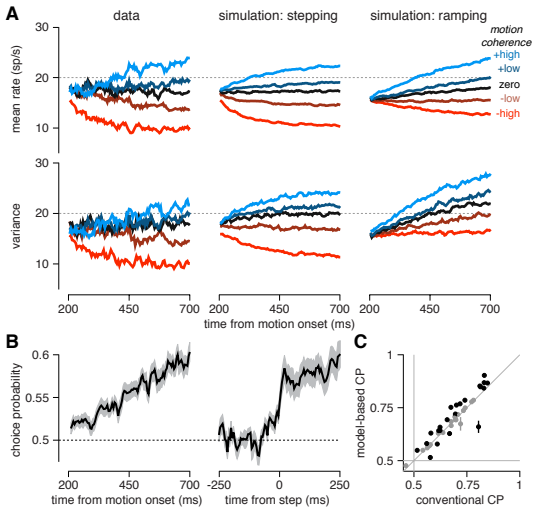

Figure B.4: Stepping model better explains variance of responses and can be used to decode choices. **A** Comparison of model fits to average population activity, sorted by stimulus strength. Spike rates and variances were calculated with a 25 ms sliding window. **B** Population average choice probability aligned to stimulus onset (left), and average CP aligned to estimated step times (right). Grey region indicates one standard error of the mean. CPs were calculated with a sliding 25 ms window. Conventional alignment suggests a ramp in choice selectivity, while the model-based alignment indicates a rapid transition. **C** Conventional choice probability based on spike counts using responses 200-700 ms after motion onset versus model-based choice probability using the probability of stepping to the up state by the end of the same period. Model-based CP is greater than conventional CP in the population (Wilcoxon signed rank test, $p < 0.05$). Stepping models were fit using 10 fold cross validation. Error bars show the standard error of CPs, as computed on each training data set. Black points indicate cells with significant differences between model-based and conventional CP (Student's t-test, $p < 0.05$), and grey indicates not significant.

was on average greater than classical CP, indicating that the states estimated under the stepping model were more informative about the animal's choice than raw spike counts (Figure B.4C).

B.3 Discussion

In conclusion, we have developed tractable, principled methods for fitting and comparing statistical models of single-neuron spike trains in which spike rates are governed by a latent stochastic process. We have applied these methods to determine the dynamics underlying neural activity in area LIP. Although neurons in this area have been largely assumed to exhibit ramping dynamics, reflecting the temporal accumulation of evidence posited by models of decision-making, statistical model comparison supports an alternative hypothesis: LIP responses were better described by randomly timed, discrete steps between underlying states. (In a supplementary analysis, we examined data from a response-time version of the dots task and found results consistent with the trend in the fixed duration version; this initial comparison will be strengthened by extending the models to account for overlapping decision and motor events, and application to larger datasets (Roitman & Shadlen 2002)) In addition to accounting better for the dynamics of the mean firing rates, only the stepping model accounts accurately for the variance of neural responses. Finally, the estimation of single-trial step times provides a novel view of choice-related activity, revealing that choice-correlated fluctuations in response are also dominated by discrete step-like dynamics.

Although these results challenge the canonical perspective of LIP dynamics during decision-making, the approach facilitates new avenues of investigation. Our analyses suggest that accumulation may be implemented by stochastic steps, but simultaneous recordings of multiple neurons will be

required to test whether population activity ramps or discretely transitions between states on single trials (Miller & Katz 2010); population-level ramping could still be implemented via step times that vary across neurons, even on the same trial. Fortunately, the statistical techniques reported here are scalable to simultaneously-recorded samples of multiple neurons, and newer recording techniques are starting to yield these multi-neuron datasets (Stevenson & Kording 2011, Bollimunta, Totten & Ditterich 2012, Kiani et al. 2014, Kaufman, Churchland, Ryu & Shenoy 2015). It is also possible that single neurons with ramping dynamics implement evidence integration elsewhere in the brain, and that LIP neurons are post-decisional or pre-motor indicators of the binary result of this computation. More generally, we believe these techniques will have broad applicability for identifying and interpreting the latent factors governing multi-neuron spike responses, allowing for principled tests of the dynamics governing cognitive computations in many brain areas.

Bibliography

Adelson, E. H. & Bergen, J. R. (1985), 'Spatiotemporal energy models for the perception of motion.', *Journal of the Optical Society of America. A, Optics and image science* **2**(2), 284–299.

Ahumada, A. (1971), 'Stimulus Features in Signal Detection', *The Journal of the Acoustical Society of America* **49**(6B), 1751.

Ahumada, A. (1975), 'Time and frequency analyses of auditory signal detection', *The Journal of the Acoustical Society of America* **57**(2), 385–390.

Albright, T. D. (1984), 'Direction and orientation selectivity of neurons in visual area MT of the macaque', *Journal of Neurophysiology* **52**(6), 1106–1130.

Allman, J. M. & Kaas, J. H. (1971), 'A representation of the visual field in the caudal third of the middle temporal gyrus of the owl monkey (Aotus trivirgatus)', *Brain research* **31**(1), 85–105.

Alonso, J.-M., Usrey, W. M., Reid, R. C. & others (1996), 'Precisely correlated firing in cells of the lateral geniculate nucleus', *Nature* **383**(6603), 815–819.

Andersen, R. A., Asanuma, C., Essick, G. & Siegel, R. M. (1990), 'Corticocortical connections of anatomically and physiologically defined subdivisions

within the inferior parietal lobule', *The Journal of comparative neurology* **296**(1), 65–113.

Andersen, R. A. & Buneo, C. A. (2002), 'Intentional maps in posterior parietal cortex', *Annual Review of Neuroscience* **25**(1), 189–220.

Andersen, R., Essick, G. & Siegel, R. (1985), 'Encoding of spatial location by posterior parietal neurons', *Science* **230**(4724), 456–458.

Anderson, J. C., Kennedy, H. & Martin, K. A. C. (2011), 'Pathways of attention: synaptic relationships of frontal eye field to V4, lateral intraparietal cortex, and area 46 in macaque monkey.', *Journal of Neuroscience* **31**(30), 10872–10881.

Arikan, R., Blake, N. M., Erinjeri, J. P., Woolsey, T. A., Giraud, L. & Highstein, S. M. (2002), 'A method to measure the effective spread of focally injected muscimol into the central nervous system with electrophysiology and light microscopy', *Journal of Neuroscience Methods* **118**(1), 51–57.

Averbeck, B. B., Latham, P. E. & Pouget, A. (2006), 'Neural correlations, population coding and computation.', *Nature Reviews Neuroscience* **7**(5), 358–366.

Bair, W. & Movshon, J. A. (2004), 'Adaptive temporal integration of motion in direction-selective neurons in macaque visual cortex.', *Journal of Neuroscience* **24**(33), 7305–7323.

Bair, W., Zohary, E. & Newsome, W. T. (2001), 'Correlated firing in macaque visual area MT: time scales and relationship to behavior', *The Journal of neuroscience : the official journal of the Society for Neuroscience* **21**(5), 1676–1697.

Balan, P. F. & Gottlieb, J. (2009), 'Functional significance of nonspatial information in monkey lateral intraparietal area.', *Journal of Neuroscience* **29**(25), 8166–8176.

Barak, O., Sussillo, D., Romo, R., Tsodyks, M. & Abbott, L. F. (2013), 'From fixed points to chaos: three models of delayed discrimination.', *Progress in neurobiology* **103**, 214–222.

Barash, S., Bracewell, R. M., Fogassi, L., Gnadt, J. W. & Andersen, R. A. (1991*a*), 'Saccade-related activity in the lateral intraparietal area. I. Temporal properties; comparison with area 7a.', *Journal of Neurophysiology* **66**(3), 1095–1108.

Barash, S., Bracewell, R. M., Fogassi, L., Gnadt, J. W. & Andersen, R. A. (1991*b*), 'Saccade-related activity in the lateral intraparietal area. II. Spatial properties.', *Journal of Neurophysiology* **66**(3), 1109–1124.

Barbas, H. & Mesulam, M. M. (1981), 'Organization of afferent input to subdivisions of area 8 in the rhesus monkey.', *The Journal of comparative neurology* **200**(3), 407–431.

Barlow, H. & Tripathy, S. P. (1997), 'Correspondence noise and signal pooling in the detection of coherent visual motion.', *The Journal of neuroscience : the official journal of the Society for Neuroscience* **17**(20), 7954–7966.

Beck, J. M., Ma, W. J., Kiani, R., Hanks, T., Churchland, A. K., Roitman, J., Shadlen, M. N., Latham, P. E. & Pouget, A. (2008), 'Probabilistic Population Codes for Bayesian Decision Making', *Neuron* **60**(6), 1142–1152.

Belmonte, J. C. I., Callaway, E. M., Churchland, P., Caddick, S. J., Feng, G., Homanics, G. E., Lee, K.-F., Leopold, D. A., Miller, C. T., Mitchell, J. F., Mitalipov, S., Moutri, A. R., Movshon, J. A., Okano, H., Reynolds, J. H., Ringach, D., Sejnowski, T. J., Silva, A. C., Strick, P. L., Wu, J. & Zhang, F. (2015), 'Perspective', *Neuron* **86**(3), 617–631.

Berens, P., Ecker, A. S., Cotton, R. J., Ma, W. J., Bethge, M. & Tolias, A. S. (2012), 'A Fast and Simple Population Code for Orientation in Primate V1.', *Journal of Neuroscience* **32**(31), 10618–10626.

Berman, R. A. & Wurtz, R. H. (2010), 'Functional Identification of a Pulvinar Path from Superior Colliculus to Cortical Area MT', *Journal of Neuroscience* **30**(18), 6342–6354.

Bishop, C. M. (2006), *Pattern Recognition and Machine Learning*, Information Science and Statistics, Springer.

Blatt, G. J., Andersen, R. A. & Stoner, G. R. (1990), 'Visual Receptive Field Organization and Cortico-Cortical Connections of the Lateral Intraparietal Area (Area LIP) in the Macaque', *The Journal of comparative neurology* **299**(4), 421–445.

Bollimunta, A., Totten, D. & Ditterich, J. (2012), 'Neural dynamics of choice: single-trial analysis of decision-related activity in parietal cortex.', *Journal of Neuroscience* **32**(37), 12684–12701.

Born, R. T. & Bradley, D. C. (2005), 'Structure and function of visual area MT.', *Annual Review of Neuroscience* **28**, 157–189.

Bosking, W. H. & Maunsell, J. H. R. (2011), 'Effects of stimulus direction on the correlation between behavior and single units in area MT during a motion detection task.', *Journal of Neuroscience* **31**(22), 8230–8238.

Bradley, D. C. & Goyal, M. S. (2008), 'Velocity computation in the primate visual system', *Nature Reviews Neuroscience* **9**(9), 686–695.

Brainard, D. H. (1997), 'The Psychophysics Toolbox.', *Spatial vision* **10**(4), 433–436.

Britten, K. H., Newsome, W. T., Shadlen, M. N., Celebrini, S. & Movshon, J. A. (1996), 'A relationship between behavioral choice and the visual responses of neurons in macaque MT.', *Visual neuroscience* **13**(1), 87–100.

Britten, K. H., Shadlen, M. N., Newsome, W. T. & Movshon, J. A. (1992), 'The Analysis of Visual Motion: A Comparison of Neuronal and Psychophysical Performance', *The Journal of neuroscience* pp. 1–21.

Britten, K. H., Shadlen, M. N., Newsome, W. T. & Movshon, J. A. (1993), 'Responses of neurons in macaque MT to stochastic motion signals.', *Visual neuroscience* **10**(6), 1157–1169.

Brody, C. (1999), 'Correlations without synchrony', *Neural Computation* **11**(7), 1537–1551.

Brunton, B. W., Botvinick, M. M. & Brody, C. D. (2013), 'Rats and humans can optimally accumulate evidence for decision-making.', *Science* **340**(6128), 95–98.

Burkhalter, A. & Van Essen, D. C. (1986), 'Processing of color, form and disparity information in visual areas VP and V2 of ventral extrastriate cortex in the macaque monkey', *The Journal of neuroscience* **6**(8), 2327–2351.

Celebrini, S. & Newsome, W. T. (1994), 'Neuronal and psychophysical sensitivity to motion signals in extrastriate area MST of the macaque monkey.', *The Journal of neuroscience : the official journal of the Society for Neuroscience* **14**(7), 4109–4124.

Chapman, B., Zahs, K. R. & Stryker, M. P. (1991), 'Relation of cortical cell orientation selectivity to alignment of receptive fields of the geniculocor-

tical afferents that arborize within a single orientation column in ferret visual cortex', *The Journal of neuroscience* **11**(5), 1347–1358.

Chen, Y., Geisler, W. S. & Seidemann, E. (2006), 'Optimal decoding of correlated neural population responses in the primate visual cortex', *Nature Neuroscience* **9**(11), 1412–1420.

Chichilnisky, E. J. (2001), 'A simple white noise analysis of neuronal light responses.', *Network (Bristol, England)* **12**(2), 199–213.

Chowdhury, S. A. & DeAngelis, G. C. (2008), 'Fine discrimination training alters the causal contribution of macaque area MT to depth perception.', *Neuron* **60**(2), 367–377.

Churchland, A. K., Kiani, R., Chaudhuri, R., Wang, X.-J., Pouget, A. & Shadlen, M. N. (2011), 'Variance as a Signature of Neural Computations during Decision Making', *Neuron* **69**(4), 818–831.

Churchland, A. K., Kiani, R. & Shadlen, M. N. (2008), 'Decision-making with multiple alternatives', *Nature Neuroscience* **11**(6), 693–702.

Churchland, M. M., Yu, B. M., Cunningham, J. P., Sugrue, L. P., Cohen, M. R., Corrado, G. S., Newsome, W. T., Clark, A. M., Hosseini, P., Scott, B. B., Bradley, D. C., Smith, M. A., Kohn, A., Movshon, J. A., Armstrong, K. M., Moore, T., Chang, S. W., Snyder, L. H., Lisberger, S. G., Priebe, N. J., Finn, I. M., Ferster, D., Ryu, S. I., Santhanam, G., Sahani, M. & Shenoy, K. V. (2010), 'Stimulus onset quenches neural

variability: a widespread cortical phenomenon', *Nature Publishing Group* **13**(3), 369–378.

Cohen, M. R. & Kohn, A. (2011), 'Measuring and interpreting neuronal correlations.', *Nature Neuroscience* **14**(7), 811–819.

Cohen, M. R. & Newsome, W. T. (2009), 'Estimates of the contribution of single neurons to perception depend on timescale and noise correlation.', *Journal of Neuroscience* **29**(20), 6635–6648.

Cook, E. P. (2004), 'Attentional Modulation of Motion Integration of Individual Neurons in the Middle Temporal Visual Area', *Journal of Neuroscience* **24**(36), 7964–7977.

Crowe, D. A., Goodwin, S. J., Blackman, R. K., Sakellaridi, S., Sponheim, S. R., MacDonald, A. W. & Chafee, M. V. (2013), 'Prefrontal neurons transmit signals to parietal neurons that reflect executive control of cognition.', *Nature Publishing Group* **16**(10), 1484–1491.

Cui, Y., Liu, L. D., Khawaja, F. A., Pack, C. C. & Butts, D. A. (2013), 'Diverse Suppressive Influences in Area MT and Selectivity to Complex Motion Features', *Journal of Neuroscience* **33**(42), 16715–16728.

Czuba, T. B., Huk, A. C., Cormack, L. K. & Kohn, A. (2014), 'Area MT encodes three-dimensional motion.', *Journal of Neuroscience* **34**(47), 15522–15533.

de Lafuente, V., Jazayeri, M. & Shadlen, M. N. (2015), 'Representation of accumulating evidence for a decision in two parietal areas.', *Journal of Neuroscience* **35**(10), 4306–4318.

DeAngelis, G. C. & Newsome, W. T. (1999), 'Organization of disparity-selective neurons in macaque area MT', *The Journal of neuroscience* **19**(4), 1398–1415.

DeAngelis, G. C. & Newsome, W. T. (2004), 'Perceptual "read-out" of conjoined direction and disparity maps in extrastriate area MT', *PLOS Biology* **2**(3), e77.

Ding, L. & Gold, J. I. (2011), 'Neural Correlates of Perceptual Decision Making before, during, and after Decision Commitment in Monkey Frontal Eye Field', *Cerebral Cortex* **22**(5), 1052–1067.

Ding, L. & Gold, J. I. (2013), 'The basal ganglia's contributions to perceptual decision making', *Neuron* **79**(4), 640–649.

Ditterich, J. (2006), 'Stochastic models of decisions about motion direction: behavior and physiology.', *Neural networks : the official journal of the International Neural Network Society* **19**(8), 981–1012.

Ditterich, J., Mazurek, M. E. & Shadlen, M. N. (2003), 'Microstimulation of visual cortex affects the speed of perceptual decisions', *Nature Neuroscience* **6**(8), 891–898.

Dodd, J. V., Krug, K., Cumming, B. G. & Parker, A. J. (2001), 'Perceptually bistable three-dimensional figures evoke high choice probabilities in cortical area MT', *The Journal of neuroscience* **21**(13), 4809–4821.

Durstewitz, D. & Deco, G. (2008), 'Computational significance of transient dynamics in cortical networks.', *The European Journal of Neuroscience* **27**(1), 217–227.

Eastman, K. M. & Huk, A. C. (2012), 'PLDAPS: a hardware architecture and software toolbox for neurophysiology requiring complex visual stimuli and online behavioral control', *Frontiers in neuroinformatics* **6**.

Ecker, A. S., Berens, P., Keliris, G. A., Bethge, M., Logothetis, N. K. & Tolias, A. S. (2010), 'Decorrelated Neuronal Firing in Cortical Microcircuits', *Science* **327**(5965), 584–587.

Ecker, A. S., Berens, P., Tolias, A. S. & Bethge, M. (2011), 'The Effect of Noise Correlations in Populations of Diversely Tuned Neurons', *Journal of Neuroscience* **31**(40), 14272–14283.

Erlich, J. C., Brunton, B. W., Duan, C. A., Hanks, T. D., Brody, C. D. & Carandini, M. (2015), 'Distinct effects of prefrontal and parietal cortex inactivations on an accumulation of evidence task in the rat', *eLife* **4**, e05457.

Ernst, M. O. & Banks, M. S. (2002), 'Humans integrate visual and haptic

information in a statistically optimal fashion', *Nature* **415**(6870), 429–433.

Fechner, G. T. (1860), *Elemente der Psychophysik*, Elemente der Psychophysik, Breitkopf und Härtel.

Felleman, D. J. & Van Essen, D. C. (1991), 'Distributed hierarchical processing in the primate cerebral cortex', *Cerebral Cortex* **1**(1), 1–47.

Ferraina, S., Paré, M. & Wurtz, R. H. (2002), 'Comparison of cortico-cortical and cortico-collicular signals for the generation of saccadic eye movements', *Journal of Neurophysiology* **87**(2), 845–858.

Friedman, J., Hastie, T. & Tibshirani, R. (2010), 'Regularization paths for generalized linear models via coordinate descent', *Journal of statistical software* **33**(1), 1.

Fuchs, A. F., Kaneko, C. & Scudder, C. A. (1985), 'Brainstem control of saccadic eye movements', *Annual Review of Neuroscience* **8**(1), 307–337.

Fusi, S., Miller, E. K. & Rigotti, M. (2016), 'Why neurons mix: high dimensionality for higher cognition.', *Current Opinion in Neurobiology* **37**, 66–74.

Georgopoulos, A., Schwartz, A. & Kettner, R. (1986), 'Neuronal population coding of movement direction', *Science* **233**(4771), 1416–1419.

Gerhard, F., Kispersky, T., Gutierrez, G. J., Marder, E., Kramer, M. & Eden, U. (2013), 'Successful reconstruction of a physiological circuit with known connectivity from spiking activity alone', *PLoS computational biology* **9**(7), e1003138.

Ghose, G. M. & Bearl, D. W. (2010), 'Vision Research', *Vision Research* **50**(4), 441–451.

Gnadt, J. W. & Andersen, R. A. (1988), 'Memory related motor planning activity in posterior parietal cortex of macaque.', *Experimental brain research. Experimentelle Hirnforschung. Expérimentation cérébrale* **70**(1), 216–220.

Gold, J. I. & Ding, L. (2013), 'How mechanisms of perceptual decision-making affect the psychometric function.', *Progress in neurobiology* **103**, 98–114.

Gold, J. I. & Shadlen, M. N. (2001), 'Neural computations that underlie decisions about sensory stimuli', *Trends in Cognitive Sciences* **5**(1), 10–16.

Gold, J. I. & Shadlen, M. N. (2007), 'The Neural Basis of Decision Making', *Annual Review of Neuroscience* **30**(1), 535–574.

Gold, J. M., Murray, R. F., Bennett, P. J. & Sekuler, A. B. (2000), 'Deriving behavioural receptive fields for visually completed contours.', *Current biology : CB* **10**(11), 663–666.

Goldman, M. S. (2015), Failure of Averaging, *in* D. Jaeger & R. Jung, eds, 'Encyclopedia of Computational Neuroscience', Springer.

Graf, A. B. A. & Andersen, R. A. (2015), 'Predicting oculomotor behaviour from correlated populations of posterior parietal neurons.', *Nature communications* **6**, 6024.

Graf, A. B. A., Kohn, A., Jazayeri, M. & Movshon, J. A. (2011), 'Decoding the activity of neuronal populations in macaque primary visual cortex', *Nature Neuroscience* **14**(2), 239–245.

Green, D. M. & Swets, J. A. (1966), 'Signal detection theory and psychophysics', *Society* **1**, 521.

Groh, J. M., Born, R. T. & Newsome, W. T. (1997), 'How Is a Sensory Map Read Out? Effects of Microstimulation in Visual Area MT on Saccades and Smooth Pursuit Eye Movements', *The Journal of neuroscience* .

Gu, Y., DeAngelis, G. C. & Angelaki, D. E. (2007), 'A functional link between area MSTd and heading perception based on vestibular signals.', *Nature Neuroscience* **10**(8), 1038–1047.

Hanks, T. D., Kopec, C. D., Brunton, B. W., Duan, C. A., Erlich, J. C. & Brody, C. D. (2015), 'Distinct relationships of parietal and prefrontal cortices to evidence accumulation.', *Nature* **520**(7546), 220–223.

Hedges, J. H., Gartshteyn, Y., Kohn, A., Rust, N. C., Shadlen, M. N., Newsome, W. T. & Movshon, J. A. (2011), 'Dissociation of neuronal and psychophysical responses to local and global motion.', *Current biology : CB* **21**(23), 2023–2028.

Heiss, J. D., Walbridge, S., Asthagiri, A. R. & Lonser, R. R. (2010), 'Image-guided convection-enhanced delivery of muscimol to the primate brain', *Journal of Neurosurgery* **112**(4), 790–795.

Herrington, T. M. & Assad, J. A. (2010), 'Temporal sequence of attentional modulation in the lateral intraparietal area and middle temporal area during rapid covert shifts of attention.', *Journal of Neuroscience* **30**(9), 3287–3296.

Hess, R. & Murata, K. (1974), 'Effects of glutamate and GABA on specific response properties of neurones in the visual cortex.', *Experimental brain research. Experimentelle Hirnforschung. Expérimentation cérébrale* **21**(3), 285–297.

Horwitz, G. D., Batista, A. P. & Newsome, W. T. (2004), 'Representation of an abstract perceptual decision in macaque superior colliculus.', *Journal of Neurophysiology* **91**(5), 2281–2296.

Huk, A. C. & Shadlen, M. N. (2005), 'Neural activity in macaque parietal cortex reflects temporal integration of visual motion signals during perceptual decision making.', *Journal of Neuroscience* **25**(45), 10420–10436.

Janssen, P. & Shadlen, M. N. (2005), 'A representation of the hazard rate of elapsed time in macaque area LIP.', *Nature Neuroscience* **8**(2), 234–241.

Jazayeri, M. & Movshon, J. A. (2006), 'Optimal representation of sensory information by neural populations', *Nature Neuroscience* **9**(5), 690–696.

Jazayeri, M. & Shadlen, M. N. (2015), 'A Neural Mechanism for Sensing and Reproducing a Time Interval.', *Current biology : CB* **25**(20), 2599–2609.

Kaufman, M. T., Churchland, M. M., Ryu, S. I. & Shenoy, K. V. (2015), 'Vacillation, indecision and hesitation in moment-by-moment decoding of monkey motor cortex', *eLife* **4**, e04677.

Kelly, R. C., Smith, M. A., Samonds, J. M., Kohn, A., Bonds, A. B., Movshon, J. A. & Lee, T. S. (2007), 'Comparison of recordings from microelectrode arrays and single electrodes in the visual cortex.', *Journal of Neuroscience* **27**(2), 261–264.

Kerkhoff, G. (2001), 'Spatial hemineglect in humans.', *Progress in neurobiology* **63**(1), 1–27.

Kiani, R., Cueva, C. J., Reppas, J. B. & Newsome, W. T. (2014), 'Dynamics of neural population responses in prefrontal cortex indicate changes of mind on single trials.', *Current biology : CB* **24**(13), 1542–1547.

Kiani, R., Hanks, T. D. & Shadlen, M. N. (2008), 'Bounded Integration in Parietal Cortex Underlies Decisions Even When Viewing Duration Is Dictated by the Environment', *Journal of Neuroscience* **28**(12), 3017–3029.

Kiani, R. & Shadlen, M. N. (2009), 'Representation of Confidence Associated with a Decision by Neurons in the Parietal Cortex', *Science* **324**(5928), 759–764.

Kim, H. R., Angelaki, D. E. & DeAngelis, G. C. (2015), 'A functional link between MT neurons and depth perception based on motion parallax.', *Journal of Neuroscience* **35**(6), 2766–2777.

Kim, S., Putrino, D., Ghosh, S. & Brown, E. N. (2011), 'A Granger Causality Measure for Point Process Models of Ensemble Neural Spiking Activity', *PLoS computational biology* **7**(3), 1–13.

Knoblauch, K. & Maloney, L. T. (2008), 'Estimating classification images with generalized linear and additive models', *Journal of Vision* **8**(16), 10–10.

Kubanek, J., Li, J. M. & Snyder, L. H. (2015), 'Motor role of parietal cortex in a monkey model of hemispatial neglect.', *Proceedings of the National Academy of Sciences of the United States of America* **112**(16), E2067–72.

Latimer, K. W., Huk, A. C. & Pillow, J. W. (2015), '7 Bayesian inference for latent stepping and ramping models of spike train data', *Advanced State Space Methods for Neural and Clinical Data* p. 160.

Latimer, K. W., Yates, J. L., Meister, M. L. R., Huk, A. C. & Pillow, J. W. (2015), 'NEURONAL MODELING. Single-trial spike trains in parietal cortex reveal discrete steps during decision-making.', *Science* **349**(6244), 184–187.

Law, C.-T. & Gold, J. I. (2008), 'Neural correlates of perceptual learning in a sensory-motor, but not a sensory, cortical area', *Nature Neuroscience* **11**(4), 505–513.

Lennie, P. (1998), 'Single units and visual cortical organization', *Perception* **27**(8), 889–935.

Leon, M. I. & Shadlen, M. N. (2003), 'Representation of time by neurons in the posterior parietal cortex of the macaque.', *Neuron* **38**(2), 317–327.

Lewis, J. W. & Van Essen, D. C. (2000), 'Corticocortical connections of visual, sensorimotor, and multimodal processing areas in the parietal lobe of the macaque monkey.', *The Journal of comparative neurology* **428**(1), 112–137.

Link, S. W. (1992), *The wave theory of difference and similarity*, Psychology Press.

Liu, S., Gu, Y., DeAngelis, G. C. & Angelaki, D. E. (2013), 'Choice-related activity and correlated noise in subcortical vestibular neurons.', *Nature Publishing Group* **16**(1), 89–97.

Liu, Y., Yttri, E. A. & Snyder, L. H. (2010), 'Intention and attention: different functional roles for LIPd and LIPv', *Nature Publishing Group* **13**(4), 495–500.

Logothetis, N. K. & Schall, J. D. (1989), 'Neuronal correlates of subjective visual perception.', *Science* **245**(4919), 761–763.

Louie, K. & Glimcher, P. W. (2012), 'Efficient coding and the neural representation of value', *Annals of the New York Academy of Sciences* **1251**(1), 13–32.

Lynch, J. C. (1992), 'Saccade initiation and latency deficits after combined lesions of the frontal and posterior eye fields in monkeys', *Journal of Neurophysiology* **68**(5), 1913–1916.

Lynch, J. C., Graybiel, A. M. & Lobeck, L. J. (1985), 'The differential projection of two cytoarchitectonic subregions of the inferior parietal lobule of macaque upon the deep layers of the superior colliculus', *The Journal of comparative neurology* **235**(2), 241–254.

Mareschal, I., Dakin, S. C. & Bex, P. J. (2006), 'Dynamic properties of orientation discrimination assessed by using classification images.', *Proceedings of the National Academy of Sciences* **103**(13), 5131–5136.

Mareschal, I., Morgan, M. J. & Solomon, J. A. (2008), 'Contextual effects on decision templates for parafoveal orientation identification.', *Vision Research* **48**(27), 2689–2695.

Markov, N. T., Vezoli, J., Chameau, P., Falchier, A., Quilodran, R., Huissoud, C., Lamy, C., Misery, P., Giroud, P., Ullman, S., Barone, P., Dehay, C., Knoblauch, K. & Kennedy, H. (2014), 'Anatomy of hierarchy: feedforward and feedback pathways in macaque visual cortex.', *The Journal of comparative neurology* **522**(1), 225–259.

Martin, J. H. (1991), 'Autoradiographic estimation of the extent of reversible inactivation produced by microinjection of lidocaine and muscimol in the rat.', *Neuroscience letters* **127**(2), 160–164.

Maunsell, J. H. & Van Essen, D. C. (1983*a*), 'Functional properties of neurons in middle temporal visual area of the macaque monkey. I. Selectivity for stimulus direction, speed, and orientation', *Journal of Neurophysiology* **49**(5), 1127–1147.

Maunsell, J. & Van Essen, D. (1983*b*), 'The connections of the middle temporal visual area (MT) and their relationship to a cortical hierarchy in the macaque monkey.', *The Journal of neuroscience : the official journal of the Society for Neuroscience* **3**(12), 2563–2586.

Mazurek, M. E., Roitman, J. D., Ditterich, J. & Shadlen, M. N. (2003), 'A Role for Neural Integrators in Perceptual Decision Making', *Cerebral Cortex* **13**(11), 1257–1269.

Mazurek, M. E. & Shadlen, M. N. (2002), 'Limits to the temporal fidelity of cortical spike rate signals.', *Nature Neuroscience* **5**(5), 463–471.

Meister, M. L. R., Hennig, J. A. & Huk, A. C. (2013), 'Signal multiplexing and single-neuron computations in lateral intraparietal area during decision-making.', *Journal of Neuroscience* **33**(6), 2254–2267.

Miller, P. & Katz, D. B. (2010), 'Stochastic transitions between neural states in taste processing and decision-making.', *Journal of Neuroscience* **30**(7), 2559–2570.

Mineault, P. J., Barthelme, S. & Pack, C. C. (2009), 'Improved classification

images with sparse priorsin a smooth basis', *Journal of Vision* **9**(10), 17–17.

Mineault, P. J., Khawaja, F. A., Butts, D. A. & Pack, C. C. (2012), 'Hierarchical processing of complex motion along the primate dorsal visual pathway.', *Proceedings of the National Academy of Sciences of the United States of America* **109**(16), E972–80.

Moreno-Bote, R., Beck, J., Kanitscheider, I., Pitkow, X., Latham, P. & Pouget, A. (2014), 'Information-limiting correlations', *Nature Publishing Group* **17**(10), 1410–1417.

Morgan, M. J. & Ward, R. (1980), 'Conditions for motion flow in dynamic visual noise.', *Vision Research* **20**(5), 431–435.

Mountcastle, V. B., Talbot, W. H., Sakata, H. & Hyvärinen, J. (1969), 'Cortical neuronal mechanisms in flutter-vibration studied in unanesthetized monkeys. Neuronal periodicity and frequency discrimination.', *Journal of Neurophysiology* **32**(3), 452–484.

Movshon, J. A., Adelson, E. H., Gizzi, M. S. & Newsome, W. T. (1985), 'The analysis of moving visual patterns', *Pattern recognition mechanisms* **54**(54), 117–151.

Movshon, J. A. & Newsome, W. T. (1996), 'Visual response properties of striate cortical neurons projecting to area MT in macaque monkeys.', *The*

Journal of neuroscience : the official journal of the Society for Neuroscience **16**(23), 7733–7741.

Murray, R. F. (2011), 'Classification images: A review', *Journal of Vision* **11**(5), 2–2.

Neri, P. (2004), 'A Stereoscopic Look at Visual Cortex', *Journal of Neurophysiology* **93**(4), 1823–1826.

Neri, P. & Heeger, D. J. (2002), 'Spatiotemporal mechanisms for detecting and identifying image features in human vision', *Nature Neuroscience* **5**(8), 812–816.

Neri, P. & Levi, D. M. (2006), 'Receptive versus perceptive fields from the reverse-correlation viewpoint', *Vision Research* **46**(16), 2465–2474.

Neri, P., Parker, A. J. & Blakemore, C. (1999), 'Probing the human stereoscopic system with reverse correlation.', *Nature* **401**(6754), 695–698.

Newsome, W. T., Britten, K. H. & Movshon, J. A. (1989), 'Neuronal correlates of a perceptual decision.', *Nature* **341**(6237), 52–54.

Newsome, W. T. & Pare, E. B. (1988), 'A selective impairment of motion perception following lesions of the middle temporal visual area (MT).', *The Journal of neuroscience : the official journal of the Society for Neuroscience* **8**(6), 2201–2211.

Newsome, W. T., Wurtz, R. H., Dürsteler, M. R. & Mikami, A. (1985), 'Deficits in visual motion processing following ibotenic acid lesions of the middle temporal visual area of the macaque monkey.', *The Journal of neuroscience : the official journal of the Society for Neuroscience* **5**(3), 825–840.

Nichols, M. J. & Newsome, W. T. (2002), 'Middle temporal visual area microstimulation influences veridical judgments of motion direction.', *Journal of Neuroscience* **22**(21), 9530–9540.

Nienborg, H. & Cumming, B. (2010), 'Correlations between the activity of sensory neurons and behavior: how much do they tell us about a neuron's causality?', *Current Opinion in Neurobiology* **20**(3), 376–381.

Nienborg, H. & Cumming, B. G. (2009), 'Decision-related activity in sensory neurons reflects more than a neuron's causal effect', *Nature* **459**(7243), 89–92.

Noudoost, B. & Moore, T. (2011), 'A reliable microinjectrode system for use in behaving monkeys.', *Journal of Neuroscience Methods* **194**(2), 218–223.

Nover, H., Anderson, C. H. & DeAngelis, G. C. (2005), 'A logarithmic, scale-invariant representation of speed in macaque middle temporal area accounts for speed discrimination performance.', *Journal of Neuroscience* **25**(43), 10049–10060.

Okamoto, H., Kawakami, S., Saito, H.-a., Hida, E., Odajima, K., Tamanoi, D. & Ohno, H. (1999), 'MT neurons in the macaque exhibited two types of bimodal direction tuning as predicted by a model for visual motion detection', *Vision Research* **39**(20), 3465–3479.

Okatan, M., Wilson, M. & Brown, E. (2005), 'Analyzing Functional Connectivity Using a Network Likelihood Model of Ensemble Neural Spiking Activity', *Neural Computation* **17**, 1927–1961.

Osborne, L. C., Bialek, W. & Lisberger, S. G. (2004), 'Time course of information about motion direction in visual area MT of macaque monkeys.', *Journal of Neuroscience* **24**(13), 3210–3222.

Paninski, L. (2004), 'Maximum likelihood estimation of cascade point-process neural encoding models.', *Network (Bristol, England)* **15**(4), 243–262.

Park, I. M., Meister, M. L. R., Huk, A. C. & Pillow, J. W. (2014), 'Encoding and decoding in parietal cortex during sensorimotor decision-making', *Nature Publishing Group* **17**(10), 1395–1403.

Parker, A. J. & Newsome, W. T. (1998), 'Sense and the single neuron: probing the physiology of perception', *Annual Review of Neuroscience* **21**(1), 227–277.

Patel, G. H., Shulman, G. L., Baker, J. T., Akbudak, E., Snyder, A. Z., Snyder, L. H. & Corbetta, M. (2010), 'Topographic organization of macaque

area LIP.', *Proceedings of the National Academy of Sciences of the United States of America* **107**(10), 4728–4733.

Pillow, J. W., Paninski, L., Uzzell, V. J., Simoncelli, E. P. & Chichilnisky, E. J. (2005), 'Prediction and decoding of retinal ganglion cell responses with a probabilistic spiking model.', *Journal of Neuroscience* **25**(47), 11003–11013.

Pillow, J. W., Shlens, J., Chichilnisky, E. J. & Simoncelli, E. P. (2013), 'A model-based spike sorting algorithm for removing correlation artifacts in multi-neuron recordings.', *PLoS ONE* **8**(5), e62123.

Pillow, J. W., Shlens, J., Paninski, L., Sher, A., Litke, A. M., Chichilnisky, E. J. & Simoncelli, E. P. (2008), 'Spatio-temporal correlations and visual signalling in a complete neuronal population', *Nature* **454**(7207), 995–999.

Pitkow, X., Liu, S., Angelaki, D. E., DeAngelis, G. C. & Pouget, A. (2015), 'How Can Single Sensory Neurons Predict Behavior?', *Neuron* **87**(2), 411–423.

Platt, M. L. & Glimcher, P. W. (1999), 'Neural correlates of decision variables in parietal cortex.', *Nature* **400**(6741), 233–238.

Price, N. S. C. & Born, R. T. (2010), 'Timescales of Sensory- and Decision-Related Activity in the Middle Temporal and Medial Superior Temporal Areas', *Journal of Neuroscience* **30**(42), 14036–14045.

Price, N. S. C. & Prescott, D. L. (2012), 'Adaptation to direction statistics modulates perceptual discrimination', *Journal of Vision* **12**(6), 32–32.

Priebe, N. J., Cassanello, C. R. & Lisberger, S. G. (2003), 'The neural representation of speed in macaque area MT/V5', *The Journal of neuroscience* **23**(13), 5650–5661.

Priebe, N. J., Churchland, M. M. & Lisberger, S. G. (2002), 'Constraints on the source of short-term motion adaptation in macaque area MT. I. the role of input and intrinsic mechanisms.', *Journal of Neurophysiology* **88**(1), 354–369.

Priebe, N. J. & Lisberger, S. G. (2002), 'Constraints on the source of short-term motion adaptation in macaque area MT. II. tuning of neural circuit mechanisms.', *Journal of Neurophysiology* **88**(1), 370–382.

Purushothaman, G. & Bradley, D. C. (2005), 'Neural population code for fine perceptual decisions in area MT.', *Nature Neuroscience* **8**(1), 99–106.

Rao, V., DeAngelis, G. C. & Snyder, L. H. (2012), 'Neural Correlates of Prior Expectations of Motion in the Lateral Intraparietal and Middle Temporal Areas', *Journal of Neuroscience* **32**(29), 10063–10074.

Raposo, D., Kaufman, M. T. & Churchland, A. K. (2014), 'A category-free neural population supports evolving demands during decision-making', *Nature Publishing Group* **17**(12), 1784–1792.

Ratcliff, R. (1978), 'A theory of memory retrieval', *Psychological review* **85**(2), 59–108.

Ratcliff, R. & Rouder, J. N. (1998), 'Modeling response times for two-choice decisions', *Psychological Science* **9**(5), 347–356.

Roitman, J. D. & Shadlen, M. N. (2002), 'Response of neurons in the lateral intraparietal area during a combined visual discrimination reaction time task.', *Journal of Neuroscience* **22**(21), 9475–9489.

Rust, N. C., Mante, V., Simoncelli, E. P. & Movshon, J. A. (2006), 'How MT cells analyze the motion of visual patterns', *Nature Neuroscience* **9**(11), 1421–1431.

Saalmann, Y. B., Pigarev, I. N. & Vidyasagar, T. R. (2007), 'Neural mechanisms of visual attention: how top-down feedback highlights relevant locations.', *Science* **316**(5831), 1612–1615.

Salzman, C., Britten, K. & Newsome, W. (1990), 'Cortical microstimulation influences perceptual judgements of motion direction', *Nature* pp. 1–4.

Salzman, C. D. & Newsome, W. T. (1994), 'Neural mechanisms for forming a perceptual decision.', *Science* **264**(5156), 231–237.

Salzman, C., Murasugi, C. & Britten, K. (2003), 'Microstimulation in Visual Area MT: Effects on Direction Discrimination Performance', *The Journal of ...* pp. 1–25.

Sanada, T. M. & DeAngelis, G. C. (2014), 'Neural representation of motion-in-depth in area MT.', *Journal of Neuroscience* **34**(47), 15508–15521.

Sarma, A., Masse, N. Y., Wang, X.-J. & Freedman, D. J. (2016), 'Task-specific versus generalized mnemonic representations in parietal and prefrontal cortices.', *Nature Publishing Group* **19**(1), 143–149.

Schwartz, O., Pillow, J. W., Rust, N. C. & Simoncelli, E. P. (2006), 'Spike-triggered neural characterization', *Journal of Vision* **6**(4), 13–13.

Seidemann, E., Zohary, E. & Newsome, W. T. (1998), 'Temporal gating of neural signals during performance of a visual discrimination task.', *Nature* **394**(6688), 72–75.

Seung, H. S. & Sompolinsky, H. (1993), 'Simple models for reading neuronal population codes.', *Proceedings of the National Academy of Sciences* **90**(22), 10749–10753.

Shadlen, M. N., Britten, K. H., Newsome, W. T. & Movshon, J. A. (1996), 'A computational analysis of the relationship between neuronal and behavioral responses to visual motion.', *The Journal of neuroscience : the official journal of the Society for Neuroscience* **16**(4), 1486–1510.

Shadlen, M. N. & Kiani, R. (2013), 'Decision making as a window on cognition.', *Neuron* **80**(3), 791–806.

Shadlen, M. N. & Kim, J.-N. (1999), 'Neural correlates of a decision in the dorsolateral prefrontal cortex of the macaque - Nature Neuroscience', *Nature Neuroscience* **2**(2), 176–185.

Shadlen, M. N. & Newsome, W. T. (1996), 'Motion perception: seeing and deciding.', *Proceedings of the National Academy of Sciences* **93**(2), 628–633.

Shadlen, M. N. & Newsome, W. T. (2001), 'Neural basis of a perceptual decision in the parietal cortex (area LIP) of the rhesus monkey.', *Journal of Neurophysiology* **86**(4), 1916–1936.

Shimozaki, S. S., Eckstein, M. P. & Abbey, C. K. (2005), 'Spatial profiles of local and nonlocal effects upon contrast detection/discrimination from classification images', *Journal of Vision* **5**(1), 5–5.

Siegel, M., Buschman, T. J. & Miller, E. K. (2015), 'BRAIN PROCESSING. Cortical information flow during flexible sensorimotor decisions.', *Science* **348**(6241), 1352–1355.

Sincich, L. C., Park, K. F., Wohlgemuth, M. J. & Horton, J. C. (2004), 'Bypassing V1: a direct geniculate input to area MT', *Nature Neuroscience* **7**(10), 1123–1128.

Spiegelhalter, D. J., Best, N. G., Carlin, B. P. & van der Linde, A. (2002), 'Bayesian measures of model complexity and fit', *Journal of the Royal Statistical Society: Series B (Statistical Methodology)* **64**(4), 583–639.

Stanton, G. B., Bruce, C. J. & Goldberg, M. E. (1995), 'Topography of projections to posterior cortical areas from the macaque frontal eye fields', *The Journal of comparative neurology* **353**(2), 291–305.

Stevenson, I. H. & Kording, K. P. (2010), 'On the similarity of functional connectivity between neurons estimated across timescales.', *PLoS ONE* **5**(2), e9206.

Stevenson, I. H. & Kording, K. P. (2011), 'How advances in neural recording affect data analysis', *Nature Publishing Group* **14**(2), 139–142.

Stevenson, I. H., London, B. M., Oby, E. R., Sachs, N. A., Reimer, J., Englitz, B., David, S. V., Shamma, S. A., Blanche, T. J., Mizuseki, K., Zandvakili, A., Hatsopoulos, N. G., Miller, L. E. & Kording, K. P. (2012), 'Functional connectivity and tuning curves in populations of simultaneously recorded neurons.', *PLoS computational biology* **8**(11), e1002775.

Stevenson, I. H., Rebesco, J. M., Miller, L. E. & Kording, K. P. (2008), 'Inferring functional connections between neurons', *Current Opinion in Neurobiology* **18**(6), 582–588.

Sugrue, L. P., Corrado, G. S. & Newsome, W. T. (2004), 'Matching Behavior and the Representation of Value in the Parietal Cortex', *Science* **304**(5678), 1782–1787.

Tauste Campo, A., Martinez-Garcia, M., Nácher, V., Luna, R., Romo, R. & Deco, G. (2015), 'Task-driven intra- and interarea communications in pri-

mate cerebral cortex.', *Proceedings of the National Academy of Sciences of the United States of America* **112**(15), 4761–4766.

Tolhurst, D. J., Movshon, J. A. & Dean, A. F. (1983), 'The statistical reliability of signals in single neurons in cat and monkey visual cortex.', *Vision Research* **23**(8), 775–785.

Tolias, A. S., Ecker, A. S., Siapas, A. G., Hoenselaar, A., Keliris, G. A. & Logothetis, N. K. (2007), 'Recording chronically from the same neurons in awake, behaving primates.', *Journal of Neurophysiology* **98**(6), 3780–3790.

Treue, S. & Maunsell, J. H. (1996), 'Attentional modulation of visual motion processing in cortical areas MT and MST.', *Nature* **382**(6591), 539–541.

Truccolo, W., Eden, U. T., Fellows, M. R., Donoghue, J. P. & Brown, E. N. (2005), 'A point process framework for relating neural spiking activity to spiking history, neural ensemble, and extrinsic covariate effects.', *Journal of Neurophysiology* **93**(2), 1074–1089.

Truccolo, W., Hochberg, L. R. & Donoghue, J. P. (2010), 'Collective dynamics in human and monkey sensorimotor cortex: predicting single neuron spikes.', *Nature Publishing Group* **13**(1), 105–111.

Tsetsos, K., Gao, J., McClelland, J. L. & Usher, M. (2012), 'Using Time-Varying Evidence to Test Models of Decision Dynamics: Bounded Diffu-

sion vs. the Leaky Competing Accumulator Model.', *frontiers in Neuroscience* **6**, 1–17.

Uka, T. & DeAngelis, G. C. (2003), 'Contribution of middle temporal area to coarse depth discrimination: comparison of neuronal and psychophysical sensitivity.', *Journal of Neuroscience* **23**(8), 3515–3530.

Uka, T. & DeAngelis, G. C. (2004), 'Contribution of area MT to stereoscopic depth perception: choice-related response modulations reflect task strategy.', *Neuron* **42**(2), 297–310.

Ungerleider, L. G. & Desimone, R. (1986), 'Cortical connections of visual area MT in the macaque', *Journal of Comparative Neurology* **248**(2), 190–222.

Van Essen, D. C., Newsome, W. T. & Maunsell, J. H. (1984), 'Van Essen, Newsome, Maunsell - 1984 - The visual field representation in striate cortex of the macaque monkey asymmetries, anisotropies, and individual variability', *Vision Research* **24**(5), 429–448.

von Helmholtz, H. & Southall, J. P. C. (1924), *Helmholtz's treatise on physiological optics*, Helmholtz's Treatise on Physiological Optics, The Optical Society of America.

Wald, A. (1947), *Sequential Analysis*, Wiley series in probability and mathematical statistics. Probability and mathematical statistics, J. Wiley & Sons, Incorporated.

Wardak, C., Olivier, E. & Duhamel, J.-R. (2004), 'A deficit in covert attention after parietal cortex inactivation in the monkey.', *Neuron* **42**(3), 501–508.

Watamaniuk, S. N., Grzywacz, N. M. & Yuille, A. L. (1993), 'Dependence of speed and direction perception on cinematogram dot density.', *Vision Research* **33**(5-6), 849–859.

Watson, A. B. & Ahumada, Jr, A. J. (1983), 'A look at motion in the frequency domain'.

Wichmann, F. A. & Hill, N. J. (2001), 'The psychometric function: I. Fitting, sampling, and goodness of fit.', *Perception & psychophysics* **63**(8), 1293–1313.

Wilke, M., Kagan, I. & Andersen, R. A. (2012), 'Functional imaging reveals rapid reorganization of cortical activity after parietal inactivation in monkeys.', *Proceedings of the National Academy of Sciences of the United States of America* **109**(21), 8274–8279.

Wimmer, K., Compte, A., Roxin, A., Peixoto, D., Renart, A. & de la Rocha, J. (2015), 'Sensory integration dynamics in a hierarchical network explains choice probabilities in cortical area MT.', *Nature communications* **6**, 6177.

Wong, K.-F., Huk, A. C., Shadlen, M. N. & Wang, X.-J. (2008), 'Neural circuit dynamics underlying accumulation of time-varying evidence during perceptual decision making.', *Frontiers in Computational Neuroscience* **1**, 1–11.

Wurtz, R. H., Sommer, M. A., Paré, M. & Ferraina, S. (2001), 'Signal transformations from cerebral cortex to superior colliculus for the generation of saccades', *Vision Research* **41**(25), 3399–3412.

Wyart, V., de Gardelle, V., Scholl, J. & Summerfield, C. (2012), 'Rhythmic fluctuations in evidence accumulation during decision making in the human brain.', *Neuron* **76**(4), 847–858.

Yttri, E. A., Liu, Y. & Snyder, L. H. (2013), 'Lesions of cortical area LIP affect reach onset only when the reach is accompanied by a saccade, revealing an active eye–hand coordination circuit', *Proceedings of the National Academy of Sciences* **110**(6), 2371–2376.

Vita

Jacob Lachenmyer Yates was born in San Francisco in 1985. After graduating from University of California at Berkeley with a degree in Psychology, he moved to Austin to join the Institute for Neuroscience at UT Austin. He plans to move to Rochester in June of 2016 to work with Jude Mitchell and Gregory DeAngelis at the University of Rochester as a postdoctoral fellow.

Permanent address: jlyates@utexas.edu

This dissertation was typeset with LaTeX[†] by the author.

[†]LaTeX is a document preparation system developed by Leslie Lamport as a special version of Donald Knuth's TeX Program.